MODELING AND NUMERICAL ANALYSIS OF SINGLE DROPLET DRYING

A THESIS SUBMITTED TO
THE GRADUATE SCHOOL OF NATURAL AND APPLIED SCIENCES
OF
MIDDLE EAST TECHNICAL UNIVERSITY

BY

NESİP DALMAZ

IN PARTIAL FULFILLMENT OF THE REQUIREMENTS
FOR
THE DEGREE OF MASTER OF SCIENCE
IN
CHEMICAL ENGINEERING

AUGUST 2005

Approval of the Graduate School of Natural and Applied Sciences

Prof. Dr. Canan ÖZGEN
Director

I certify that this thesis satisfies all the requirements as a thesis for the degree of Master of Science.

Prof. Dr. Nurcan BAÇ
Head of Department

This is to certify that we have read this thesis and that in our opinion it is fully adequate, in scope and quality, as a thesis and for the degree of Master of Science.

Asst. Prof. Dr. Yusuf ULUDAĞ
Co-Supervisor

Prof. Dr. H. Önder ÖZBELGE
Supervisor

Examining Committee Members

Prof. Dr. A. Tülay ÖZBELGE (METU, CHE)________________________

Prof. Dr. H. Önder ÖZBELGE (METU, CHE)________________________

Asst. Prof. Dr. Yusuf ULUDAĞ (METU, CHE)________________________

Assoc. Prof. Dr. Ahmet N. ERASLAN (METU, ES) ________________________

Asst. Prof. Dr. Halil KALIPÇILAR (METU, CHE)________________________

I hereby declare that all information in this document has been obtained and presented in accordance with academic rules and ethical conduct. I also declare that, as required by these rules and conduct, I have fully cited and referenced all material and results that are not original to this work.

Name, Last name : Nesip DALMAZ

Signature :

ABSTRACT

MODELING AND NUMERICAL ANALYSIS OF SINGLE DROPLET DRYING

DALMAZ, Nesip
M.Sc., Department of Chemical Engineering
Supervisor: Prof. Dr. H. Önder ÖZBELGE
Co-Supervisor: Asst. Prof. Dr. Yusuf ULUDAĞ

August 2005, 120 pages

A new single droplet drying model is developed that can be used as a part of computational modeling of a typical spray drier. It is aimed to describe the drying behavior of a single droplet both in constant and falling rate periods using receding evaporation front approach coupled with the utilization of heat and mass transfer equations. A special attention is addressed to develop two different numerical solution methods, namely the Variable Grid Network (VGN) algorithm for constant rate period and the Variable Time Step (VTS) algorithm for falling rate period, with the requirement of moving boundary analysis. For the assessment of the validity of the model, experimental weight and temperature histories of colloidal silica (SiO_2), skimmed milk and sodium sulfate decahydrate ($Na_2SO_4 \cdot 10H_2O$) droplets are compared with the model predictions. Further, proper choices of the numerical parameters are sought in order to have successful iteration loops.

The model successfully estimated the weight and temperature histories of colloidal silica, dried at air temperatures of 101^oC and 178^oC, and skimmed milk, dried at air temperatures of 50^oC and 90^oC, droplets. However, the model failed to predict both the weight and the temperature histories of $Na_2SO_4 \cdot 10H_2O$ droplets dried at air temperatures of 90^oC and 110^oC. Using the vapor pressure expression of pure water, which neglects the non-idealities introduced by solid-liquid interactions, in model calculations is addressed to be the main reason of the model resulting poor estimations. However, the developed model gives the flexibility to use a proper vapor pressure expression without much effort for estimation of the drying history of droplets having highly soluble solids with strong solid-liquid interactions.

Initial droplet diameters, which were calculated based on the estimations of the critical droplet weights, were predicted in the range of 1.5-2.0 mm, which are in good agreement with the experimental measurements.

It is concluded that the study has resulted a new reliable drying model that can be used to predict the drying histories of different materials.

Keywords: Spray drying, single droplet, modeling, finite difference method, moving boundary

ÖZ

TEK DAMLACIK KURUMASININ MODELLENMESİ VE NÜMERİK ÇÖZÜMLEMESİ

DALMAZ, Nesip
Yüksek Lisans, Kimya Mühendisliği
Tez Yöneticisi: Prof. Dr. H. Önder ÖZBELGE
Yardımcı Tez Yöneticisi: Y. Doç. Dr. Yusuf ULUDAĞ

Ağustos 2005, 120 sayfa

Sprey kurutucularının modellenmesinde kullanılabilecek yeni bir tek damlacık kuruma modeli geliştirilmiştir. Isı ve kütle transferi denklemleri yardımıyla, değişken pozisyonlu buharlaşma yüzü yaklaşımı kullanılarak, tek damlacığın sabit ve azalan hız rejimlerindeki kuruma davranışı tanımlanmaya çalışılmıştır. Sabit ve azalan hız rejimleri için, Değişken Grid Ağı (VGN) ve Değişken Zaman Aralığı (VTS) algoritması adlı iki farklı nümerik çözüm metodu, değişken pozisyonlu sınır analizinin gerekleri göz önünde bulundurularak geliştirilmiştir. Modelin geçerliliğini sınamak amacıyla silisyum dioksit (SiO_2), yağsız süt ve sodyum sülfat dekahidrat ($Na_2SO_4 \cdot 10H_2O$) damlacıklarına ait deneysel ağırlık ve sıcaklık ölçümleri model sonuçlarıyla karşılaştırılmıştır. Bunun yanında, algoritmalarda kullanılan döngülerin doğru çalışması gereği düşünülerek nümerik parametrelerin uygun değerleri araştırılmıştır.

Geliştirilen model 101^{o}C de ve 178^{o}C de kurutulan silisyum dioksit (SiO_2) damlacıklarıyla 50^{o}C de ve 90^{o}C de kurutulan süt damlacıklarına ait ağırlık ve sıcaklık değerlerini başarıyla hesaplamıştır. Ancak, 90^{o}C de ve 110^{o}C de kurutulan sodyum sülfat dekahidrat ($Na_2SO_4 \cdot 10H_2O$) damlacıklarına ait ağırlık ve sıcaklık değerlerini hesaplamada model başarısız olmuştur. Bunun temel nedeni olarak, modelin saf suya ait olan ve katı-sıvı etkileşimlerini gözardı eden bir buhar basıncı denkliği kullanması öngörülmüştür. Ancak, geliştirilen model yüksek çözünürlüğe sahip katı-sıvı etkileşimi güçlü damlacıklara ait kuruma geçmişini belirlemeye uygun bir buhar basıncı denkliğini az bir çabayla kullanmayı sağlayacak esnekliğe sahiptir.

Damlacıkların kritik ağırlık temel alınarak hesaplanan ilk andaki çapları 1.5-2.0 mm olarak bulunmuş olup, bu değerler deneysel sonuçlarla uyum göstermiştir.

Sonuç olarak, bu çalışma farklı damlacıklara ait kuruma geçmişini belirlemede kullanılabilecek olan yeni ve güvenilir bir model ortaya çıkarmıştır.

Anahtar sözcükler: Sprey kurutma, tek damlacık, modelleme, sabit farklar metodu, değişken pozisyonlu sınır

To My Beloved Brother Mustafa

ACKNOWLEDGEMENTS

I would like to express my sincere appreciation to my supervisors Prof. Dr. H. Önder ÖZBELGE and Asst. Prof. Dr. Yusuf ULUDAĞ for their guidance, patience and unforgettable encouragements throughout not only in this study but also in my academic career.

I extend my sincere appreciation to Assoc. Prof. Dr. Ahmet N. Eraslan for his solutions and suggestions. His continuous support is greatly acknowledged.

I wish to thank my father and my mother for their endless, unforgettable supports in the very hard times of our life. My appreciation to you can not be put into words.

I would like to extend my appreciation to my brothers Mustafa and Yasin for their unforgettable tolerance and encouragement throughout this study.

I wish to thank aunt Nuran, uncle Osman and cousin Yasemin for their endless support and motivation.

Very special thanks are due to cousin Abdullah for his logical support.

Finally, I would like to thank my grandmother for her tasteful meals.

TABLE OF CONTENTS

PLAGIARISM …………………………………………………………………… iii

ABSTRACT ………………………………………………………………….... iv

ÖZ ………………………………………………………………………….... vi

DEDICATION ……………………………………………………………….... viii

ACKNOWLEDGEMENTS …………………………………………………..... ix

TABLE OF CONTENTS ……………………………………………………... x

LIST OF TABLES ……………………………………………………………. xii

LIST OF FIGURES …………………………………………………………… xiii

CHAPTER

1. INTRODUCTION ………………………………………………. 1
2. LITERATURE REVIEW ……………………………………….. 7
3. MODELING ……………………………………………………. 13
    - 3.1 Modeling in Constant Rate Period ……………………….. 13
    - 3.2 Modeling in Falling Rate Period ………………………….... 22
4. NUMERICAL CALCULATIONS ……………………………... 32
    - 4.1 Numerical Calculations in Constant Rate Period …………. 34
    - 4.2 Numerical Calculations in Falling Rate Period …………… 41
    - 4.3 Calculation of Drying Parameters ……………………….. 51

5. RESULTS & DISCUSSION ………………………………………. 52

5.1 Drying of Colloidal Silica Droplets ……………………….. 52

5.2 Drying of Skimmed Milk Droplets ………………………... 64

5.3 Drying of Sodium Sulfate Decahydrate Droplets …………. 72

5.4 Drying & Numerical Model Parameters …………………... 80

5.5 Comparison of Different Model Results …………………... 83

6. CONCLUSION ……………………………………………………. 92

7. RECOMMENDATIONS ………………………………………….. 95

REFERENCES ………………………………………………………………... 96

APPENDICES

A. PHYSICAL PROPERTIES USED BY THE MODEL …….. 99

B. PROGRAM FILE LISTING OF VGN ALGORITHM …….. 101

C. PROGRAM FILE LISTING OF VTS ALGORITHM ……... 111

LIST OF TABLES

TABLE

5.1 Parameters used for drying of a colloidal silica droplet at 101^{o}C …. 53

5.2 Parameters used for drying of a colloidal silica droplet at 178^{o}C …. 59

5.3 Parameters used for drying of a skimmed milk droplet at 50^{o}C …… 64

5.4 Parameters used for drying of a skimmed milk droplet at 90^{o}C …… 69

5.5 Parameters used for drying of a $Na_2SO_4 \cdot 10H_2O$ droplet at 90^{o}C ….. 72

5.6 Parameters used for drying of a $Na_2SO_4 \cdot 10H_2O$ droplet at 110^{o}C … 76

5.7 Comparison of experimental and predicted droplet diameters …….. 81

LIST OF FIGURES

FIGURE

1.1 A typical counter-current spray drier ………………………………………. 2

1.2 Typical drying rate-moisture content and weight-time curves …………... 3

1.3 Drying behavior of a typical droplet …………………………………….. 4

3.1 Droplet drying in constant rate period …………………………………… 14

3.2 Droplet drying in falling rate period ……………………………………... 22

4.1 Grid distributions in constant rate period ………………………………... 34

4.2 Schematic description of VGN algorithm ……………………………….. 39

4.3 Grid distributions in falling rate period ………………………………….. 41

4.4 Schematic description of VTS algorithm ………………………………... 49

5.1 Weight history of a colloidal silica droplet dried at 101^{o}C ……………… 54

5.2 Temperature history of a colloidal silica droplet dried at 101^{o}C ………… 55

5.3 Temperature profiles of a colloidal silica droplet dried at 101^{o}C ……….. 57

5.4 Concentration profiles of a colloidal silica droplet dried at 101^{o}C ……… 59

5.5 Weight history of a colloidal silica droplet dried at 178^{o}C ……………… 60

5.6 Temperature history of a colloidal silica droplet dried at 178^{o}C ………… 61

5.7 Temperature profiles of a colloidal silica droplet dried at 178^{o}C ……….. 63

5.8 Concentration profiles of a colloidal silica droplet dried at 178^{o}C ……… 63

5.9 Weight history of a skimmed milk droplet dried at 50°C ……………….. 65
5.10 Temperature history of a skimmed milk droplet dried at 50°C ………….. 66
5.11 Temperature profiles of a skimmed milk droplet dried at 50°C ………… 67
5.12 Concentration profiles of a skimmed milk droplet dried at 50°C ……….. 68
5.13 Weight history of a skimmed milk droplet dried at 90°C ……………….. 69
5.14 Temperature history of a skimmed milk droplet dried at 90°C ………….. 70
5.15 Temperature profiles of a skimmed milk droplet dried at 90°C ………… 71
5.16 Concentration profiles of a skimmed milk droplet dried at 90°C ……….. 71
5.17 Weight history of a $Na_2SO_4 \cdot 10H_2O$ droplet dried at 90°C ……………… 73
5.18 Temperature history of a $Na_2SO_4 \cdot 10H_2O$ droplet dried at 90°C ………… 74
5.19 Temperature profiles of a $Na_2SO_4 \cdot 10H_2O$ droplet dried at 90°C ……….. 75
5.20 Concentration profiles of a $Na_2SO_4 \cdot 10H_2O$ droplet dried at 90°C ……… 76
5.21 Weight history of a $Na_2SO_4 \cdot 10H_2O$ droplet dried at 110°C …………….. 77
5.22 Temperature history of a $Na_2SO_4 \cdot 10H_2O$ droplet dried at 110°C ……….. 78
5.23 Temperature profiles of a $Na_2SO_4 \cdot 10H_2O$ droplet dried at 110°C ……… 79
5.24 Concentration profiles of a $Na_2SO_4 \cdot 10H_2O$ droplet dried at 110°C …….. 79
5.25 Effect of different critical weight choices on weight history …………… 80
5.26 Effect of different critical weight choices on temperature history ……… 81
5.27 Relationship of the falling rate numerical parameters …………………… 83
5.28 Predictions for weight history of a colloidal silica droplet at 101°C …….. 83
5.29 Predictions for temperature history of a colloidal silica droplet at 101°C . 84
5.30 Predictions for weight history of a colloidal silica droplet at 178°C …….. 84
5.31 Predictions for temperature history of a colloidal silica droplet at 178°C . 85
5.32 Predictions for weight history of a skimmed milk droplet at 50°C ……… 85

5.33 Predictions for temperature history of a skimmed milk droplet at 50°C … 86

5.34 Predictions for weight history of a skimmed milk droplet at 90°C ……… 86

5.35 Predictions for temperature history of a skimmed milk droplet at 90°C … 87

5.36 Predictions for weight history of a $Na_2SO_4 \cdot 10H_2O$ droplet at 90°C ……... 87

5.37 Predictions for temperature history of a $Na_2SO_4 \cdot 10H_2O$ droplet at 90°C .. 88

5.38 Predictions for weight history of a $Na_2SO_4 \cdot 10H_2O$ droplet at 110°C ……. 88

5.39 Predictions for temperature history of a $Na_2SO_4 \cdot 10H_2O$ droplet at 110°C . 89

5.40 Results for weight history of a colloidal silica droplet at 178°C ………… 89

5.41 Results for temperature history of a colloidal silica droplet at 178°C …… 90

5.42 Results for weight history of a skimmed milk droplet at 90°C ………….. 90

5.43 Results for temperature history of a skimmed milk droplet at 90°C …….. 91

CHAPTER 1

INTRODUCTION

Industrial drying operations require the removal of moisture from a solid, semi-solid or liquid feedstock via application of heat. Heat supplied by conduction, convection or radiation evaporates some portion of the volatile liquid and a carrier gas, which passes through or over the feed, removes the vapor from the drying medium. Most commonly, drying is accomplished by the removal of water into a hot air stream, but drying may also encompass the removal of any volatile liquid into any heated gas.

Drying has found applications in many fields such as chemical, agricultural, food, polymer, pharmaceutical, ceramics and mineral processing industries. Thus there are numerous dryer designs available to meet the demand of each individual industry. Generally, nature of the feedstock, operating conditions and desired quality of the product are the determinants of a drier design. In addition, energy efficiency is very important for a drier because a large amount of energy is utilized to evaporate water, which has high latent heat of vaporization.

Spray drying is one of the most widely used drying operations due to its flexibility in meeting product requirements as well as its high energy efficiency compared to other methods [15]. In a typical spray drying operation, which is shown in Figure 1.1, a liquid, slurry or paste feedstock is sprayed into a drying chamber where low moisture containing hot air stream is blown through. Atomization of the feed into small droplets generates large surface area for both heat and mass transfer. Heat supplied by air evaporates moist water within the droplets and the vapor is transferred to air. Drying proceeds until the droplets reach equilibrium moisture content, which is prescribed by temperature and moisture content of the drying air. Nature of the material also determines when drying stops, since different materials show different equilibrium moisture content curves.

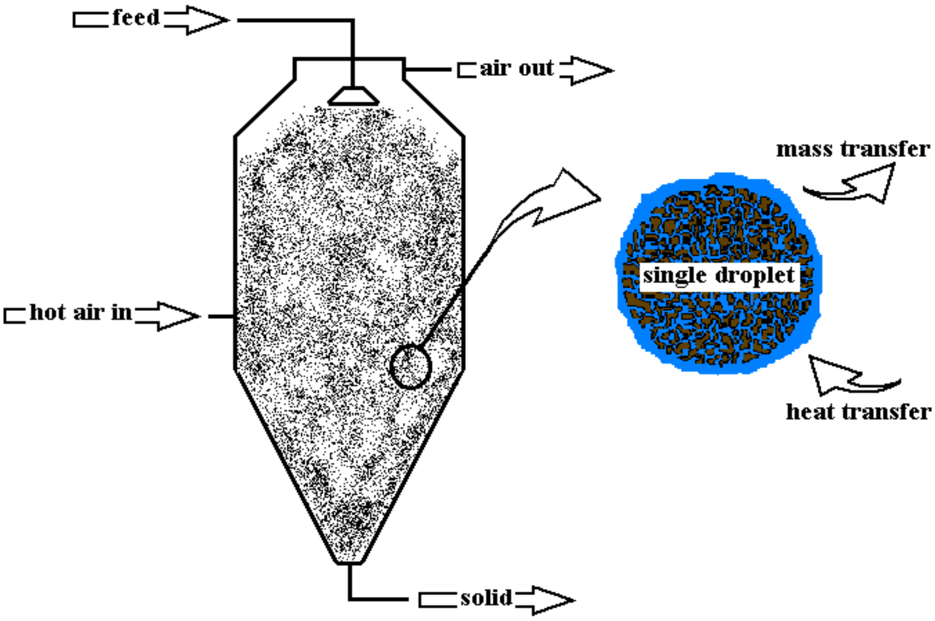

Figure 1.1 A typical counter-current spray drier

An in-depth understanding of the drying behavior of a single feed droplet is essential for the design of a spray drier. Experimentation [3,10,26,31] on drying of drops containing suspended or dissolved solids has shown that evaporation first occurs at a constant rate, followed by a falling rate similar to what is usually observed in other drying operations. In the constant rate period, which is shown in Figure 1.2, drying rate is generally controlled by the velocity, flow pattern, temperature and humidity of the drying air. After an initial adjustment, droplet temperature reaches air wet-bulb temperature in this period, in which heat transferred from air is counter-balanced by the heat required to evaporate free water on the surface of the drop. In the case of drops containing dissolved solids, vapor pressure at the drop surface is lowered due to solid-liquid interactions, which causes a reduction in mass transfer rate. Surface temperature of the drop consequently exceeds thermodynamic wet-bulb temperature. For drops containing suspended solids, vapor pressure lowering effects are generally negligible.

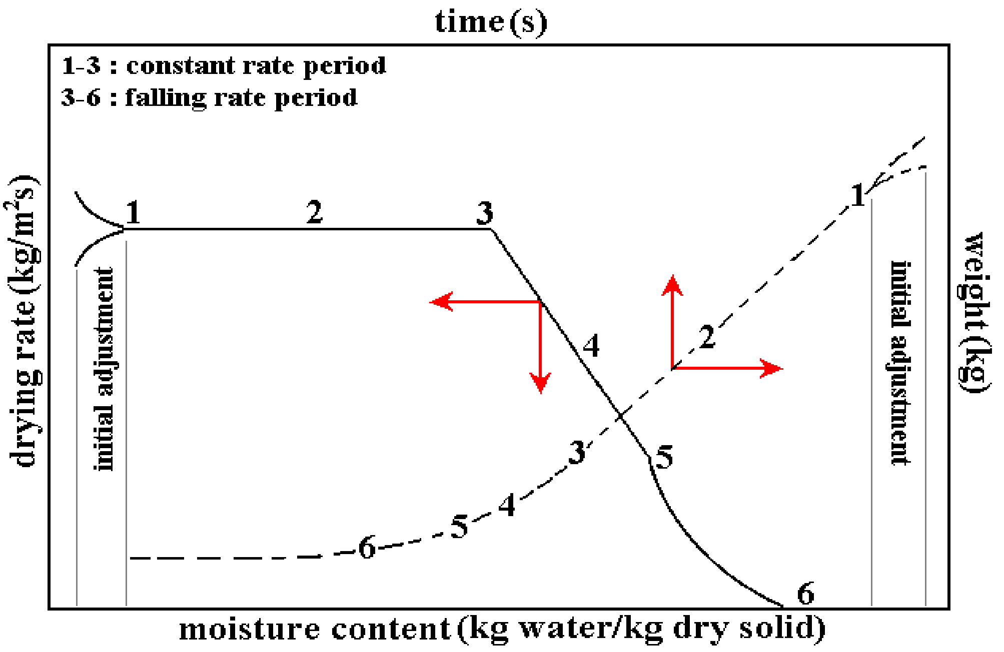

Figure 1.2 Typical drying rate-moisture content and weight-time curves

As drying proceeds in constant rate period, free water on the surface of the droplet is evaporated gradually. At critical moisture content (point 3 in Figure 1.2), water supply from interior to surface of the droplet becomes inadequate and dry spots commence at the points of maximum mass transfer, which is shown in Figure 1.3. Unsaturated surface drying (path 3-5 in Figures 1.2&1.3) conditions prevail until surface of the droplet dries completely. Internal movement of heat and mass within the droplet controls drying afterwards (path 5-6 in Figures 1.2&1.3).

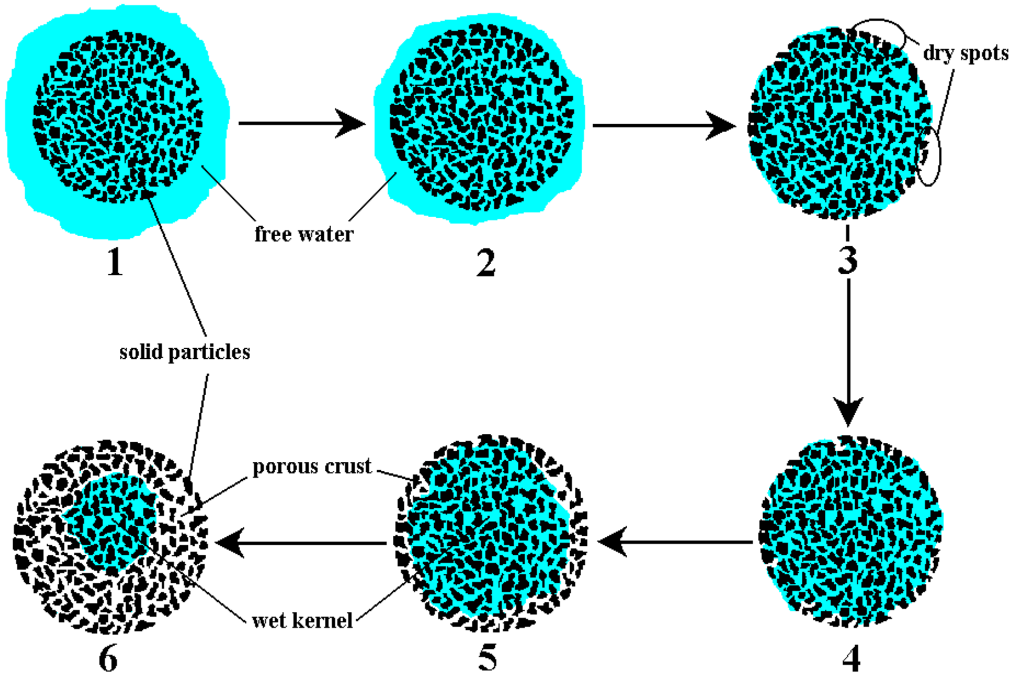

Figure 1.3 Drying behavior of a typical droplet

In falling rate period, an additional resistance to both heat and mass transfer arises due to formation of a porous solid layer. Temperature gradients within the droplet are greater compared to constant rate period since surface temperature of the droplet continuously changes from wet-bulb temperature to dry-bulb temperature of air as drying proceeds. Migration of moisture within the droplet is a much more complicated phenomenon since different mechanisms predominate at different times during the drying cycle, especially in falling rate period. Three generally accepted theories have been proposed for the migration of moisture in porous media: the diffusion theory, the capillary flow theory and the evaporation-condensation theory.

Diffusion theory proposed by Sherwood [30] suggests that moisture can either be transferred as liquid water through pores followed by evaporation on the surface, or by evaporation of water below the surface followed by vapor diffusion thorough the pores. A Fickian type of expression with an effective diffusion coefficient is usually used to describe the diffusion of water.

In capillary flow theory [1,2], the term capillary potential is used to describe the motion of liquid water in pores. The theory assumes that water moves towards a high water concentration region provided that the region has a fine pore structure. Darcy's law [4,24,32] type of an expression is generally used with an effective permeability.

Evaporation-condensation theory [12,16] assumes that moisture is in a pendulum-like state. Liquid water exists at the waists of the pores and moisture moves in vapor phase by evaporation-condensation sequence.

It should be noted that the validity of above mentioned theories depend highly on the nature of the spray-dried material, that is, the material's being hygroscopic or non-hygroscopic and solid's being soluble or insoluble in water. External conditions of temperature and humidity of the drying air also determine how moisture is transferred as well as the structural changes that occur during the course of drying such as formation of crust, pore size change, shrinkage, inflation, fracture etc., which all make the drying of a single droplet a very complicated phenomenon. Such complications are not only limited to spray drying operation.

In the past, spray driers have been designed depending on field experience and know-how followed by experimentation in pilot plant trials. Problems associated with scale-up and hydrodynamics of the driers have resulted limited success. The advent of Computational Fluid Dynamics (CFD) in 1980s has enabled to solve the equations of fluid flow within the spray chamber without any restrictive assumptions, which has resulted in better spray drier designs [17]. Such approaches usually require sub-models that describe the drying behavior of a single drop of feed, since a robust model of heat and mass transfer mechanisms within the droplet is essential for the macroscopic modeling.

The objective of this study is therefore to develop a model for the numerical solution of the governing heat and mass transfer equations associated with the drying of a single droplet. It is aimed to describe the drying behavior both in constant and falling rate periods using receding evaporation front approach. Fick's law of diffusion and Fourrier's law of conduction with effective coefficients are used to describe mass and heat transfer, respectively. The model is actually obtained by further improvements of the existing studies [5,6,7,11,22] utilizing the same approach mentioned. A special attention is addressed to develop two different numerical solution methods, one for the constant rate period and one for the falling rate period, with the requirement of moving boundary analysis. Numerical solutions yield temperature and moisture concentration distributions within the droplet over course of drying. It is also objected to validate the results of the model with the available experimental data [22].

CHAPTER 2

LITERATURE REVIEW

Drying of single droplets has been extensively studied by many investigators [5-7] and a wide variety of models have been developed. In those studies, mainly drying in the falling rate period was investigated. It is certain that there has been no general agreement among the researchers on which driving forces predominate during the course of drying, since different materials show quite different moisture migration behavior. Generally, in most of the models, an appropriate moisture migration mechanism is assumed to be valid and the derived equations governing heat and mass transfer within the droplet are solved. Contrary to the utilization of different mass transfer mechanisms, thermal conduction inside the droplet is generally accepted to be the mode of heat transfer.

Luikov [18] developed a unique approach to describe the drying of porous bodies based on the application of the principles of irreversible thermodynamics. According to Luikov's model, in the falling rate period, the drying material is divided into dry and wet zones, each having a different moisture migration mechanism. The zones are separated by an evaporation front, which recedes as drying proceeds. This approach has the advantage of not requiring the assumption of any controlling mechanism of internal moisture migration. However, the resulting set of the governing differential equations requires the use of the experimentally determined diffusion and thermal conduction coefficients, which puts a limitation on the applicability of the model.

Based on Luikov's two-zone model, Mikhailov [19] presented approximate analytical solutions of the heat and mass transfer equations for a porous half-space system with the simplifying assumption that moisture migration in dry zone is in vapor phase only.

Wijlhuizen et al. [33] developed a solid sphere and hollow sphere model for the drying of skimmed milk droplets. They were mainly interested in the phosphatase inactivation. In solid sphere model, liquid water is assumed to diffuse throughout the droplet and evaporate at the surface. The diffusion equation with a binary diffusion coefficient varying both with temperature and moisture content is utilized. In hollow sphere model, an initial gas bubble of known size having uniform vapor concentration is assumed to exist in the droplet. Movement of water due to contraction or expansion of the gas bubble is also included in the diffusion equation. In both of the models, temperature variations within the droplet are neglected. Further, by not allowing the formation of the crust, the study shows overestimated results especially in the falling rate period.

A more realistic model was developed by Sano and Keey [28] for the drying of droplets containing colloidal particles. In their study, an initial voidless spherical droplet is assumed to inflate and form a hollow sphere by deformation with subsequent fracture. Inflation is proposed to occur if the vapor pressure of water inside the droplet exceeds the ambient pressure. Deformation of hollow sphere is explained by increase of the void radius keeping outer radius constant or by decrease of the outer radius keeping void radius constant. Diffusion of liquid water in both voidless and inflated droplets is described by a Fickian type expression with temperature and moisture content dependent diffusion coefficient, which is obtained experimentally. Although a special attention is addressed for the migration of moisture, the study neglects the heat transfer resistances within the droplet, which is quite unrealistic. Further, their computation requires an experimentally determined inflation ratio, which is defined as the ratio of maximum radius obtained after inflation to the radius of voidless sphere. Actually, the possibility of such inflations arises only if the drying air temperature is higher than the boiling point of water [3], which puts a limitation on the validity of such a model.

Sano and Yamamoto [29] predicted the drying rate of polyacrylonitrile in dimethyl formamide by modifying Sano and Keey's model [28] with the assumption of shrinkage due to solvent loss. They also assumed no radial variation of concentration except for a region, defined as penetration depth. A diffusion equation with an empirically derived diffusion coefficient was used to describe the variation of liquid solvent concentration throughout the penetration depth.

Cheong et al. [7] developed a receding interface model for the drying of sodium sulfate decahydrate droplets. In their study, the droplet is divided into dry and wet regions separated by an evaporation interface, which moves towards the center as drying proceeds. Diffusion of water vapor in the dry region is described by a Fickian type expression with an effective diffusion coefficient. Both heat and mass transfer resistances of the wet region are neglected as well as sensible heating of the dry region. Actually, the assumption of linear temperature distribution in dry region, which is not valid for spherical geometry, is the major drawback of this model, since such an assumption underestimates the resistance to heat transferred to the interface, which yields higher drying rates than the actual case. Further, although their experimentation shows an apparent constant rate period, in the model, falling rate conditions prevail for the whole drying history.

Nesic and Vodnik [22] studied the drying of colloidal silica, sodium sulfate and skimmed milk droplets. They also developed a shrinking core model describing heat and mass transfer mechanisms of droplet drying with the utilization of a five-stage concept. According to this concept, the droplet temperature passes through five different paths: initial heating, quasi-equilibrium evaporation, crust formation, boiling and drying above boiling. Initial heating corresponds to a stage in which droplet temperature changes from initial temperature to the equilibrium temperature, that is usually the wet-bulb temperature of air surrounding the droplet. In quasi-equilibrium evaporation stage, temperature of the droplet steadily increases above the wet-bulb temperature due to the vapor pressure lowering effects caused by the solid-liquid interactions. Such deviations from the wet-bulb temperature in this stage are actually negligible in the absence of solid-liquid interactions, as in the case of drying of colloidal silica droplets. A solid crust forms at the surface of the droplet when the surface concentration of solids exceeds the saturation value, which indicates the beginning of the crust formation stage. Due to the introduction of a new resistance to transferred heat, droplet temperature rises gradually until it reaches the boiling point of the liquid. Crust also increases in thickness in this period. Boiling stage is observed only if the air temperature is above the boiling point of the liquid for a given total pressure. Finally, bound water is removed in drying above boiling stage as the temperature of droplet reaches the air temperature.

In the model of Nesic and Vodnik [22], heat transfer resistance of the wet core region is neglected as well as the effect of diffusing water vapor through the crust to heat transfer. Usually, if the Biot number is higher than 0.1, which is valid for drying of droplets having highly conductive solids and liquid, heat transfer resistance of the wet core region can be neglected. Similarly, heating effect of vapor in the pores can be negligible for low temperature drying conditions and for the early stages of the drying process, since the concentration of vapor is small for these conditions. In initial heating and quasi-equilibrium evaporation stages, a transient diffusion equation is solved with an effective diffusion coefficient determined experimentally in order to assess the starting of the crust formation stage. Although the model results are in good agreement with the measurements, experimental determination of the diffusion coefficients for different materials puts a limitation on the applicability of the model.

More recently, Chen and Xie [5] developed a model based on reaction engineering approach for the drying of milk droplets. Their model does not consider the variations of both temperature and moisture within the droplet but a proper activity coefficient is assumed to change the vapor pressure of water at the surface of the droplet. Decreasing drying rates in the falling rate period is then explained by the introduction of such a water activity expression. Chen et al. [6] then improved this model by introducing the crust mass transfer resistance. Although their results show good agreement with the experimental drying rates, the models fail to describe the temperature history of the milk droplets.

The reason that such models [7,28,29,33] result unrealistic temperature histories is mainly because of assuming Biot number for heat transfer to be less than 0.1. Although the diameters of the droplets in such studies are small (1-2 mm), low values of crust thermal conductivities fail the validity of small Biot number assumption.

Recently, Farid [11] developed a more realistic model with the utilization of transient heat conduction equations for both wet core and dry crust regions. The model is actually based on the assumption that both internal conduction and external convection resistances control the drying rate. Mass transfer resistance of the crust region is neglected as well as the heating effect of water vapor diffusing through the pores of the crust, which can be neglected for the early stages of the falling rate period only. The results of the model are fitted to the measurements by varying the physical properties of both core and crust regions. Farid’s work has shown that the only physical parameter that effect drying rate significantly is the crust thermal conductivity, which implies that drying in the falling rate period is mainly controlled by the heat transfer resistance of the dry crust region. Further, the model assumes that, during the course of drying, temperature of the evaporation interface is kept at the wet-bulb temperature of drying air. Such an assumption is unrealistic since the concentration of water vapor at the interface is higher than the bulk concentration, which directly implies that the temperature of the interface, as long as equilibrium conditions prevail, should be higher than the wet-bulb temperature of air.

It is observed that, generally, previous studies on drying of single droplets have restrictive assumptions that significantly effect drying rate calculations. Some of them [5,28,33] are concentrated mainly on the mass transfer mechanisms by ignoring heat transfer resistances, while some other [7,11] take into account only the heat transfer resistances for drying rate calculations. However, in this study, it is objected to develop a physical model with the aid of receding evaporation front approach that takes into account both heat and mass transfer resistances, which predominantly control the drying rate.

CHAPTER 3

MODELING

The drying model developed in this study is based on a receding evaporation front approach, which is utilized in many droplet drying studies [7,11,18,19,22]. This approach assumes that there exists a front that liquid water evaporates from, thus droplet loses moisture as the front moves. It is also assumed that drying is carried out in constant and falling rate periods. The governing heat and mass transfer equations, which consider all the heat transfer resistances and the mass transfer resistance of the dry crust region, are derived for both periods of drying.

3.1 Modeling in Constant Rate Period

In constant rate period, heat is transferred convectively from surrounding air to the surface of the droplet and causes the evaporation of free water until it is depleted totally (Figure 3.1). Water vapor is removed by convection from the surface. The following assumptions are made in obtaining the governing differential equations:

1. Droplet is in spherical shape.
2. Conduction is the mechanism of heat transfer within the droplet.
3. Inner radius of the droplet is constant.

4. Depletion of free water at the surface is described by the receding of the outer radius of the droplet.
5. Constant drying conditions prevail in which humidity, temperature and the velocity of air surrounding the droplet are constant.

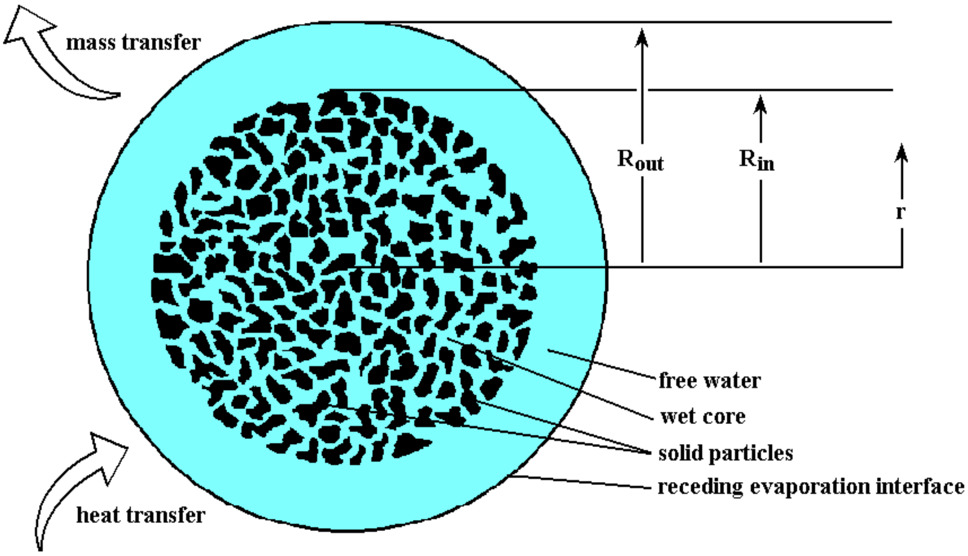

Figure 3.1 Droplet drying in constant rate period

6. Internal circulation of water and capillary effects are negligible.
7. There is no physical or chemical interaction between solids and water.
8. Air-water vapor mixture obeys the ideal gas law.
9. Temperature varies only in radial direction.
10. Physical and transport properties are constant with respect to position and time.
11. Evaporation occurs instantly so that a thermal and concentration equilibrium condition is established on the evaporation interface.
12. Solid particles and liquid water surrounding them are in thermal equilibrium.

13. Physical properties of liquid water and solid are calculated at an average temperature defined as the arithmetic average of initial droplet temperature and air temperature.

Taking a differential volume element in wet core region and carrying out heat balances, the following transfer equation is obtained as

For *0 < r <R_{in} , t > 0*

$$\frac{\partial}{\partial t}\left[\varepsilon\rho_w Cp_w T_{co} + (1-\varepsilon)\rho_s Cp_s T_{co}\right] = -\frac{1}{r^2}\frac{\partial}{\partial r}\left(r^2 q_{co}\right) \tag{3.1.1}$$

where ε in Equation 3.1.1 is the volume fraction of water in the wet core region. Similarly, subscripts *w*, *s* and *co* represent liquid water, solid and wet core region, respectively. Using Fourrier's law of conduction Equation 3.1.1 takes the form as

$$\frac{\partial}{\partial t}\left[\varepsilon\rho_w Cp_w T_{co} + (1-\varepsilon)\rho_s Cp_s T_{co}\right] = \frac{1}{r^2}\frac{\partial}{\partial r}\left(r^2 k_{co}\frac{\partial T_{co}}{\partial r}\right) \tag{3.1.2}$$

where k_{co} is the effective diffusion coefficient defined as

$$k_{co} = \varepsilon k_w + (1-\varepsilon)k_s\,. \tag{3.1.3}$$

Equation 3.1.2 takes the final form by a slight modification as

$$\alpha_1\frac{\partial T_{co}}{\partial t} = \frac{\partial^2 T_{co}}{\partial r^2} + \frac{2}{r}\frac{\partial T_{co}}{\partial r} \tag{3.1.4}$$

where

$$\alpha_1 = \frac{\varepsilon\rho_w Cp_w + (1-\varepsilon)\rho_s Cp_s}{k_{co}}\,. \tag{3.1.5}$$

In order to solve Equation 3.1.4 an initial condition and two boundary conditions at the center and at the inner radius of the droplet are required, which are given by Equations 3.1.6-8 as

For $0 \leq r \leq R_{in}$, $t = 0$

$$T_{co} = T_{init} . \tag{3.1.6}$$

For $r = 0$, $t > 0$

$$-k_{co} \frac{\partial T_{co}}{\partial r} = 0 . \tag{3.1.7}$$

For $r = R_{in}$, $t > 0$

$$T_{co} = T_{w} \tag{3.1.8}$$

where T_{init} is the initial droplet temperature.

Taking a differential volume element in free water region and carrying out heat balances, heat transfer equation for free water region can be obtained as

For $R_{in} < r < R_{out}(t)$, $t > 0$

$$\frac{\partial}{\partial t}\left[\rho_{w} Cp_{w} T_{w}\right] = -\frac{1}{r^{2}} \frac{\partial}{\partial r}\left(r^{2} q_{w}\right) \tag{3.1.9}$$

where

$$q_{w} = -k_{w} \frac{\partial T_{w}}{\partial r} . \tag{3.1.10}$$

Using Equations 3.1.9&10 the final form of the heat transfer equation for free water region is obtained as

$$\alpha_{2} \frac{\partial T_{w}}{\partial t} = \frac{\partial^{2} T_{w}}{\partial r^{2}} + \frac{2}{r} \frac{\partial T_{w}}{\partial r} \tag{3.1.11}$$

where

$$\alpha_{2} = \frac{\rho_{w} Cp_{w}}{k_{w}} . \tag{3.1.12}$$

Initial condition and two boundary conditions required for Equation 3.1.12 are

For $R_{in} \leq r \leq R_{out}(t)$, $t = 0$

$$T_w = T_{init} . \tag{3.1.13}$$

For $r = R_{in}$, $t > 0$

$$-k_{co} \frac{\partial T_{co}}{\partial r} = -k_w \frac{\partial T_w}{\partial r} . \tag{3.1.14}$$

For $r = R_{out}(t)$, $t > 0$

$$\lambda_w \rho_w \frac{dR_{out}}{dt} = k_h \left(T_w - T_{gas} \right) + k_w \frac{\partial T_w}{\partial r} \tag{3.1.15}$$

where λ_w is the latent heat of evaporation of water and k_h is the convective heat transfer coefficient. T_{gas} is the temperature of drying air. Equation 3.1.15 is actually obtained by carrying out a heat balance at the evaporation interface $R_{out}(t)$, in that the difference between the heat transferred convectively to the surface of the droplet and the heat conducted to the interior of the droplet is utilized to evaporate some portion of the free water. Further modification of Equation 3.1.15 yields

$$\lambda_w \frac{dR_{out}}{dt} = \alpha_3 \left(T_w - T_{gas} \right) + \alpha_4 \frac{\partial T_w}{\partial r} \tag{3.1.16}$$

where

$$\alpha_3 = \frac{k_h}{\rho_w} \tag{3.1.17}$$

and

$$\alpha_4 = \frac{k_w}{\rho_w} . \tag{3.1.18}$$

In order to track the motion of the interface between free water and air, a simple mass balance at $R_{out}(t)$ is carried out, in which the change of mass of the droplet is equal to the convective mass flux of water vapor from the evaporation interface, which yields

For $r = R_{out}(t)$, $t > 0$

$$\rho_w \frac{dR_{out}}{dt} = -k_m Mw\left(C_{wv} - C_{gas}\right) \tag{3.1.19}$$

where k_m is the convective mass transfer coefficient and Mw is the molecular weight of water. C_{wv} and C_{gas} are the concentrations of water vapor at the surface of the droplet and in air, respectively. C_{wv} in Equation 3.1.19 is defined as

$$C_{wv} = \frac{P^{vap}\left(T_s\right)}{R_{gas}T_s} \tag{3.1.20}$$

where P^{vap} is the vapor pressure evaluated at surface temperature. R_{gas} in Equation 3.1.19 is the universal gas constant. Further modification of Equation 3.1.19 yields

$$\frac{dR_{out}}{dt} = -\alpha_5\left(C_{wv} - C_{gas}\right) \tag{3.1.21}$$

where

$$\alpha_5 = \frac{k_m Mw}{\rho_w}. \tag{3.1.22}$$

In order to solve Equation 3.1.21, an initial condition is also required as

For $r = R_{out}(t)$, $t = 0$

$$R_{out}(t) = R_{init} \tag{3.1.23}$$

where R_{init} is the initial value of the outer radius.

For the ease of the numerical calculations, a dimensionless distance is defined as

$$\xi = \frac{r}{R_{init}} \tag{3.1.24}$$

and the Equations 3.1.4-23 are modified accordingly. The resulting set of differential equations then forms the drying model in the constant rate period, which are given as

For $0 < \xi < \xi_{in}$, $t > 0$

$$\alpha'_1 \frac{\partial T_{co}}{\partial t} = \frac{\partial^2 T_{co}}{\partial \xi^2} + \frac{2}{\xi}\frac{\partial T_{co}}{\partial \xi} \tag{3.1.25}$$

where

$$\alpha'_1 = \frac{R^2_{init}\left(\varepsilon \rho_w C p_w + (1-\varepsilon)\rho_s C p_s\right)}{k_{co}}. \tag{3.1.26}$$

Initial and boundary conditions of Equation 3.1.25 are

For $0 \le \xi \le \xi_{in}$, $t = 0$

$$T_{co} = T_{init}. \tag{3.1.27}$$

For $\xi = 0$, $t > 0$

$$-k_{co}\frac{\partial T_{co}}{\partial \xi} = 0. \tag{3.1.28}$$

For $\xi = \xi_{in}$, $t > 0$

$$T_{co} = T_w. \tag{3.1.29}$$

For $\xi_{in} < \xi < \xi_{out}(t)$, $t > 0$

$$\alpha'_2 \frac{\partial T_w}{\partial t} = \frac{\partial^2 T_w}{\partial \xi^2} + \frac{2}{\xi}\frac{\partial T_w}{\partial \xi} \tag{3.1.30}$$

where

$$\alpha'_2 = \frac{R^2_{init}\rho_w C p_w}{k_w}. \tag{3.1.31}$$

Initial and boundary conditions of Equation 3.1.30 are

For $\xi_{in} \leq \xi \leq \xi_{out}(t)$, $t = 0$

$$T_w = T_{init}. \tag{3.1.32}$$

For $\xi = \xi_{in}$, $t > 0$

$$-k_{co}\frac{\partial T_{co}}{\partial \xi} = -k_w \frac{\partial T_w}{\partial \xi}. \tag{3.1.33}$$

For $\xi = \xi_{out}(t)$, $t > 0$

$$\lambda_w \frac{d\xi_{out}}{dt} = \alpha'_3\left(T_w - T_{gas}\right) + \alpha'_4 \frac{\partial T_w}{\partial \xi} \tag{3.1.34}$$

where

$$\alpha'_3 = \frac{k_h}{R_{init}\rho_w} \tag{3.1.35}$$

and

$$\alpha'_4 = \frac{k_w}{R^2_{init}\rho_w}. \tag{3.1.36}$$

For $\xi = \xi_{out}(t)$, $t > 0$

$$\frac{d\xi_{out}}{dt} = -\alpha'_5\left(C_{wv} - C_{gas}\right) \tag{3.1.37}$$

where

$$\alpha'_5 = \frac{k_m Mw}{R_{init}\rho_w}. \tag{3.1.38}$$

Initial condition of Equation 3.1.37 is

For $\xi = \xi_{out}(t)$, $t = 0$

$$\xi_{out}\left(t\right) = 1. \tag{3.1.39}$$

In order to calculate the convective heat and mass transfer coefficients, an empirical correlation, which is a slight modification of Ranz and Marshall [26] correlation with a coefficient of 0.65, is used as

$$Nu = 2 + 0.65 Re^{0.5} Pr^{0.33} \tag{3.1.40}$$

$$Sh = 2 + 0.65 Re^{0.5} Sc^{0.33} \tag{3.1.41}$$

where

$$Re = \frac{D_p V_a \rho_a}{\mu_a}. \tag{3.1.42}$$

$$Pr = \frac{Cp_a}{\mu_a k_a}. \tag{3.1.43}$$

$$Sc = \frac{\mu_a}{\rho_a D_{wv}}. \tag{3.1.44}$$

$$Sh = \frac{k_m D_p}{D_{wv}}. \tag{3.1.45}$$

$$Nu = \frac{k_h D_p}{k_a}. \tag{3.1.46}$$

In Equations 3.1.42-46, subscripts *a*, *p* and *wv* represents air, particle and water vapor, respectively. Similarly, V_a, k_a, μ_a, Cp_a and ρ_a are the velocity, thermal conductivity, viscosity, heat capacity and density of the air, respectively. D_p is the outer diameter of the droplet and D_{wv} is the diffusivity of water vapor in air. The properties of air, water vapor and air-water vapor mixture used by the model are documented in Appendix-A. The properties used to estimate the convective heat and mass transfer coefficients are calculated at an average temperature defined as the arithmetic average of the surface temperature of the droplet and the air temperature.

3.2 Modeling in Falling Rate Period

Constant rate period of drying ends when all of the free water at the surface of the droplet is depleted, in which R_{out} approaches R_{in} (Figure 3.1). Actually, there is a transition period between constant and falling rate periods of drying, in which the surface of the droplet is partially wet, having some dry spots commencing at the points of maximum mass transfer. The transition period ends when the surface of the droplet is totally dry. Since variations of both temperature and concentration are only considered in radial direction, such transition period is not taken into account by the developed model.

In the falling rate period, a receding evaporation front is assumed to exist which separates the droplet into wet core and dry crust regions. As water is evaporated interface recedes into the center of the droplet, which is shown in Figure 3.2. The following assumptions are also made in obtaining the governing differential equations:

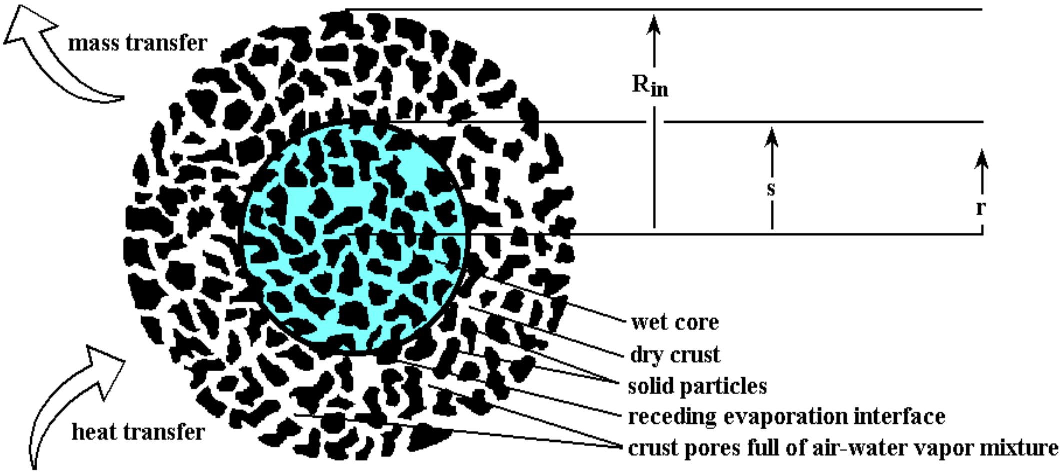

Figure 3.2 Droplet drying in falling rate period

1. Droplet is in spherical shape.
2. Conduction is the mechanism of heat transfer within the droplet.
3. Heat is transferred convectively to the surface of the droplet.
4. Depletion of the liquid water in the pores of the droplet is described by the receding of the radius of the wet core region.
5. Radius of the droplet, R_{in}, does not change during drying.
6. Constant drying conditions prevail in which humidity, temperature and the velocity of the air surrounding the droplet remain constant.
7. Internal circulation of water and capillary effects are negligible in the wet core region.
8. Dissolution of solids in water is neglected.
9. Air-water vapor mixture obeys the ideal gas law.
10. Pores of the dry crust region are filled by air, which is stagnant, and water vapor diffuses through these pores.
11. Temperature and water vapor concentration vary only in radial direction.
12. Physical and transport properties are constant with respect to both position and time.
13. Evaporation occurs instantly so that a thermal and concentration equilibrium condition is established on the evaporation interface.
14. Physical properties of liquid water and solid are calculated at an average temperature defined as the arithmetic average of initial droplet temperature and air temperature.
15. Physical and transport properties of water vapor is calculated at an average temperature defined as the arithmetic average of surface temperature of the wet core region and the surface temperature of the droplet.
16. Fick's law of diffusion with an effective diffusion coefficient describes diffusion of water vapor through the pores of the dry crust.

17. Solid particles and the surrounding media are in thermal equilibrium.

18. The morphology of the droplet does not change during drying.

Taking a differential volume element and carrying out heat balances, the following transfer equation for the wet core region is obtained as

For $0 < r < s(t)\, ,\, t > 0$

$$\frac{\partial}{\partial t}\left[\varepsilon \rho_w C p_w T_{co} + (1-\varepsilon)\rho_s C p_s T_{co}\right] = -\frac{1}{r^2}\frac{\partial}{\partial r}\left(r^2 q_{co}\right) \tag{3.2.1}$$

where same subscript notation utilized for the constant rate period modeling is also used for the model equations derived for the falling rate period. Similar to the derivation of Equation 3.1.4, a slight modification of Equation 3.2.1 yields the final form of the heat transfer equation for the wet core region as

$$\beta_1 \frac{\partial T_{co}}{\partial t} = \frac{\partial^2 T_{co}}{\partial r^2} + \frac{2}{r}\frac{\partial T_{co}}{\partial r} \tag{3.2.2}$$

where

$$\beta_1 = \frac{\varepsilon \rho_w C p_w + (1-\varepsilon)\rho_s C p_s}{k_{co}} \tag{3.2.3}$$

and k_{co} is the effective diffusion coefficient defined as

$$k_{co} = \varepsilon k_w + (1-\varepsilon) k_s\, . \tag{3.2.4}$$

Initial and boundary conditions required for the solution of Equation 3.2.2 are

For $0 \le r \le s(t)\, ,\, t = 0$

$$T_{co} = T_{f,init}\, . \tag{3.2.5}$$

For $r = 0\, ,\, t > 0$

$$-k_{co}\frac{\partial T_{co}}{\partial r} = 0\, . \tag{3.2.6}$$

For $r = s(t)$, $t > 0$

$$T_{co} = T_{cr} \tag{3.2.7}$$

where subscript *cr* represents the crust region and $T_{f,init}$ is the droplet temperature calculated at the end of constant rate period.

In order to derive the crust heat transfer equation heat balances are carried out on a differential volume element taken in the dry crust region to yield

For $s(t) < r < R_{in}$, $t > 0$

$$\frac{\partial}{\partial t}\left[(1-\varepsilon)\rho_s C p_s T_{cr}\right] = -\frac{1}{r^2}\frac{\partial}{\partial r}\left(r^2 q_{cr}\right) - \frac{1}{r^2}\frac{\partial}{\partial r}\left(r^2 T_{cr} C p_{wv} j_{cr}\right) \tag{3.2.8}$$

where

$$q_{cr} = -k_{cr}\frac{\partial T_{cr}}{\partial r} \tag{3.2.9}$$

and

$$j_{cr} = -D_{cr} M w \frac{\partial C_{wv}}{\partial r}. \tag{3.2.10}$$

Left hand side of Equation 3.2.8 does not include the time rate of change of heat of water vapor in the pores, which is considered much less than that of solid particles. C_{wv} in Equation 3.2.10 represents the concentration of water vapor in the pores of the dry crust. D_{cr} [23] and k_{cr} in Equations 3.2.9&10 are the effective diffusion coefficients given as

$$D_{cr} = \frac{2\varepsilon D_{wv}}{3-\varepsilon} \tag{3.2.11}$$

$$k_{cr} = \varepsilon k_m + (1-\varepsilon) k_s \tag{3.2.12}$$

where k_m is the thermal conductivity of air-water vapor mixture existing in the pores of the dry crust. Further modification of Equation 3.2.8 yields

$$\beta_2 \frac{\partial T_{cr}}{\partial t} = \frac{1}{r^2}\frac{\partial}{\partial r}\left(r^2 \frac{\partial T_{cr}}{\partial r}\right) + \frac{\beta_3}{r^2}\frac{\partial}{\partial r}\left(r^2 T_{cr} \frac{\partial C_{wv}}{\partial r}\right) \tag{3.2.13}$$

where

$$\beta_2 = \frac{(1-\varepsilon)\rho_s Cp_s}{k_{cr}} \tag{3.2.14}$$

and

$$\beta_3 = \frac{D_{cr} Mw Cp_{wv}}{k_{cr}}. \tag{3.2.15}$$

Collecting similar terms in Equation 3.2.13 yields final form of crust heat transfer equation as

$$\beta_2 \frac{\partial T_{cr}}{\partial t} = \frac{\partial^2 T_{cr}}{\partial r^2} + \left(\frac{2}{r} + \beta_3 \frac{\partial C_{wv}}{\partial r}\right)\frac{\partial T_{cr}}{\partial r} + \left(\frac{2\beta_3}{r}\frac{\partial C_{wv}}{\partial r} + \beta_3 \frac{\partial^2 C_{wv}}{\partial r^2}\right) T_{cr}. \tag{3.2.16}$$

Initial and boundary conditions of Equation 3.2.16 are

For $s(t) \le r \le R_{in}$, $t = 0$

$$T_{cr} = T_{f,init}. \tag{3.2.17}$$

For $r = s(t)$, $t > 0$

$$\varepsilon \rho_w \lambda_w \frac{ds}{dt} = -k_{cr} \frac{\partial T_{cr}}{\partial r} + k_{co} \frac{\partial T_{co}}{\partial r}. \tag{3.2.18}$$

For $r = R_{in}$, $t > 0$

$$-k_{cr} \frac{\partial T_{cr}}{\partial r} = k_h \left(T_{cr} - T_{gas}\right). \tag{3.2.19}$$

Equation 3.2.18 is actually obtained by carrying out a heat balance at the evaporation interface, in which the difference between the heat transferred from the crust to interface and the heat transferred to core from the interface is used to evaporate some portion of the liquid water existing in the pores of the wet core. Further simplification of Equation 3.2.18 yields

$$\lambda_w \frac{ds}{dt} = -\beta_4 \frac{\partial T_{cr}}{\partial r} + \beta_5 \frac{\partial T_{co}}{\partial r} \tag{3.2.20}$$

where

$$\beta_4 = \frac{k_{cr}}{\varepsilon \rho_w} \tag{3.2.21}$$

and

$$\beta_5 = \frac{k_{co}}{\varepsilon \rho_w}. \tag{3.2.22}$$

In order to solve Equation 3.2.16 and to obtain the concentration profile of water vapor in the pores of the crust, a mass balance is made by taking a differential volume element in the dry crust region yielding

For $s(t) < r < R_{in}$, $t > 0$

$$\frac{\partial}{\partial t}\left[\varepsilon M w C_{wv}\right] = -\frac{1}{r^2}\frac{\partial}{\partial r}\left(r^2 j_{cr}\right). \tag{3.2.23}$$

Further modification of Equation 3.2.23 gives

$$\beta_6 \frac{\partial C_{wv}}{\partial t} = \frac{\partial^2 C_{wv}}{\partial r^2} + \frac{2}{r}\frac{\partial C_{wv}}{\partial r} \tag{3.2.24}$$

where

$$\beta_6 = \frac{\varepsilon}{D_{cr}}. \tag{3.2.25}$$

Initial and boundary conditions required for the solution of Equation 3.2.24 are

For $s(t) \leq r \leq R_{in}$, $t = 0$

$$C_{wv} = \frac{P^{vap}\left(T_{f,init}\right)}{R_{gas} T_{f,init}}. \tag{3.2.26}$$

For *r = s(t) , t > 0*

$$C_{wv} = \frac{P^{vap}\left(T_{cr}\right)}{R_{gas}T_{cr}}. \tag{3.2.27}$$

For *r = R_{in} , t > 0*

$$-D_{cr}\frac{\partial C_{wv}}{\partial r} = k_m\left(C_{wv} - C_{gas}\right). \tag{3.2.28}$$

A mass balance at the evaporation interface yields the equation that is used to track the motion of the interface as

For *r = s(t) , t > 0*

$$\varepsilon\rho_w\frac{ds}{dt} = D_{cr}Mw\frac{\partial C_{wv}}{\partial r}. \tag{3.2.29}$$

Further modification of Equation 3.2.29 gives

$$\frac{ds}{dt} = \beta_7\frac{\partial C_{wv}}{\partial r} \tag{3.2.30}$$

where

$$\beta_7 = \frac{D_{cr}Mw}{\varepsilon\rho_w}. \tag{3.2.31}$$

Initial condition required for the solution of Equation 3.2.31 is

For *r = s(t) , t = 0*

$$s\left(t\right) = R_{in}. \tag{3.2.32}$$

For the ease of the numerical calculations, a dimensionless distance is defined as

$$\zeta = \frac{r}{R_{in}} \tag{3.2.33}$$

and the Equations 3.2.2-32 are modified accordingly to give the final form of the model equations as

For *$0 < \zeta < s'(t)$, $t > 0$*

$$\beta'_1 \frac{\partial T_{co}}{\partial t} = \frac{\partial^2 T_{co}}{\partial \zeta^2} + \frac{2}{\zeta}\frac{\partial T_{co}}{\partial \zeta} \tag{3.2.34}$$

where *$s'(t)$* is the dimensionless wet core radius and *β'_1* is

$$\beta'_1 = \frac{R^2_{in}\left(\varepsilon \rho_w C p_w + (1-\varepsilon)\rho_s C p_s\right)}{k_{co}}. \tag{3.2.35}$$

Initial and boundary conditions of Equation 3.2.34 are

For *$0 \le \zeta \le s'(t)$, $t = 0$*

$$T_{co} = T_{f,init}. \tag{3.2.36}$$

For *$\zeta = 0$, $t > 0$*

$$-k_{co}\frac{\partial T_{co}}{\partial \zeta} = 0. \tag{3.2.37}$$

For *$\zeta = s'(t)$, $t > 0$*

$$T_{co} = T_{cr}. \tag{3.2.38}$$

For *$s'(t) < \zeta < 1$, $t > 0$*

$$\beta'_2 \frac{\partial T_{cr}}{\partial t} = \frac{\partial^2 T_{cr}}{\partial \zeta^2} + \left(\frac{2}{\zeta} + \beta'_3 \frac{\partial C_{wv}}{\partial \zeta}\right)\frac{\partial T_{cr}}{\partial \zeta} + \left(\frac{2\beta'_3}{\zeta}\frac{\partial C_{wv}}{\partial \zeta} + \beta'_3 \frac{\partial^2 C_{wv}}{\partial \zeta^2}\right) T_{cr} \tag{3.2.39}$$

where

$$\beta'_2 = \frac{R^2_{in}\left((1-\varepsilon)\rho_s C p_s\right)}{k_{cr}} \tag{3.2.40}$$

and

$$\beta'_3 = \frac{D_{cr} Mw Cp_{wv}}{k_{cr}}. \tag{3.2.41}$$

Initial and boundary conditions of Equation 3.2.39 are

For *s'(t) ≤ ζ ≤ 1 , t = 0*

$$T_{cr} = T_{f,init}. \tag{3.2.42}$$

For *ζ = s'(t) , t > 0*

$$\lambda_w \frac{ds'}{dt} = -\beta'_4 \frac{\partial T_{cr}}{\partial \zeta} + \beta'_5 \frac{\partial T_{co}}{\partial \zeta}. \tag{3.2.43}$$

For *ζ = 1 , t > 0*

$$-k_{cr} \frac{\partial T_{cr}}{\partial \zeta} = R_{in} k_h \left(T_{cr} - T_{gas} \right) \tag{3.2.44}$$

where

$$\beta'_4 = \frac{k_{cr}}{R^2_{in} \varepsilon \rho_w} \tag{3.2.45}$$

and

$$\beta'_5 = \frac{k_{co}}{R^2_{in} \varepsilon \rho_w}. \tag{3.2.46}$$

For *s'(t) < ζ < 1 , t > 0*

$$\beta'_6 \frac{\partial C_{wv}}{\partial t} = \frac{\partial^2 C_{wv}}{\partial \zeta^2} + \frac{2}{\zeta} \frac{\partial C_{wv}}{\partial \zeta} \tag{3.2.47}$$

where

$$\beta'_6 = \frac{R^2_{in} \varepsilon}{D_{cr}}. \tag{3.2.48}$$

Initial and boundary conditions of Equation 3.2.47 are

For *s'(t) ≤ ζ ≤ 1 , t = 0*

$$C_{wv} = \frac{P^{vap}\left(T_{f,init}\right)}{R_{gas}T_{f,init}}. \tag{3.2.49}$$

For *ζ = s'(t) , t > 0*

$$C_{wv} = \frac{P^{vap}\left(T_{cr}\right)}{R_{gas}T_{cr}}. \tag{3.2.50}$$

For *ζ = 1 , t > 0*

$$-D_{cr}\frac{\partial C_{wv}}{\partial \zeta} = R_{in}k_m\left(C_{wv} - C_{gas}\right). \tag{3.2.51}$$

For *ζ = s'(t) , t > 0*

$$\frac{ds'}{dt} = \beta'_7\frac{\partial C_{wv}}{\partial \zeta} \tag{3.2.52}$$

where

$$\beta'_7 = \frac{D_{cr}Mw}{R^2_{in}\varepsilon\rho_w}. \tag{3.2.53}$$

Initial condition of Equation 3.2.52 is

For *ζ = s'(t) , t = 0*

$$s'(t) = 1. \tag{3.2.54}$$

Same correlations given by Equations 3.1.40&41 are used to calculate the convective heat and mass transfer coefficients in the falling rate period.

CHAPTER 4

NUMERICAL CALCULATIONS

Solution of the drying model equations developed requires numerical techniques with the application of moving boundary analysis. Depending on the nature of the model equations, two different numerical solution methods are utilized, namely the Variable Grid Network (VGN) method for constant rate period and the Variable Time Step (VTS) method for the falling rate period. Actually, VGN and VTS methods are obtained by making slight modifications to the front tracking methods developed for the solution of free and moving boundary problems [9].

Second order finite difference equations with the utilization of a fully implicit numerical scheme are used for the discretization of the differential equations. A fully implicit numerical scheme is chosen since it has the advantage of not requiring any stability criterion. First order spatial derivatives are discretized using forward, backward or central difference schemes (Equations 4.1-3) where appropriate, and second order spatial derivatives are discretized using central difference scheme (Equation 4.4).

$$\frac{\partial \varphi}{\partial r} = \frac{\varphi_{i+1} - \varphi_i}{(\Delta r)}. \tag{4.1}$$

$$\frac{\partial \varphi}{\partial r} = \frac{\varphi_i - \varphi_{i-1}}{(\Delta r)} . \tag{4.2}$$

$$\frac{\partial \varphi}{\partial r} = \frac{\varphi_{i+1} - \varphi_{i-1}}{2(\Delta r)} . \tag{4.3}$$

$$\frac{\partial^2 \varphi}{\partial r^2} = \frac{\varphi_{i+1} - 2\varphi_i + \varphi_{i-1}}{(\Delta r)^2} . \tag{4.4}$$

φ in Equations 4.1-4 represents any dependent variable and r represents independent variable. Also, subscript i represents the grid level. The fully implicit scheme requires the discretization of time derivatives as

$$\frac{\partial \varphi}{\partial t} = \frac{\varphi_i^{t+\Delta t} - \varphi_i^{t}}{\Delta t} . \tag{4.5}$$

Discretization of each of the differential equations utilized in the drying model with the aid of the second order difference schemes generates a set of algebraic equations, which is shown in matrix notation as

$$\begin{bmatrix} -A_1 & B_1 & 0 & 0 & 0 & 0 & 0 \\ C_2 & -A_2 & B_2 & 0 & 0 & 0 & 0 \\ 0 & \ddots & \ddots & \ddots & 0 & 0 & 0 \\ 0 & 0 & C_i & -A_i & B_i & 0 & 0 \\ 0 & 0 & 0 & \ddots & \ddots & \ddots & 0 \\ 0 & 0 & 0 & 0 & C_{N-1} & -A_{N-1} & B_{N-1} \\ 0 & 0 & 0 & 0 & 0 & C_N & -A_N \end{bmatrix} \begin{bmatrix} \varphi_1 \\ \varphi_2 \\ \vdots \\ \varphi_i \\ \vdots \\ \varphi_{N-1} \\ \varphi_N \end{bmatrix} = \begin{bmatrix} D_1 \\ D_2 \\ \vdots \\ D_i \\ \vdots \\ D_{N-1} \\ D_N \end{bmatrix} \tag{4.6}$$

where N in above notation is the total grid number. A_i, B_i and C_i are the coefficients of the unknowns φ_i, φ_{i+1} and φ_{i-1}, and D_i is the forcing term. The tridiagonal matrix solver utilized in both VGN and VTS algorithms requires the input of the coefficients A_i, B_i, C_i and the forcing term D_i in the following manner

$$A_i \varphi_i = B_i \varphi_{i+1} + C_i \varphi_{i-1} + D_i \tag{4.7}$$

thus the form of the Equation 4.7 is used when modifying the discretized form of the differential equations.

4.1 Numerical Calculations in Constant Rate Period

The model developed for the constant rate period of drying requires the simultaneous solution of heat transfer equations of wet core and free water regions with the aid of interface equation. Discretization of the governing differential equations is carried out according to the grid numbering shown in Figure 4.1.

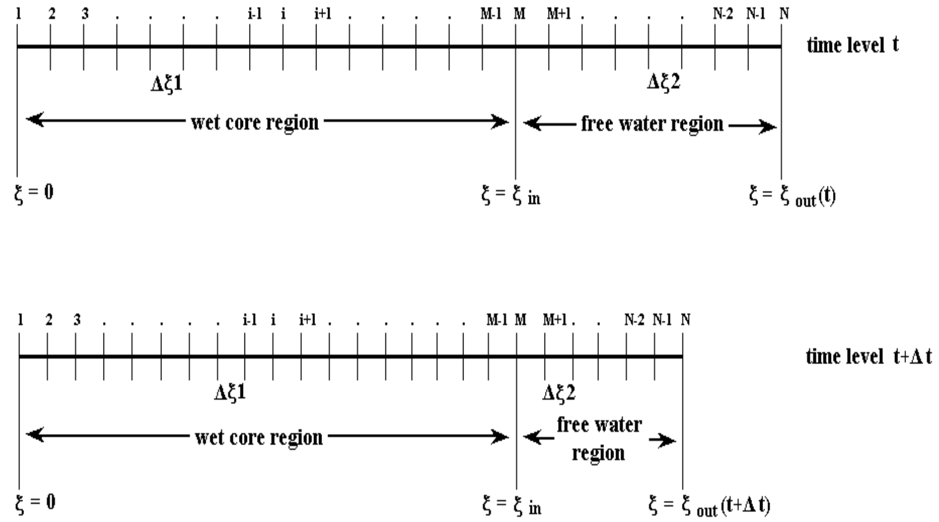

Figure 4.1 Grid distributions in constant rate period

Model equations derived in Chapter 3 for the constant rate period are

For $0 < \xi < \xi_{in}$, $t > 0$

$$\alpha'_1 \frac{\partial T_{co}}{\partial t} = \frac{\partial^2 T_{co}}{\partial \xi^2} + \frac{2}{\xi} \frac{\partial T_{co}}{\partial \xi} . \tag{4.1.1}$$

Initial and boundary conditions of Equation 4.1.1 are

For $0 \le \xi \le \xi_{in}$, $t = 0$

$$T_{co} = T_{init} . \tag{4.1.2}$$

For $\xi = 0$, $t > 0$

$$-k_{co}\frac{\partial T_{co}}{\partial \xi} = 0. \tag{4.1.3}$$

For $\xi = \xi_{in}$, $t > 0$

$$T_{co} = T_{w}. \tag{4.1.4}$$

For $\xi_{in} < \xi < \xi_{out}(t)$, $t > 0$

$$\alpha'_{2}\frac{\partial T_{w}}{\partial t} = \frac{\partial^{2} T_{w}}{\partial \xi^{2}} + \frac{2}{\xi}\frac{\partial T_{w}}{\partial \xi}. \tag{4.1.5}$$

Initial and boundary conditions of Equation 4.1.5 are

For $\xi_{in} \le \xi \le \xi_{out}(t)$, $t = 0$

$$T_{w} = T_{init}. \tag{4.1.6}$$

For $\xi = \xi_{in}$, $t > 0$

$$-k_{co}\frac{\partial T_{co}}{\partial \xi} = -k_{w}\frac{\partial T_{w}}{\partial \xi}. \tag{4.1.7}$$

For $\xi = \xi_{out}(t)$, $t > 0$

$$\lambda_{w}\frac{d\xi_{out}}{dt} = \alpha'_{3}\left(T_{w} - T_{gas}\right) + \alpha'_{4}\frac{\partial T_{w}}{\partial \xi}. \tag{4.1.8}$$

For $\xi = \xi_{out}(t)$, $t > 0$

$$\frac{d\xi_{out}}{dt} = -\alpha'_{5}\left(C_{wv} - C_{gas}\right). \tag{4.1.9}$$

Initial condition of Equation 4.1.9 is

For $\xi = \xi_{out}(t)$, $t = 0$

$$\xi_{out}\left(t\right) = 1. \tag{4.1.10}$$

In order to get the coefficients *C*, *A* and *B*, and the forcing term *D* at node *1*, Equation 4.1.3 is discretized using the forward difference scheme to yield

$$-k_{co}\frac{T_1-T_2}{\Delta\xi 1}=0\,. \tag{4.1.11}$$

Since temperature distribution is continuous throughout the droplet, subscripts *co* and *w* are dropped. *Δξ1* and *Δξ2* are the distances between two adjacent nodes in wet core and free water regions, respectively. Further modification of Equation 4.1.11 according to the form given by Equation 4.7 yields

$$\begin{aligned}C_1&=0\\A_1&=1\\B_1&=1\\D_1&=0\end{aligned}\,. \tag{4.1.12}$$

In order to obtain *C*, *A*, *B*, *D* at nodes *2* to *M-1*, Equation 4.1.1 is discretized yielding

For $2\le i\le M-1$

$$\alpha'_1\frac{T_i-T_i^*}{\Delta t}=\frac{T_{i+1}-2T_i+T_{i-1}}{(\Delta\xi 1)^2}+\frac{2}{\xi_i}\frac{T_{i+1}-T_{i-1}}{2(\Delta\xi 1)} \tag{4.1.13}$$

where *M* is the grid level which corresponds to the inner radius of the droplet. T_i^* is the temperature of the node *i* at time level *t*. Others are the temperatures at time level *t+Δt*. Further modification of Equation 4.1.13 yields

$$\begin{aligned}C_i&=\frac{(\Delta t)}{\alpha'_1(\Delta\xi 1)^2}-\frac{(\Delta t)}{\alpha'_1\,\xi_i\,(\Delta\xi 1)}\\A_i&=1+\frac{2(\Delta t)}{\alpha'_1(\Delta\xi 1)^2}\\B_i&=\frac{(\Delta t)}{\alpha'_1(\Delta\xi 1)^2}+\frac{(\Delta t)}{\alpha'_1\,\xi_i\,(\Delta\xi 1)}\\D_i&=T_i^*\end{aligned}\,. \tag{4.1.14}$$

In order to get *C*, *A*, *B*, *D* at node *M*, Equations 4.1.4&7 are used to give

$$-k_{co}\frac{T_M - T_{M-1}}{(\Delta\xi 1)} = -k_w \frac{T_{M+1} - T_M}{(\Delta\xi 2)}. \qquad (4.1.15)$$

Further simplification of Equation 4.1.15 yields

$$\begin{aligned} C_M &= \frac{k_{co}}{(\Delta\xi 1)} \\ A_M &= \frac{k_{co}}{(\Delta\xi 1)} + \frac{k_w}{(\Delta\xi 2)}. \\ B_M &= \frac{k_w}{(\Delta\xi 2)} \\ D_M &= 0 \end{aligned} \qquad (4.1.16)$$

In order to get *C*, *A*, *B*, *D* at nodes *M+1* to *N-1*, Equation 4.1.5 is discretized yielding

For $M+1 \le i \le N-1$

$$\alpha'_2 \frac{T_i - T_i^*}{\Delta t} = \frac{T_{i+1} - 2T_i + T_{i-1}}{(\Delta\xi 2)^2} + \frac{2}{\xi_i}\frac{T_{i+1} - T_{i-1}}{2(\Delta\xi 2)} \qquad (4.1.17)$$

where *N* is the final grid level. Further modification of Equation 4.1.17 yields

$$\begin{aligned} C_i &= \frac{(\Delta t)}{\alpha'_2(\Delta\xi 2)^2} - \frac{(\Delta t)}{\alpha'_2 \xi_i (\Delta\xi 2)} \\ A_i &= 1 + \frac{2(\Delta t)}{\alpha'_2(\Delta\xi 2)^2} \qquad . \\ B_i &= \frac{(\Delta t)}{\alpha'_2(\Delta\xi 2)^2} + \frac{(\Delta t)}{\alpha'_2 \xi_i (\Delta\xi 2)} \\ D_i &= T_i^* \end{aligned} \qquad (4.1.18)$$

In order to obtain *C*, *A*, *B* and *D* at node *N*, Equation 4.1.8 is used to give

$$\left(3.15\cdot 10^6 - 2.38\cdot 10^3 T_N\right)\frac{\xi_{out} - \xi_{out}^*}{\Delta t} = \alpha'_3\left(T_N - T_{gas}\right) + \alpha'_4 \frac{T_N - T_{N-1}}{(\Delta\xi 2)}. \qquad (4.1.19)$$

The term in parenthesis on the left of Equation 4.1.19 is the temperature dependent latent heat of evaporation of water, which is obtained from reference [8]. Although physical properties are assumed to be constant, temperature dependent latent heat expression is used in order to increase accuracy. ξ_{out}^* and ξ_{out} are the dimensionless outer radii of the droplet at time levels *t* and $t+\Delta t$, respectively. Further simplification of Equation 4.1.19 yields

$$\begin{aligned}
C_N &= -\frac{\alpha'_4}{(\Delta\xi 2)} \\
A_N &= -\frac{2.38\cdot 10^3\left(\xi_{out}-\xi_{out}^*\right)}{(\Delta t)} - \alpha'_3 - \frac{\alpha'_4}{(\Delta\xi 2)}. \\
B_N &= 0 \\
D_N &= -\frac{3.15\cdot 10^6\left(\xi_{out}-\xi_{out}^*\right)}{(\Delta t)} - \alpha'_3\, T_{gas}
\end{aligned} \tag{4.1.20}$$

Finally, Equation 4.1.9 is discretized to give

$$\frac{\xi_{out}-\xi_{out}^*}{\Delta t} = -\alpha'_5\left(C_{wv}-C_{gas}\right) \tag{4.1.21}$$

where C_{wv} in Equation 4.1.21 is calculated as

$$C_{wv} = \frac{P^{vap}(T_N)}{R_{gas}T_N} \tag{4.1.22}$$

where vapor pressure expression obtained from reference [8] is given as

$$P^{vap}(T) = \frac{\exp\left(20.21 - \frac{5104.05}{T}\right)}{760}. \tag{4.1.23}$$

VGN algorithm solves the set of the algebraic equations, whose coefficient matrix is given by Equation sets 4.1.12, 14, 16, 18 and 20, with the aid of interface equation (Equation 4.1.21) to yield temperature profile and outer radius of the droplet at different time levels. Further, when ξ_{out} is equal to ξ_{in}, constant rate period ends, which is used as the termination criterion. A schematic description of VGN algorithm is presented in Figure 4.2. A program file listing, which is written in FORTRAN language, utilizing VGN algorithm is documented in Appendix-B.

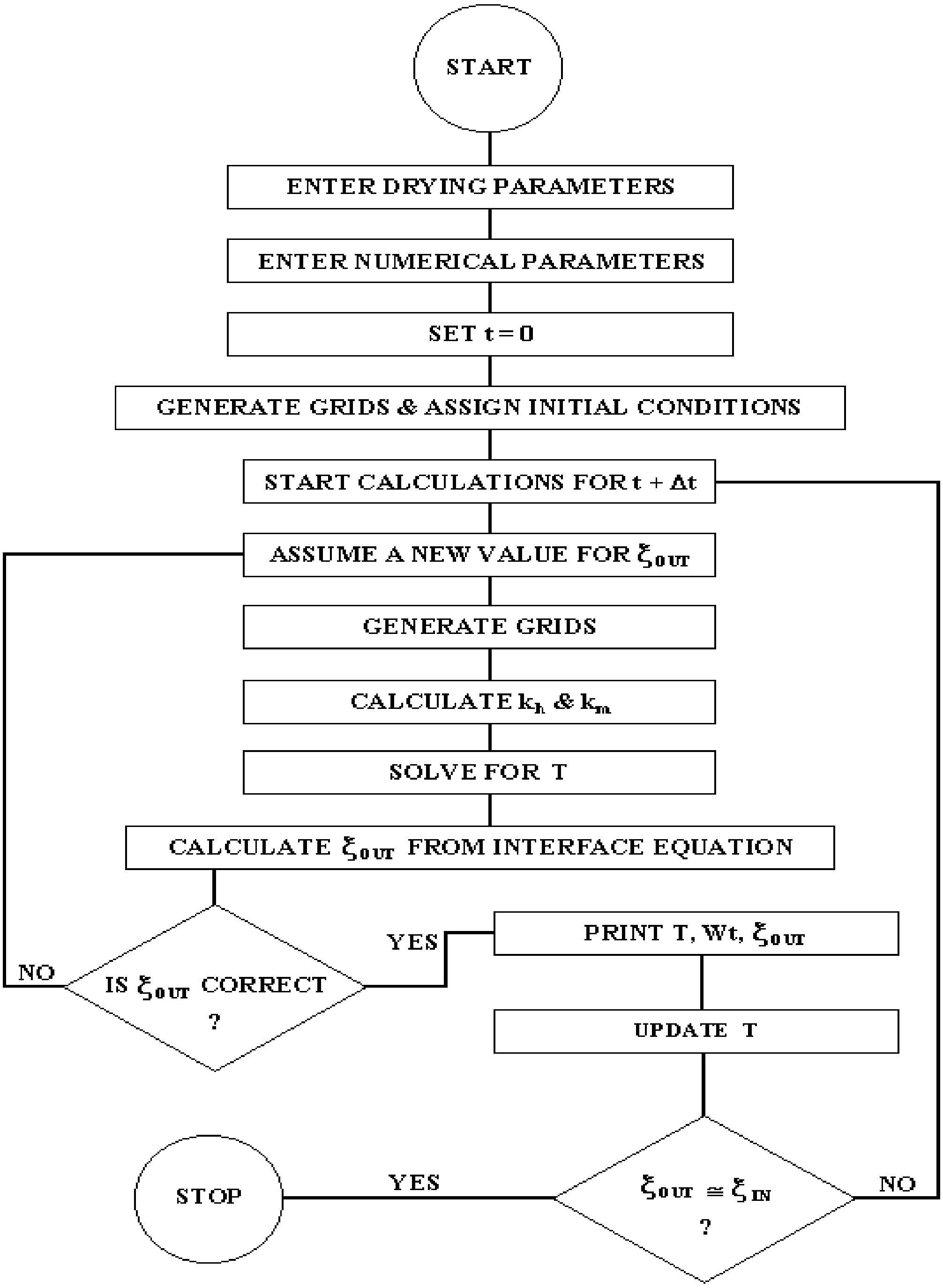

Figure 4.2 Schematic description of VGN algorithm

There exists an iteration loop in VGN algorithm (Figure 4.2) for the estimation of the interface position ξ_{out} using the known value of ξ^*_{out}. At each iteration level, ξ_{out} is estimated as

$$\xi_{out} = \xi^*_{out} - i(\delta\xi) \qquad i = 1, 2, 3 \ldots, I_{max} \tag{4.1.24}$$

where i and $(\delta\xi)$ in Equation 4.1.24 represent iteration level and incremental decrease, respectively. I_{max} is the maximum number of iteration. Having an initial estimate for ξ_{out}, temperature profile is obtained. Then using Equation 4.1.21 ξ_{out} is recalculated. Iterations are carried out until these two values converge to each other by less than a given tolerance. The convergence criterion is defined as

$$\frac{\left|\left(\xi_{out} - \xi^*_{out}\right)_C\right| - \left|\left(\xi_{out} - \xi^*_{out}\right)_E\right|}{\left|\left(\xi_{out} - \xi^*_{out}\right)_E\right|} \times 100 \leq \Phi_\xi \tag{4.1.25}$$

where subscripts C and E in Equation 4.1.25 represent calculated and estimated expressions, respectively. Φ_ξ is the percent tolerance. Similarly, the termination criterion of VGN algorithm is defined as

$$N - M = 2 \tag{4.1.26}$$

where N and M correspond to the grid levels (Figure 4.1) at ξ_{out} and ξ_{in}, respectively.

A simple mass balance expression yields the weight of the droplet as

$$Wt(t) = \frac{4}{3}\pi\left[\rho_w\left(R^3_{out}(t) - R^3_{in}\right) + \rho_w \varepsilon R^3_{in} + \rho_s(1-\varepsilon)R^3_{in}\right] \tag{4.1.27}$$

where

$$R_{out}(t) = R_{init}\xi_{out}(t). \tag{4.1.28}$$

Droplet average temperature is calculated as

$$T_{av} = \frac{3}{R^3_{out}(t)} \int_0^{R_{out}(t)} r^2 T(r)\,dr \tag{4.1.29}$$

where the integral in Equation 4.1.29 is evaluated using trapezoidal rule [13].

4.2 Numerical Calculations in Falling Rate Period

The model developed for the falling rate period of drying requires the simultaneous solution of the heat transfer equations of wet core and dry crust regions and mass transfer equation of the dry crust region with the aid of the interface equation. Discretization of the governing differential equations is carried out according to the grid numbering shown in Figure 4.3. Contrary to the utilization of moving grids in the constant rate period, a fixed grid network is used in the falling rate period.

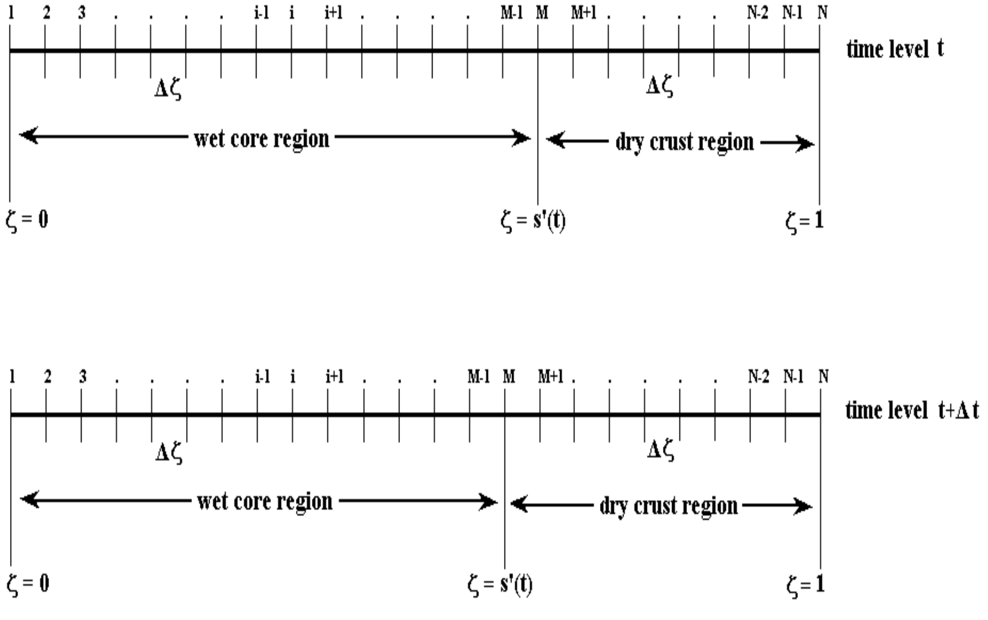

Figure 4.3 Grid distributions in falling rate period

Model equations for the falling rate period, which are derived in Chapter 3, are

For $0 < \zeta < s'(t)\,,\ t > 0$

$$\beta'_1 \frac{\partial T_{co}}{\partial t} = \frac{\partial^2 T_{co}}{\partial \zeta^2} + \frac{2}{\zeta}\frac{\partial T_{co}}{\partial \zeta}\,. \tag{4.2.1}$$

Initial and boundary conditions of Equation 4.2.1 are

For $0 \le \zeta \le s'(t)$, $t = 0$

$$T_{co} = T_{f,init} . \tag{4.2.2}$$

For $\zeta = 0$, $t > 0$

$$-k_{co} \frac{\partial T_{co}}{\partial \zeta} = 0 . \tag{4.2.3}$$

For $\zeta = s'(t)$, $t > 0$

$$T_{co} = T_{cr} . \tag{4.2.4}$$

For $s'(t) < \zeta < 1$, $t > 0$

$$\beta'_2 \frac{\partial T_{cr}}{\partial t} = \frac{\partial^2 T_{cr}}{\partial \zeta^2} + \left(\frac{2}{\zeta} + \beta'_3 \frac{\partial C_{wv}}{\partial \zeta} \right) \frac{\partial T_{cr}}{\partial \zeta} + \left(\frac{2\beta'_3}{\zeta} \frac{\partial C_{wv}}{\partial \zeta} + \beta'_3 \frac{\partial^2 C_{wv}}{\partial \zeta^2} \right) T_{cr} . \tag{4.2.5}$$

Initial and boundary conditions of Equation 4.2.5 are

For $s'(t) \le \zeta \le 1$, $t = 0$

$$T_{cr} = T_{f,init} . \tag{4.2.6}$$

For $\zeta = s'(t)$, $t > 0$

$$\lambda_w \frac{ds'}{dt} = -\beta'_4 \frac{\partial T_{cr}}{\partial \zeta} + \beta'_5 \frac{\partial T_{co}}{\partial \zeta} . \tag{4.2.7}$$

For $\zeta = 1$, $t > 0$

$$-k_{cr} \frac{\partial T_{cr}}{\partial \zeta} = R_{in} k_h \left(T_{cr} - T_{gas} \right) . \tag{4.2.8}$$

For $s'(t) < \zeta < 1$, $t > 0$

$$\beta'_6 \frac{\partial C_{wv}}{\partial t} = \frac{\partial^2 C_{wv}}{\partial \zeta^2} + \frac{2}{\zeta} \frac{\partial C_{wv}}{\partial \zeta} . \tag{4.2.9}$$

Initial and boundary conditions of Equation 4.2.9 are

For *s'(t) ≤ ζ ≤ 1 , t = 0*

$$C_{wv} = \frac{P^{vap}\left(T_{f,init}\right)}{R_{gas}T_{f,init}}. \tag{4.2.10}$$

For *ζ = s'(t) , t > 0*

$$C_{wv} = \frac{P^{vap}\left(T_{cr}\right)}{R_{gas}T_{cr}}. \tag{4.2.11}$$

For *ζ = 1 , t > 0*

$$-D_{cr}\frac{\partial C_{wv}}{\partial \zeta} = R_{in}k_m\left(C_{wv} - C_{gas}\right). \tag{4.2.12}$$

For *ζ = s'(t) , t > 0*

$$\frac{ds'}{dt} = \beta'_7\frac{\partial C_{wv}}{\partial \zeta}. \tag{4.2.13}$$

Initial condition of Equation 4.2.13 is

For *ζ = s'(t) , t = 0*

$$s'(t) = 1. \tag{4.2.14}$$

In order to get the coefficients *CT*, *AT* and *BT*, and the forcing term *DT* at node *1*, Equation 4.2.3 is discretized using the forward difference scheme yielding

$$-k_{co}\frac{T_1 - T_2}{\Delta\zeta} = 0 \tag{4.2.15}$$

where *CT*, *AT* and *BT*, and the forcing term *DT* refer to the coefficients of the algebraic equation system of temperature profile. Since temperature distribution is continuous throughout the droplet, subscripts *co* and *cr* are dropped. *Δζ* is the distance between two adjacent nodes. Further modification of Equation 4.2.15 yields

$$\begin{aligned} &CT_1 = 0 \\ &AT_1 = 1 \\ &BT_1 = 1 \\ &DT_1 = 0 \end{aligned} \quad . \tag{4.2.16}$$

In order to obtain *CT*, *AT*, *BT*, *DT* at nodes *2* to *M-1*, Equation 4.2.1 is discretized as

For $2 \leq i \leq M\text{-}1$

$$\beta'_1 \frac{T_i - T_i^*}{\Delta t} = \frac{T_{i+1} - 2T_i + T_{i-1}}{(\Delta\zeta)^2} + \frac{2}{\zeta_i}\frac{T_{i+1} - T_{i-1}}{2(\Delta\zeta)} \tag{4.2.17}$$

where node *M* corresponds to the interface position. T_i^* is the temperature of the node *i* at time level *t*. Others are the temperatures at time level $t+\Delta t$. Further modification of Equation 4.2.17 yields

$$\begin{aligned} &CT_i = \frac{(\Delta t)}{\beta'_1 (\Delta\zeta)^2} - \frac{(\Delta t)}{\beta'_1 \zeta_i (\Delta\zeta)} \\ &AT_i = 1 + \frac{2(\Delta t)}{\beta'_1 (\Delta\zeta)^2} \\ &BT_i = \frac{(\Delta t)}{\beta'_1 (\Delta\zeta)^2} + \frac{(\Delta t)}{\beta'_1 \zeta_i (\Delta\zeta)} \\ &DT_i = T_i^* \end{aligned} \quad . \tag{4.2.18}$$

For the ease of the numerical calculations concentration of water vapor in wet core region $0 \leq \zeta < s'(t)$ is assigned to zero by generating the appropriate coefficients *AC*, *BC*, *CC* and the forcing term *DC* as

For $1 \leq i \leq M\text{-}1$

$$\begin{aligned} &CC_i = 0 \\ &AC_i = 1 \\ &BC_i = 0 \\ &DC_i = 0 \end{aligned} \quad . \tag{4.2.19}$$

In order to get *CT*, *AT*, *BT* and *DT* at node *M*, Equations 4.2.4&7 are used to give

$$\left(3.15\cdot10^{6}-2.38\cdot10^{3}\,T_M\right)\frac{s'-s'^{*}}{\Delta t}=-\beta'_4\frac{T_{M+1}-T_M}{(\Delta\zeta)}+\beta'_5\frac{T_M-T_{M-1}}{(\Delta\zeta)} \tag{4.2.20}$$

where *s'* and *s'** represent the interface positions at time levels *t* and *t+Δt*, respectively. Further simplification of Equation 4.2.20 yields

$$\begin{aligned}
CT_M &= -\frac{\beta'_5}{(\Delta\zeta)}\\
AT_M &= -\frac{2.38\cdot10^{3}\left(s'-s'^{*}\right)}{(\Delta t)}-\frac{\beta'_4}{(\Delta\zeta)}-\frac{\beta'_5}{(\Delta\zeta)}\\
BT_M &= -\frac{\beta'_4}{(\Delta\zeta)}\\
DT_M &= -\frac{3.15\cdot10^{6}\left(s'-s'^{*}\right)}{(\Delta t)}
\end{aligned}\quad. \tag{4.2.21}$$

Coefficients *CC*, *AC*, *BC* and the forcing term *DC* required for the calculation of water vapor concentration at node *M*, Equation 4.2.11 is used, yielding

$$C'_M=\frac{P^{vap}\left(T_M\right)}{R_{gas}T_M} \tag{4.2.22}$$

where C'_M represents the concentration of water vapor at node *M*. Subscript *wv* is dropped when representing concentration in the discretized form of the equations. Further simplification of Equation 4.2.22 yields

$$\begin{aligned}
CC_M &= 0\\
AC_M &= 1\\
BC_M &= 0\\
DC_M &= \frac{P^{vap}\left(T_M\right)}{R_{gas}T_M}
\end{aligned}\quad. \tag{4.2.23}$$

Same vapor pressure expression given by Equation 4.1.23 is also used in Equation 4.2.22 to evaluate the concentration of water vapor.

To obtain *CT*, *AT*, *BT* and *DT* at nodes *M+1 to N-1*, Equation 4.2.5 is discretized as

For *M+1 ≤ i ≤N-1*

$$\beta'_2\frac{T_i-T_i^*}{\Delta t}=\frac{T_{i+1}-2T_i+T_{i-1}}{(\Delta\zeta)^2}+\left(\frac{2}{\zeta_i}+\beta'_3\frac{C'_{i+1}-C'_{i-1}}{2(\Delta\zeta)}\right)\frac{T_{i+1}-T_{i-1}}{2(\Delta\zeta)}$$
$$+\left(\frac{2\beta'_3}{\zeta_i}\frac{C'_{i+1}-C'_{i-1}}{2(\Delta\zeta)}+\beta'_3\frac{C'_{i+1}-2C'_i+C'_{i-1}}{(\Delta\zeta)^2}\right)T_i \qquad (4.2.24)$$

where *N* is the node number corresponding to *ζ = 1*. Equation 4.2.24 is simplified as

$$\begin{aligned}
CT_i &= \frac{(\Delta t)}{\beta'_2(\Delta\zeta)^2}-\frac{(\Delta t)}{2\beta'_2(\Delta\zeta)}\left(\frac{2}{\zeta_i}+\beta'_3\frac{C'_{i+1}-C'_{i-1}}{2(\Delta\zeta)}\right)\\
AT_i &= 1+\frac{2(\Delta t)}{\beta'_2(\Delta\zeta)^2}-\frac{(\Delta t)}{\beta'_2}\left(\frac{2\beta'_3}{\zeta_i}\frac{C'_{i+1}-C'_{i-1}}{2(\Delta\zeta)}+\beta'_3\frac{C'_{i+1}-2C'_i+C'_{i-1}}{(\Delta\zeta)^2}\right).\\
BT_i &= \frac{(\Delta t)}{\beta'_2(\Delta\zeta)^2}+\frac{(\Delta t)}{2\beta'_2(\Delta\zeta)}\left(\frac{2}{\zeta_i}+\beta'_3\frac{C'_{i+1}-C'_{i-1}}{2(\Delta\zeta)}\right)\\
DT_i &= T_i^*
\end{aligned} \qquad (4.2.25)$$

In order to get *CC*, *AC*, *BC* and *DC* at nodes *M+1* to *N-1*, Equation 4.2.9 is used as

For *M+1 ≤ i ≤N-1*

$$\beta'_6\frac{C'_i-C'^*_i}{\Delta t}=\frac{C'_{i+1}-2C'_i+C'_{i-1}}{(\Delta\zeta)^2}+\frac{2}{\zeta_i}\frac{C'_{i+1}-C'_{i-1}}{2(\Delta\zeta)}. \qquad (4.2.26)$$

Further simplification of Equation 4.2.26 yields

$$\begin{aligned}
CC_i &= \frac{(\Delta t)}{\beta'_6(\Delta\zeta)^2}-\frac{(\Delta t)}{\beta'_6\zeta_i(\Delta\zeta)}\\
AC_i &= 1+\frac{2(\Delta t)}{\beta'_6(\Delta\zeta)^2} \quad .\\
BC_i &= \frac{(\Delta t)}{\beta'_6(\Delta\zeta)^2}+\frac{(\Delta t)}{\beta'_6\zeta_i(\Delta\zeta)}\\
DC_i &= C'^*_i
\end{aligned} \qquad (4.2.27)$$

In order to obtain *CT*, *AT*, *BT* and *DT* at node *N*, Equation 4.2.8 is used to give

$$-k_{cr}\frac{T_N - T_{N-1}}{(\Delta\zeta)} = R_{in}k_h\left(T_N - T_{gas}\right). \tag{4.2.28}$$

Further simplification of Equation 4.2.28 yields

$$\begin{aligned} CT_N &= 1 \\ AT_N &= 1 + \frac{R_{in}k_h(\Delta\zeta)}{k_{cr}} \\ BT_N &= 0 \\ DT_N &= \frac{R_{in}k_h(\Delta\zeta)}{k_{cr}}T_{gas} \end{aligned} . \tag{4.2.29}$$

In order to obtain *CC*, *AC*, *BC* and *DC* at node *N*, Equation 4.2.12 is discretized as

$$-D_{cr}\frac{C'_N - C'_{N-1}}{(\Delta\zeta)} = R_{in}k_m\left(C'_N - C'_{gas}\right) \tag{4.2.30}$$

where C'_{gas} is the concentration of water vapor in air surrounding the droplet. Further modification of Equation 4.2.30 according to the form of Equation 4.7 yields

$$\begin{aligned} CC_N &= 1 \\ AC_N &= 1 + \frac{R_{in}k_m(\Delta\zeta)}{D_{cr}} \\ BC_N &= 0 \\ DC_N &= \frac{R_{in}k_m(\Delta\zeta)}{D_{cr}}C'_{gas} \end{aligned} . \tag{4.2.31}$$

Finally, Equation 4.2.13 is discretized to give

$$\frac{s' - s'^*}{\Delta t} = \beta'_7\frac{C'_{M+1} - C'_M}{(\Delta\zeta)} . \tag{4.2.32}$$

VTS algorithm solves the two sets of algebraic equations, whose coefficient matrix is given by Equation sets 4.2.16, 18, 21, 25 and 29 for temperature and Equation sets 4.2.19, 23, 27 and 31 for concentration of water vapor, with the aid of the interface equation (Equation 4.2.32) to yield temperature and concentration profiles, and radius of the wet core region at different time levels. Furthermore, when *s'(t)* approaches to zero, liquid water in the pores of the wet core region is completely evaporated. At that instant, falling rate period ends and VTS algorithm is terminated. A schematic description of VTS algorithm is presented in Figure 4.4. A program file listing, which is written in FORTRAN language, is documented in Appendix-C.

There exist two iteration loops in VTS algorithm (Figure 4.4), one for the estimation of the successful time step Δt and one for the estimation of the interface temperature T_M (Figure 4.3). In order to move from t to the next time level $t+\Delta t$, time step Δt is estimated as

$$\Delta t = \Delta t_{guess} - k(\delta t) \qquad k = 1, 2, 3\ldots, K_{max} \qquad (4.2.33)$$

where k is the iteration level and K_{max} is the maximum number of iterations. (δt) is the incremental time and Δt_{guess} is the initial guess of time step. Having an initial estimate for Δt and with the assumption that interface s' recedes by a single grid spacing $\Delta\zeta$, temperature and concentration profiles are obtained via the governing iteration loop for interface temperature T_M. Then, interface position is recalculated using Equation 4.2.32. Δt is iteratively decreased until the decrease in s', which is calculated using Equation 4.2.32, approaches $\Delta\zeta$, where the convergence criterion is defined as

$$\frac{\left|\left|\left(s'-s'^{*}\right)_C\right|-\Delta\zeta\right|}{\Delta\zeta}\times 100 \leq \Phi_s \qquad (4.2.34)$$

where subscript C in Equation 4.2.34 represents calculated expression. Φ_s is the percent tolerance.

The iteration loop for interface temperature (Figure 4.4) requires an estimate of T_M in order to obtain concentration profile at time level $t+\Delta t$, in which T_M at time level t is used as an initial estimate. Having a value for T_M, concentration and temperature profiles are obtained. Then the calculated value of T_M is used as the estimate value for the new iteration level. Iterations are carried out until the values of T_M between

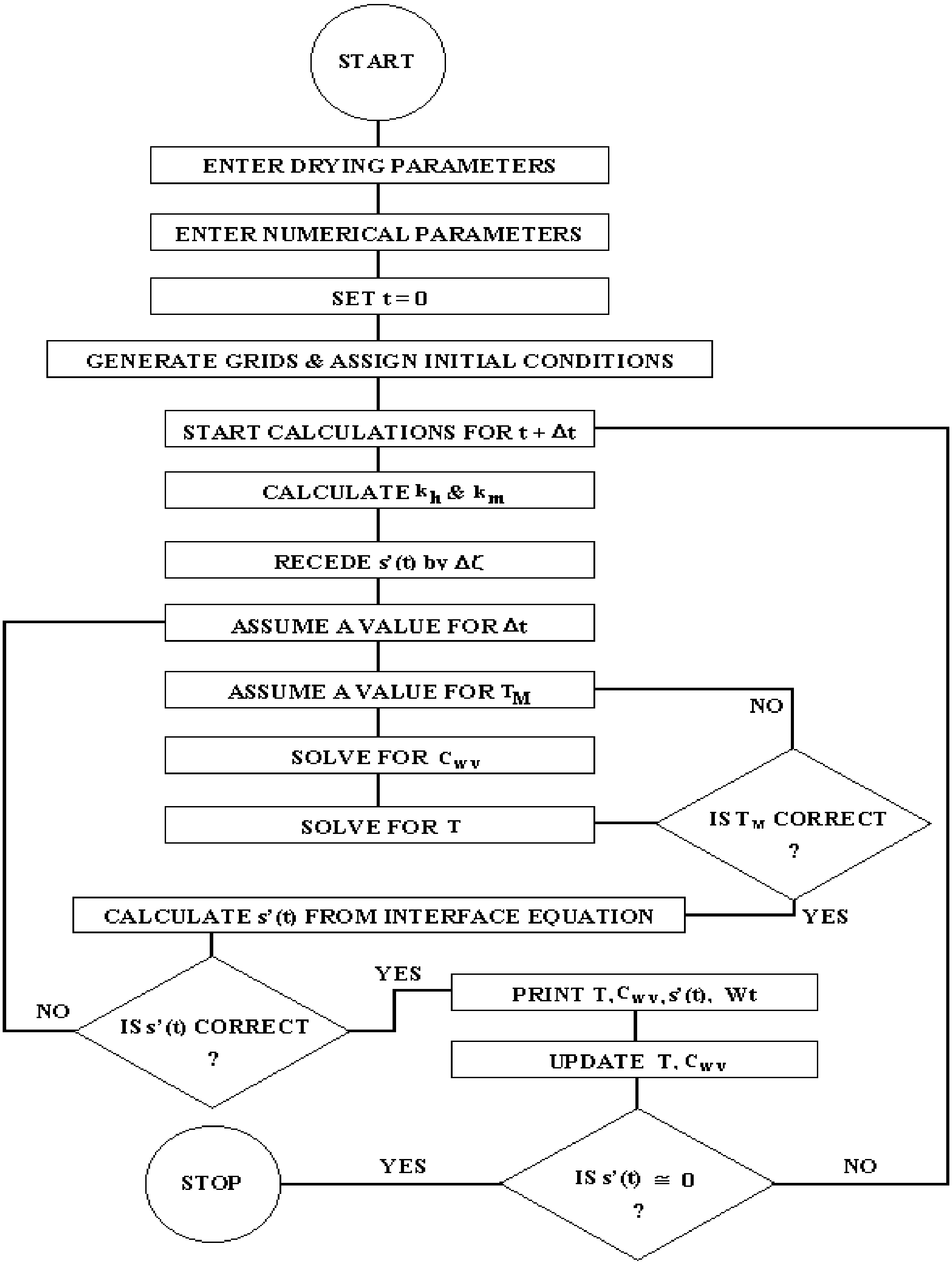

Figure 4.4 Schematic description of VTS algorithm

two successive iteration levels approach to each other, where the convergence criterion is defined as

$$\frac{\left|T_M^{j+1} - T_M^j\right|}{T_M^{j+1}} \times 100 \leq \Phi_T \qquad j = 1, 2, 3\ldots, J_{max} \tag{4.2.35}$$

where *j* represents iteration level and J_{max} is the maximum number of iterations.

VTS algorithm terminates when the dimensionless wet core radius *s'(t)* is 3 % of the dimensionless droplet radius since it is not possible to carry out numerical calculations when *s'(t)* is close to zero due to some numerical difficulties associated with the interface node exceeding the array bound of the coefficient matrices of temperature and concentration profiles. Furthermore, in order to start numerical calculations in the falling rate period, an initial crust thickness is required, which is chosen to be the 0.2 % of the dimensionless droplet radius.

Weight of the droplet at different time levels is calculated as

$$Wt(t) = \frac{4}{3}\pi\left[\rho_w \varepsilon s^3(t) + \rho_s(1-\varepsilon)R_{in}^3\right] \tag{4.2.36}$$

where

$$s(t) = R_{in} s'(t) \tag{4.2.37}$$

Similarly, droplet average temperature is calculated as

$$T_{av} = \frac{3}{R_{in}^3} \int_0^{R_{in}} r^2 T(r)\,dr \tag{4.2.38}$$

where the integral in Equation 4.2.38 is evaluated using trapezoidal rule.

4.3 Calculation of Drying Parameters

In order to carry out validation studies of the model results, inner radius of the droplet R_{in}, initial value of the outer radius of the droplet R_{init} and the porosity ε have to be evaluated using

$$\frac{4}{3}\pi\left[\rho_w\left(R^3_{init}-R^3_{in}\right)+\rho_w\varepsilon R^3_{in}+\rho_s\left(1-\varepsilon\right)R^3_{in}\right]=Wt_{init} \tag{4.3.1}$$

$$\frac{4}{3}\pi\left[\rho_w\varepsilon R^3_{in}+\rho_s\left(1-\varepsilon\right)R^3_{in}\right]=Wt_{crit} \tag{4.3.2}$$

$$\frac{4}{3}\pi\left[\rho_s\left(1-\varepsilon\right)R^3_{in}\right]=Wt_{final} \tag{4.3.3}$$

where Wt_{init} and Wt_{final} are the initial and final weight of the droplet. Similarly, Wt_{crit} is the weight of the droplet at critical moisture content. The values of the droplet weight Wt_{init}, Wt_{crit} and Wt_{final} are obtained using the experimental weight vs. time data [22]. Simultaneous solution of Equations 4.3.1-3 gives R_{init}, R_{in} and ε, which are then used as drying parameters in numerical calculations.

CHAPTER 5

RESULTS & DISCUSSION

In this study, a new single droplet drying model is developed using receding evaporation front approach coupled with the utilization of heat and mass transfer equations. For the assessment of the validity of the model, experimental [22] weight and temperature histories of colloidal silica (SiO_2), skimmed milk and sodium sulfate decahydrate ($Na_2SO_4 \cdot 10H_2O$) droplets are compared with the model predictions. In order to obtain the best fit of the model results to experimental data [22], at each run, weight of the droplet at critical moisture content is varied since the estimation of such a critical weight from available experimental data is quite difficult. Further, proper choices of the numerical parameters are also sought in order to have successful iteration loops. Temperature and water vapor concentration profiles of the droplets are also documented as well as the drying and numerical parameters used at each run.

5.1 Drying of Colloidal Silica Droplets

Colloidal silica droplets, which have initial SiO_2 mass fraction of 0.3, having small silica particles (16nm in diameter) are dried at air temperatures of 101°C and 178°C [22]. Model parameters used for drying at 101°C are given in Table 5.1.

Table 5.1 Parameters used for drying of a colloidal silica droplet at 101°C

Drying Parameters					
Parameter	**Value**	**Unit**	**Parameter**	**Value**	**Unit**
ρ_{solid} [14]	2220	kg/m^3	R_{in}	$7.934\cdot10^{-4}$	m
k_{solid} [14]	1.445	W/m.K	ε	0.588	-
Cp_{solid} [14]	825	J/kg.K	*Wt_{init}	4.582	mg
ρ_{water} [14]	1000	kg/m^3	*Wt_{crit}	3.145	mg
k_{water} [14]	0.660	W/m.K	*Wt_{final}	1.916	mg
Cp_{water} [14]	4188	J/kg.K	V_{air}	1.73	m/s
$R_{out}(t = 0)$	$9.445\cdot10^{-4}$	m	H_{air}	0.01	$kg_{wv}/kg_{dry\ air}$
Constant Rate Numerical Parameters			**Falling Rate Numerical Parameters**		
Parameter	**Value**	**Unit**	**Parameter**	**Value**	**Unit**
Δt	1.0	s	(δt)	$1.0\cdot10^{-5}$	s
$(\delta\xi)$	$1.0\cdot10^{-6}$	-	Φ_s	0.1 %	-
Φ_ξ	0.05 %	-	Φ_T	$1.0\cdot10^{-10}$ %	-

* independent parameters

Figure 5.1 shows model predictions and experimental weight measurements of drying of a colloidal silica droplet at 101°C. Vertical axis gives dimensionless droplet weight, which is obtained by dividing each droplet weight reading to initial weight, and horizontal axis gives time.

Generally, when a droplet is dried, a constant rate period is followed by a falling rate period [3,10,31], where the introduction of new heat and mass transfer resistances due to the formation of a dry crust region is addressed for the decreasing drying rate, which is directly proportional to the slope of the weight loss curve of the droplet. However, both experimental measurements and the model predictions of drying of a colloidal silica droplet at 101°C (Figure 5.1) show that drying rate does not change significantly except for the final stages of drying. This unique behavior of silica droplets could be a result of SiO_2 having a higher thermal conductivity value (1.445 W/m.K) compared to that of skimmed milk powder (0.370 W/m.K) and $Na_2SO_4\cdot10H_2O$ (0.545 W/m.K), since the dry crust formed by a conductive material probably has a thermal conductivity value close to that of the wet core as long as the crust is not highly porous. Similarly, a slight decrease in drying rate observed at the final stages of drying (Figure 5.1) could be resulted by further increase of both heat and mass transfer resistances due to increasing thickness of the dry crust.

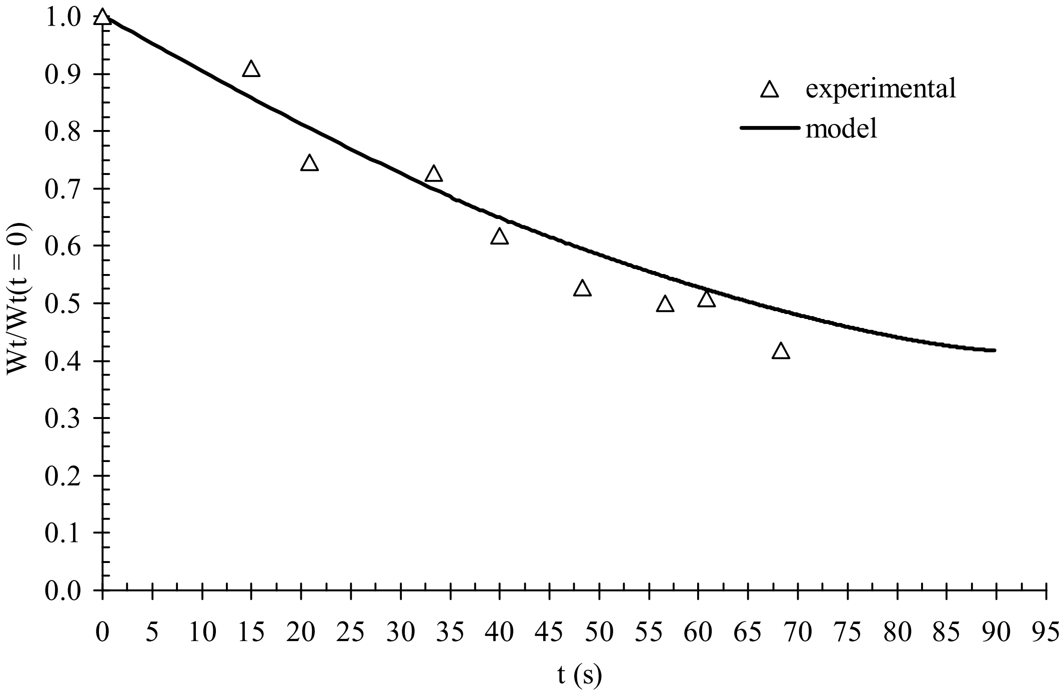

Figure 5.1 Weight history of a colloidal silica droplet dried at 101°C

It is observed that model predictions and the experimental measurements of drying of a colloidal silica droplet at 101°C (Figure 5.1) are in good agreement, which probably indicates that the estimated weight of droplet at critical moisture content, which is the only experimental data used by the model, is properly chosen.

Figure 5.2 shows predicted volume average and surface temperatures as well as the experimental [22] temperature measurements of drying of a colloidal silica droplet at 101°C. Vertical axis gives temperature readings and horizontal axis gives time. The model shows that after an initial adjustment, average droplet temperature reaches the wet-bulb temperature of air in the constant rate period. Experimental temperature readings also display similar trend in constant rate period, where the heat transferred convectively from air to droplet surface is counter-balanced by the heat required to evaporate some portion of free water on the surface. Since temperature variation within the droplet in constant rate period is negligibly small due to Biot number being less than 0.1, predicted surface temperature and average droplet temperature coincide (Figure 5.2).

In the falling rate period (Figure 5.2), model shows that average droplet temperature gradually increases from wet-bulb temperature to dry-bulb temperature of air. The slopes of both average and surface temperatures through the end of drying increase. This occurs probably because of increasing value of the convective heat transfer coefficient.

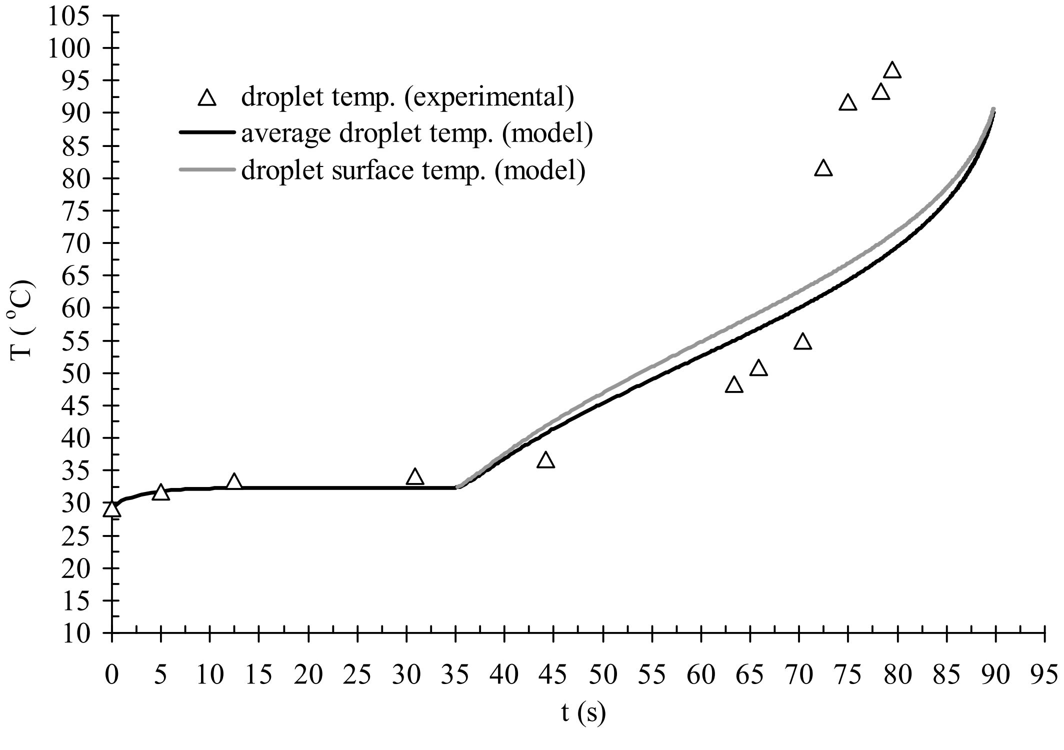

Figure 5.2 Temperature history of a colloidal silica droplet dried at 101°C

Contrary to what has been observed in constant rate period, small temperature gradients exist within the droplet in falling rate period (Figures 5.2&3), which indicates that although the droplet diameter is small (1.89 mm), Biot number is higher than 0.1 due to formation of the dry crust region having smaller thermal conductivity value compared to that of the wet core region. Similarly, estimated droplet surface temperature is not significantly different from average droplet temperature, which indicates that the value of the heat transfer resistance of the dry crust region is not significantly large. Such a behavior of the colloidal silica droplet having small temperature gradients (Figure 5.2) also supports the cause proposed for drying rate being not significantly different in constant and falling rate periods (Figure 5.1).

It is observed in Figure 5.2 that predicted average droplet temperature and the experimental temperature measurements are in good agreement in constant rate period. Since solid-liquid interactions are quite insignificant [22] for colloidal silica droplets, model successfully predicts the wet-bulb temperature of air (Figure 5.2).

At the beginning of the falling rate period (Figure 5.2), estimated average droplet temperature deviates slightly from experimental measurements, which probably has negligibly small effect on the weight history of the droplet (Figure 5.1). Experimentation [8,22] on drying of droplets has shown that in the transition stage between constant and falling rate periods, measured droplet temperature slightly increases due to dry spots commencing at the surface. As the number of dry spots increases, droplet temperature further increases. In addition, shrinkage of the droplet at the transition stage as well as the morphological changes occurring may also cause similar changes in droplet temperature, where such effects apply for the whole stages of the falling rate period. Since the model does not take into account such effects, a small deviation of predicted average droplet temperature from measured one is observed (Figure 5.2). Similarly, through the end of the falling rate period, average droplet temperature deviates significantly from the experimental measurements.

Experimental [22] weight and temperature histories were obtained by suspending individual droplets at the tip of a glass filament and at the tip of a micro-thermocouple. It is stated [22] that the heat transferred to the droplet from the filament support can be up to 10 % of the total heat transferred to the droplet. Heating effect of the filament could be the reason for such a significant deviation of average droplet temperature from experimental readings through the end of the falling rate period. Since the amount of heat transferred from filament is smaller at early stages, the effect is not observed at early periods of drying.

At the final stage of drying, when the position of the interface corresponds to 3 % of the droplet radius, VTS algorithm is terminated. Actually, heating of the droplet continues until the droplet temperature equals to drying air temperature. Since the model does not take into account this sensible heating period, average droplet temperature does not reach the air temperature in any of the runs.

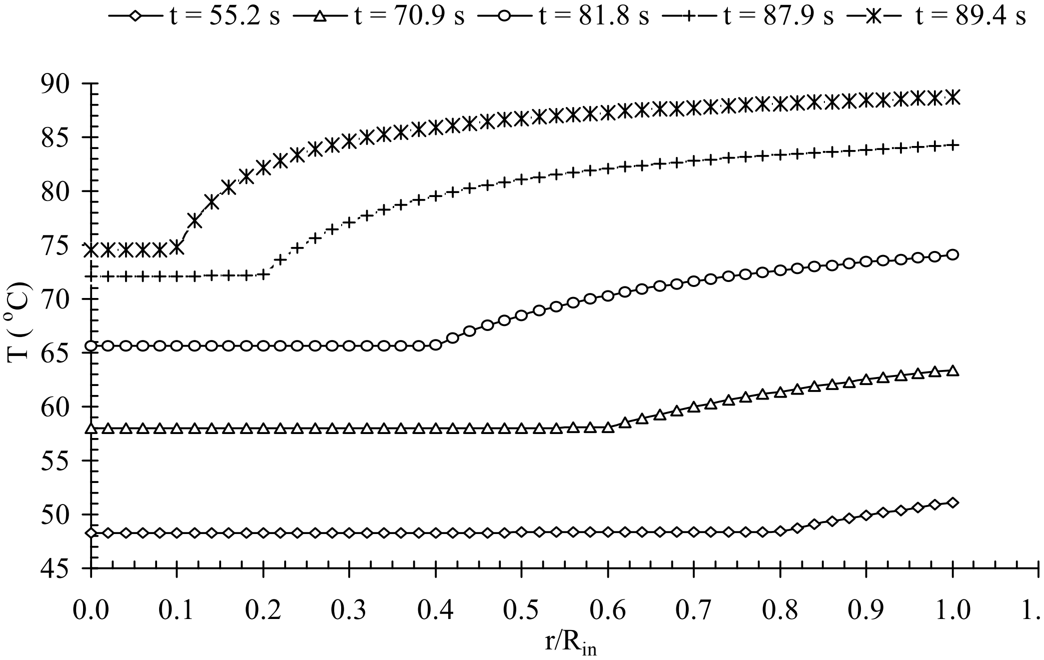

Figure 5.3 Temperature profiles of a colloidal silica droplet dried at 101°C

Figure 5.3 shows predicted temperature profiles in the falling rate period of drying of a colloidal silica droplet at 101^{o}C. Vertical axis gives temperature readings and the horizontal axis gives dimensionless droplet radius. In the constant rate period, variation of temperature within the droplet is negligibly small due to Biot number being less than 0.1. It is observed in Figure 5.3 that, even the droplet diameter is small (1.89mm) and the value of the crust thermal conductivity is respectively high (0.596 W/m.K), temperature variations exist within the droplet, which probably indicates that Biot number in falling rate period is higher than 0.1. As the dry crust thickens, which directly increases heat transfer resistance, the difference between the droplet surface temperature and wet core temperature increases. Linear variation of the dry crust temperature observed at early periods of drying also changes to convex variation at later periods. This could be a result of the heating effect of diffusing water vapor through the pores of the dry crust. Since water vapor concentration is respectively small at early periods (Figure 5.4), such a heating effect is not observed at these periods of drying.

Figure 5.4 shows predicted water vapor concentration profiles in the falling rate period of drying of a colloidal silica droplet at 101^{o}C. Vertical axis gives vapor concentration and the horizontal axis gives time. It is observed that the value of the interface concentration, which is the maximum value of each profile, increases as drying proceeds, since the interface concentration is calculated using the value of the interface temperature, which gradually increases due to thermal conduction effect. Furthermore, the difference between the two values of the interface concentration and the surface concentration probably increases due to gradual increase in mass transfer resistance of the dry crust region (Figure 5.4). It is also observed that the surface concentration values are close to each other, which could be a result of the convective boundary condition used for the solution of the governing differential equation for mass transfer.

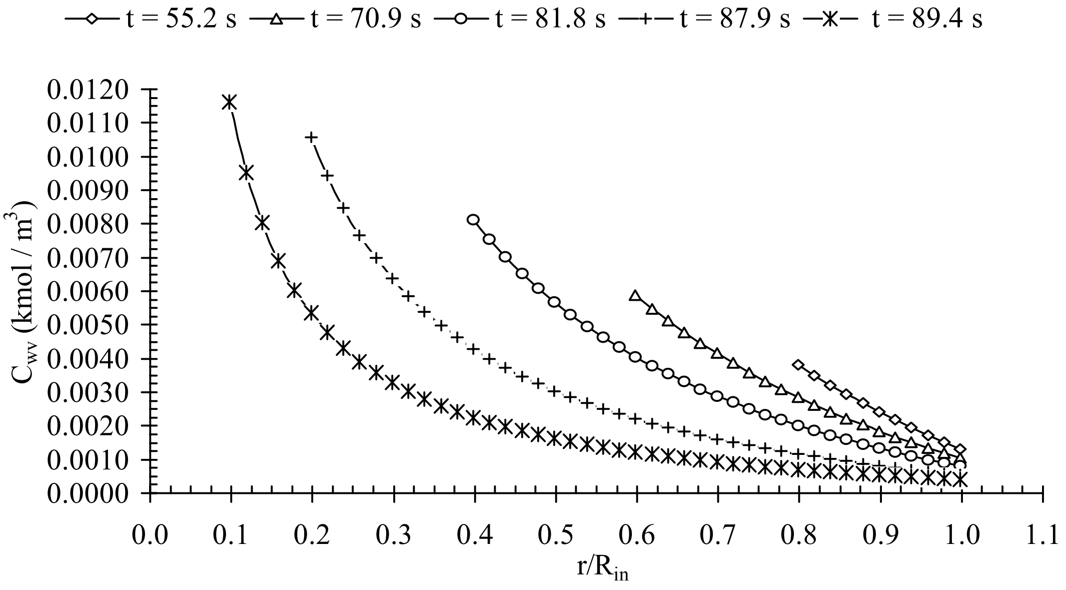

Figure 5.4 Concentration profiles of a colloidal silica droplet dried at 101°C

Table 5.2 shows the model parameters used for drying of a colloidal silica droplet at 178°C. The model uses a slightly higher porosity value of 0.602 compared to the value of porosity (0.588) used for drying at air temperature of 101°C.

Table 5.2 Parameters used for drying of a colloidal silica droplet at 178°C

Drying Parameters					
Parameter	**Value**	**Unit**	**Parameter**	**Value**	**Unit**
ρ_{solid} [14]	2220	kg/m^3	R_{in}	$7.572 \cdot 10^{-4}$	m
k_{solid} [14]	1.495	W/m.K	ε	0.602	-
Cp_{solid} [14]	875	J/kg.K	*Wt_{init}	4.248	mg
ρ_{water} [14]	1000	kg/m^3	*Wt_{crit}	2.655	mg
k_{water} [14]	0.680	W/m.K	*Wt_{final}	1.608	mg
Cp_{water} [14]	4215	J/kg.K	V_{air}	1.40	m/s
$R_{out}(t = 0)$	$9.296 \cdot 10^{-4}$	m	H_{air}	0.01	$kg_{wv}/kg_{dry\ air}$
Constant Rate Numerical Parameters			**Falling Rate Numerical Parameters**		
Parameter	**Value**	**Unit**	**Parameter**	**Value**	**Unit**
Δt	1.0	s	(δt)	$1.0 \cdot 10^{-6}$	s
$(\delta \xi)$	$1.0 \cdot 10^{-6}$	-	Φ_s	0.1 %	-
Φ_ξ	0.05 %	-	Φ_T	$1.0 \cdot 10^{-10}$ %	-

* independent parameters

Figure 5.5 shows model predictions and the experimental weight measurements of drying of a colloidal silica droplet at 178°C. Similar to what has been observed in Figure 5.1, drying rate does not change significantly during the course of drying, except for a slight decrease observed through the end of the falling rate period. Both model predictions and the experimental measurements [22] show this kind of behavior (Figure 5.5). It is also observed that, since the drying rate for the air temperature of 178°C is higher than the drying rate for the air temperature of 101°C, which can be observed by comparing the slopes of the curves shown by Figures 5.1&5, time required for drying of the colloidal silica droplet at 178°C is shorter (45s for air temperature of 178°C and 90s for air temperature of 101°C).

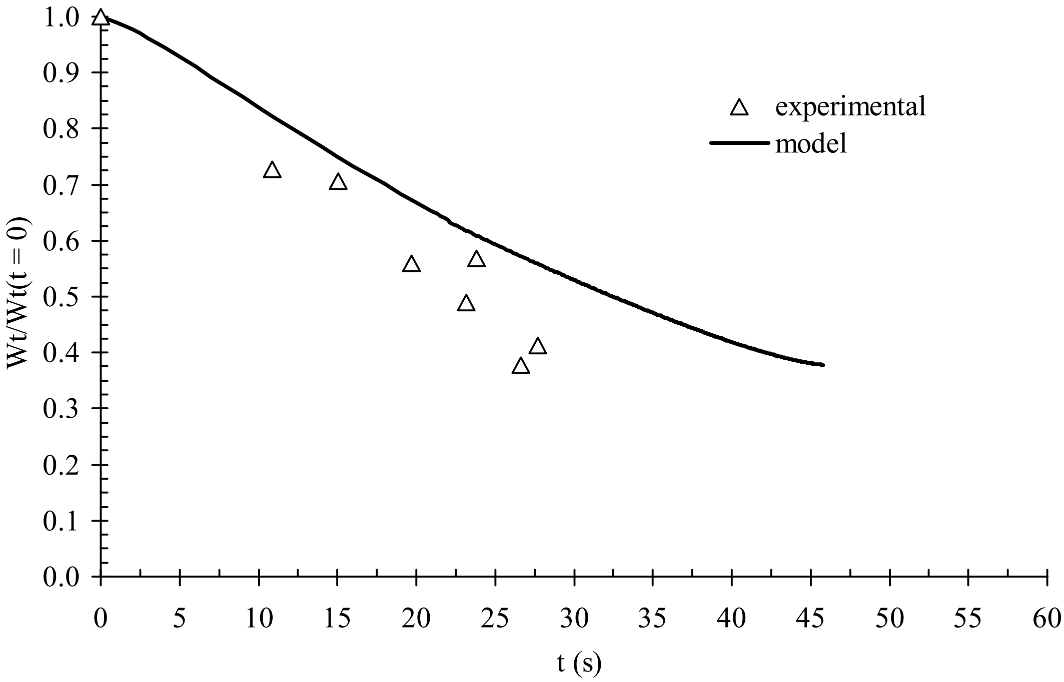

Figure 5.5 Weight history of a colloidal silica droplet dried at 178°C

It is observed in Figure 5.5 that the model predictions and the experimental measurements are not in good agreement. The reason for such a deviation could be a result of high amount of heat transferred from the filament support [22] even at the early stages of drying. Furthermore, the model estimates the drying rates by using a vapor pressure expression with the assumption that water vapor behaves ideally. Since the drying air temperature is above the boiling point of liquid water at 1 atm total pressure, estimated values of water vapor concentration at interface, which is directly used in weight loss calculations, could deviate significantly from the actual values. This could also be the reason for the significant deviation of the model results from experimental measurements (Figure 5.5). Experimentation [3,10,31] on drying of single droplets has shown that if the drying air temperature is above the boiling point of liquid water for a given total pressure, there is the possibility of cracking and fracturing of the dry crust, which is not taken into account by the model, formed in the falling rate period, where such cracks and fractures decrease both heat and mass transfer resistances significantly, which can also cause experimental drying rates being higher than the drying rates predicted by the model.

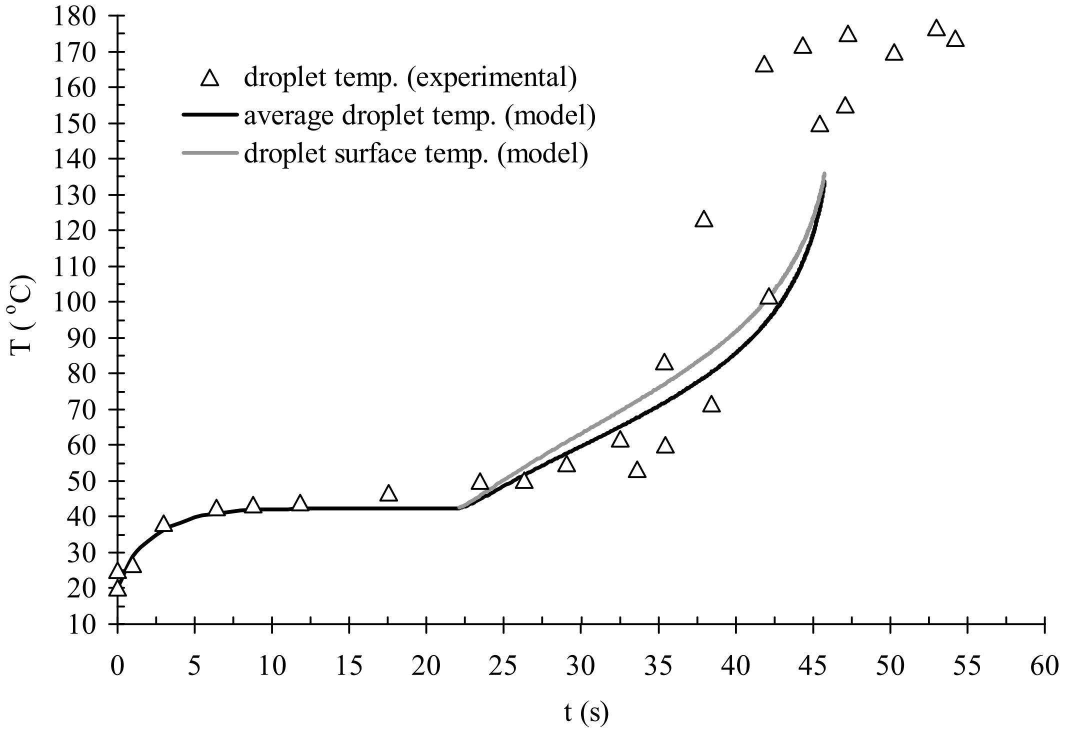

Figure 5.6 Temperature history of a colloidal silica droplet dried at 178°C

Figure 5.6 shows model predictions and the experimental measurements of drying of a colloidal silica droplet at 178°C. Similar to what has been observed in Figure 5.2, volume average droplet temperature reaches air wet-bulb temperature after an initial adjustment in constant rate period (Figure 5.6). Similar trend in experimental temperature measurements is also observed. In the falling rate period, average droplet temperature gradually increases to air temperature due to introduction of new heat and mass transfer resistances. There exists a small difference between the volume average droplet temperature and the droplet surface temperature, since heat transfer resistance of the dry crust region is respectively small.

Model predictions and the experimental temperature measurements in constant rate period are in good agreement (Figure 5.6). The model successfully estimates the wet-bulb temperature of drying air. However, the model predictions deviate slightly from experimental measurements at the beginning of the falling rate period. Furthermore, a significant deviation is observed between the average droplet temperature values and the experimental temperature measurements through the end of the falling rate period. Similarly, the same discussion, which is held for the temperature history of the colloidal silica droplet dried at 101°C, is also valid for the temperature history of the colloidal silica droplet dried at 178°C (Figure 5.6).

Predicted temperature profiles of a colloidal silica droplet dried at air temperature of 178°C are given in Figure 5.7. Contrary to small gradients observed at early stages of drying (Figure 5.3) at 101°C, there exist large temperature gradients within the droplet (Figure 5.7) even at the early periods, since the drying air temperature is high at 178°C, which directly indicates that the heat transfer rate from air to the droplet is respectively higher.

Predicted concentration profiles of a colloidal silica droplet dried at 178°C are given in Figure 5.8. Similar trend, which is observed in Figure 5.4, is also observed with the only exception of higher vapor concentration values for drying at 178°C.

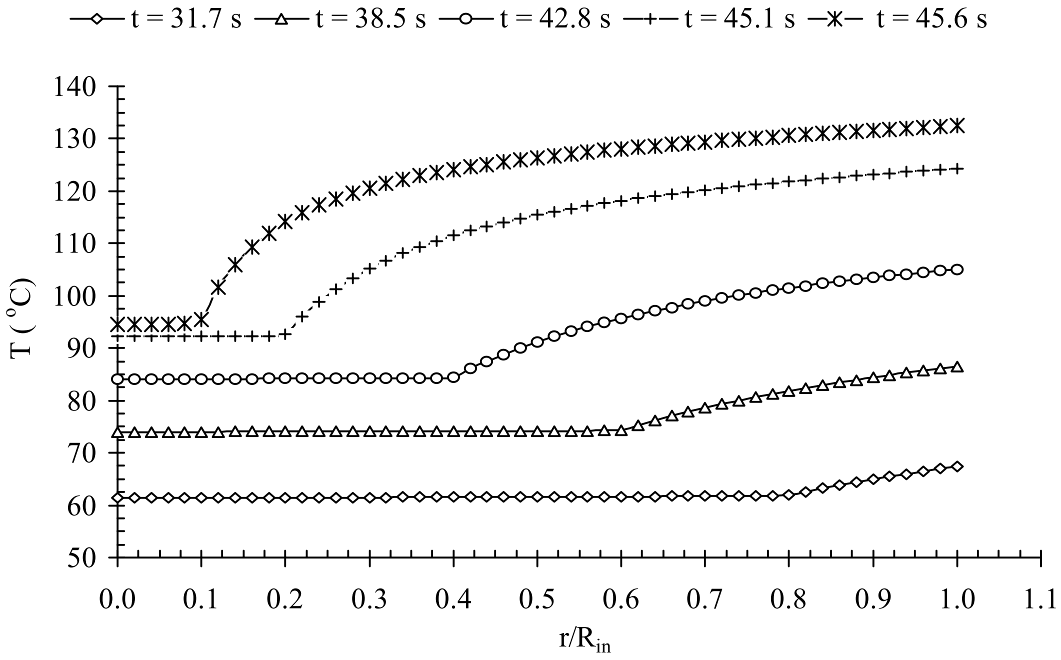

Figure 5.7 Temperature profiles of a colloidal silica droplet dried at 178^{o}C

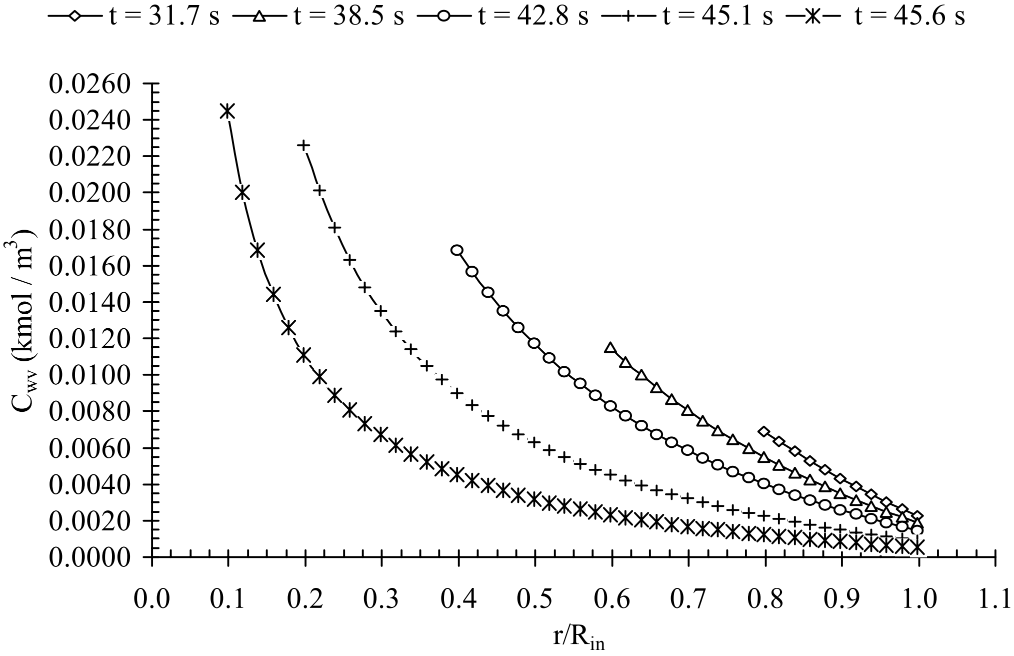

Figure 5.8 Concentration profiles of a colloidal silica droplet dried at 178^{o}C

5.2 Drying of Skimmed Milk Droplets

Skimmed milk droplets, which have initial solid mass fraction of approximately 0.2, are dried at air temperatures of 50°C and 90°C [22]. It is assumed that the only volatile component of skimmed milk droplets is liquid water. Properties of the milk powder are estimated using reference [25]. Model parameters used for drying at air temperature of 50°C are given in Table 5.3.

Table 5.3 Parameters used for drying of a skimmed milk droplet at 50°C

Drying Parameters					
Parameter	**Value**	**Unit**	**Parameter**	**Value**	**Unit**
ρ_{solid} [25]	1281	kg/m^3	R_{in}	$6.845 \cdot 10^{-4}$	m
k_{solid} [25]	0.372	W/m.K	ε	0.651	-
Cp_{solid} [25]	1791	J/kg.K	$*Wt_{init}$	2.875	mg
ρ_{water} [14]	1000	kg/m^3	$*Wt_{crit}$	1.475	mg
k_{water} [14]	0.620	W/m.K	$*Wt_{final}$	0.600	mg
Cp_{water} [14]	4178	J/kg.K	V_{air}	0.75	m/s
$R_{out}(t = 0)$	$8.684 \cdot 10^{-4}$	m	H_{air}	0.01	$kg_{wv}/kg_{dry\ air}$
Constant Rate Numerical Parameters			**Falling Rate Numerical Parameters**		
Parameter	**Value**	**Unit**	**Parameter**	**Value**	**Unit**
Δt	1.0	s	(δt)	$5.0 \cdot 10^{-5}$	s
$(\delta\xi)$	$1.0 \cdot 10^{-6}$	-	Φ_s	0.1 %	-
Φ_ξ	0.05 %	-	Φ_T	$1.0 \cdot 10^{-10}$ %	-

* independent parameters

Figure 5.9 shows model results and experimental weight measurements at 50°C. Similar to Figures 5.1&5, vertical axis gives dimensionless weight and horizontal axis gives drying time (Figure 5.9). Contrary to what has been observed in drying of colloidal silica droplets, drying rates in constant and falling rate periods are quite different from each other for drying of a skimmed milk droplet at 50°C. This is probably the result of wet core and dry crust regions having significantly different thermal conductivity values (k_{co} = 0.533 W/m.K, k_{cr} = 0.130 W/m.K), since the resistance to heat transferred is inversely proportional to thermal conductivity.

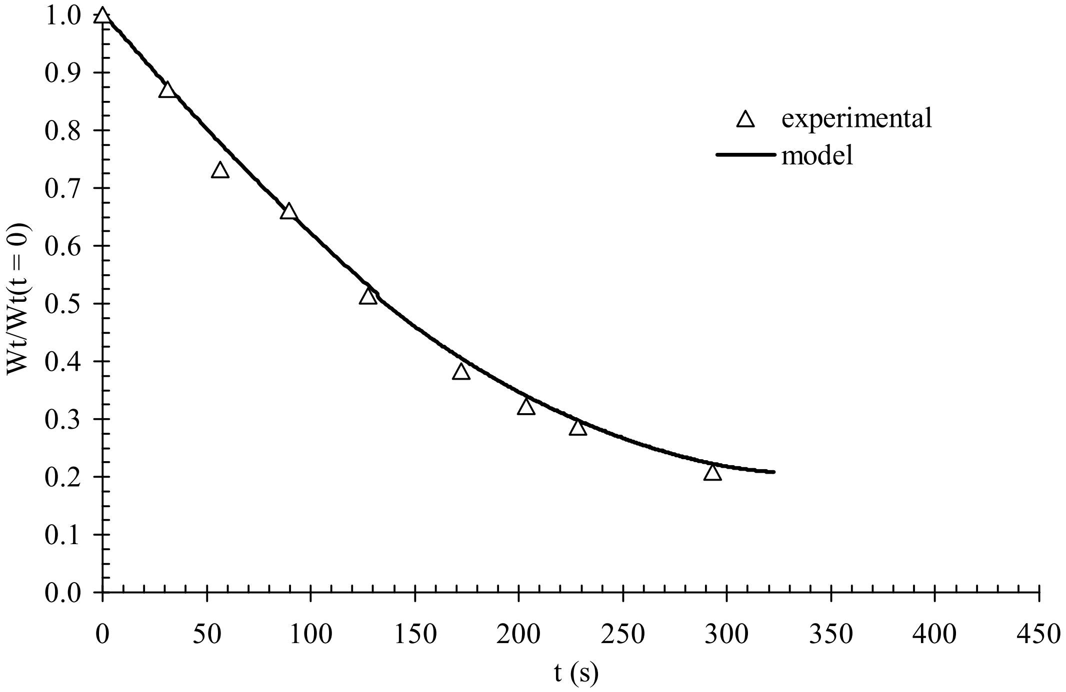

Figure 5.9 Weight history of a skimmed milk droplet dried at 50°C

It is observed in Figure 5.9 that the experimental measurements and the model predictions are in good agreement, which probably indicates that the critical droplet weight is properly chosen. Furthermore, since the heating effect of the filament support [22] is negligibly small due to relatively low air temperature, deviation of the predictions from experimental measurements through the end of the falling rate period is not observed (Figure 5.9).

Figure 5.10 shows predicted volume average and surface temperatures as well as the experimental [22] temperature measurements of drying of a skimmed milk droplet at 50°C. Similar trend, which is observed in drying of colloidal silica droplets, is also followed by model predictions and the experimental measurements: an initial adjustment period followed by the slight variation of temperature in constant rate period and gradual increase of droplet temperature in the falling rate period. Furthermore, the difference between the average droplet temperature and droplet surface temperature is respectively higher. As stated, this occurs probably because the crust heat transfer resistance of the skimmed milk droplet is higher than that of the colloidal silica droplet. Through the end of the falling rate period, average droplet temperature and the droplet surface temperature coincide (Figure 5.10). This is because as the wet core shrinks, volume fraction of wet core, which is at a lower temperature than dry crust, in the calculations of the average droplet temperature decreases, thus the average droplet temperature gets closer to the droplet surface temperature, where such a behavior is also valid for all of the runs.

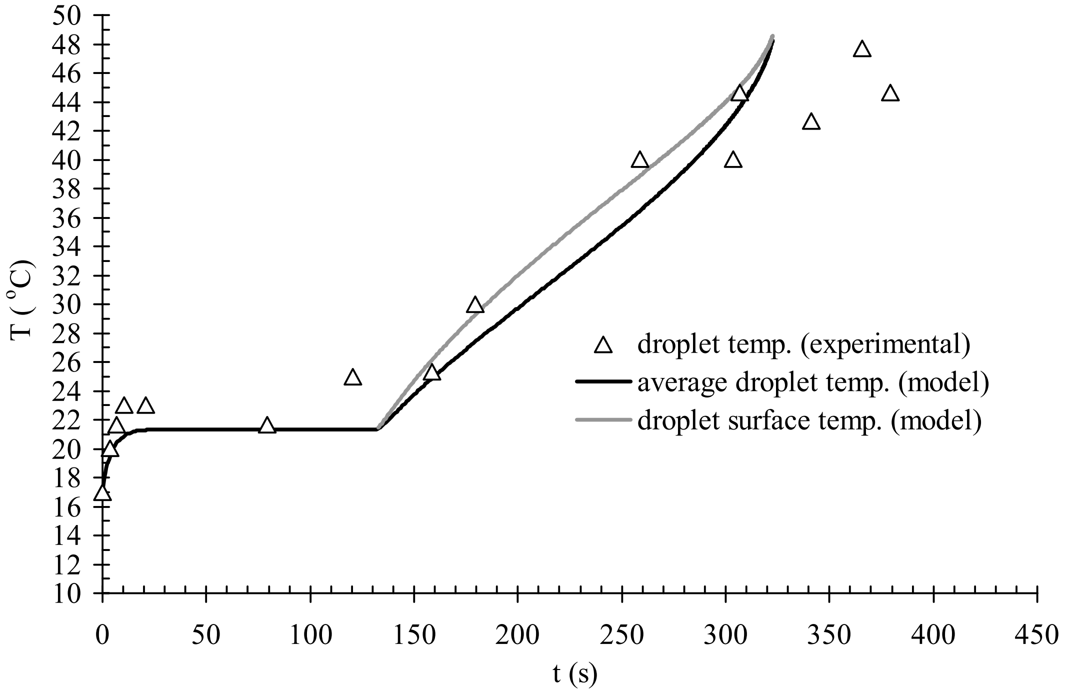

Figure 5.10 Temperature history of a skimmed milk droplet dried at 50^{o}C

Figure 5.10 shows that model results and experimental temperature measurements at 50^{o}C are in good agreement except for the constant rate period. Since the model does not take into account the solid-liquid interactions, it probably predicts the average droplet temperature values lower than the measurements in the constant rate period.

Predicted temperature profiles of a skimmed milk droplet dried at air temperature of 50°C are given in Figure 5.11, where the vertical axis shows temperature and the horizontal axis shows dimensionless droplet radius. As stated, large temperature gradients exist within the droplet, since the crust heat transfer resistance is high. Due to using a convective boundary condition at the droplet surface, surface temperature gradually increases. Similarly, increasing heating effect of the diffusing water vapor through the pores of the dry crust probably gives the convex shape to the profiles through the end of the falling rate period.

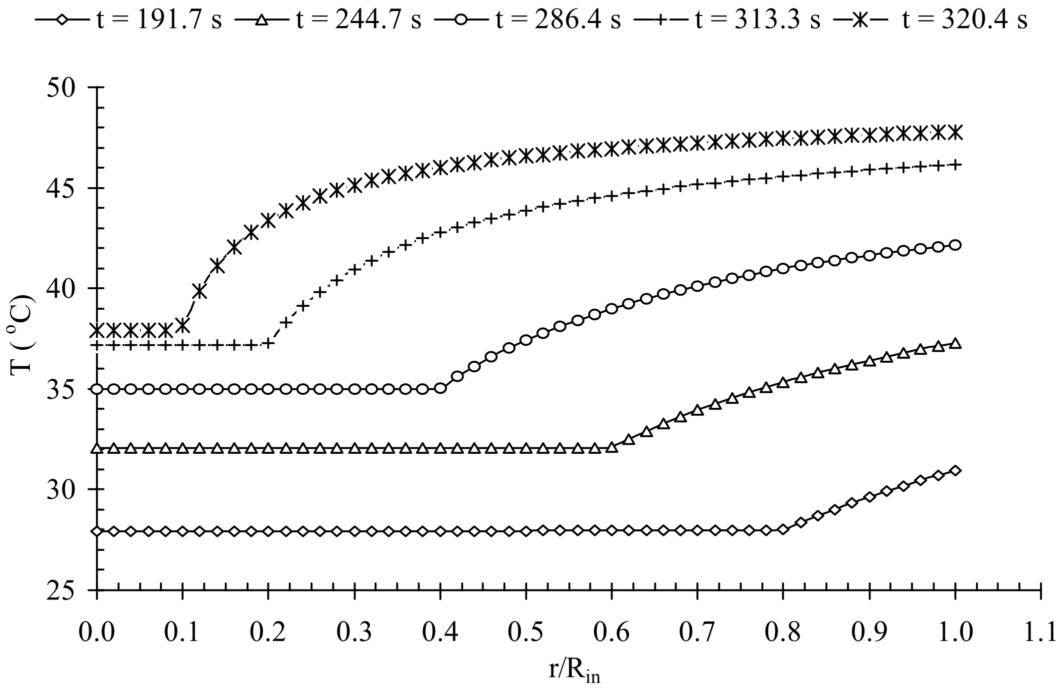

Figure 5.11 Temperature profiles of a skimmed milk droplet dried at 50°C

Predicted concentration profiles of a skimmed milk droplet dried at air temperature of 50°C are given in Figure 5.12. The trend of decreasing concentration values and the existence of gradients probably indicates that the mass transfer resistance of the dry crust significantly changes drying rates in the falling rate period.

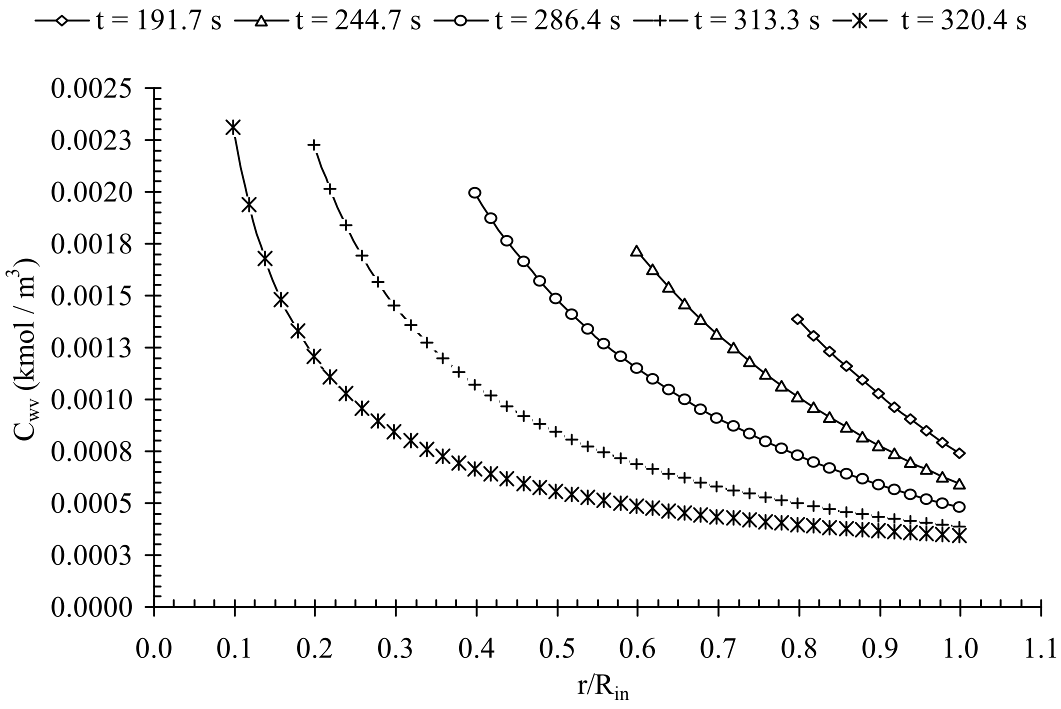

Figure 5.12 Concentration profiles of a skimmed milk droplet dried at 50°C

Table 5.4 shows the model parameters used for drying of a skimmed milk droplet at 90°C. Weight history of the skimmed milk droplet dried at 90°C is also given in Figure 5.13. Similar to what has been observed in drying at 50°C, drying rates in constant and falling rate periods are quite different. Furthermore, higher drying rates are observed in drying at 90°C when compared with drying at 50°C. Decreasing drying rates in the falling rate period is probably the result of increasing heat and mass transfer resistances of the dry crust region as it thickens during the course of drying (Figure 5.13).

It is observed in Figure 5.13 that model results and the experimental measurements are in good agreement, which indicates that the droplet weight at critical moisture content is properly chosen. In addition, the model successfully estimates the drying rates both in constant and falling rate periods (Figure 5.13). However, the model slightly overestimates the drying rates through the end of the falling rate period.

Table 5.4 Parameters used for drying of a skimmed milk droplet at 90°C

Drying Parameters					
Parameter	**Value**	**Unit**	**Parameter**	**Value**	**Unit**
ρ_{solid} [25]	1274	kg/m^3	R_{in}	$6.729 \cdot 10^{-4}$	m
k_{solid} [25]	0.366	W/m.K	ε	0.646	-
Cp_{solid} [25]	1811	J/kg.K	$^*Wt_{init}$	2.575	mg
ρ_{water} [14]	1000	kg/m^3	$^*Wt_{crit}$	1.400	mg
k_{water} [14]	0.645	W/m.K	$^*Wt_{final}$	0.575	mg
Cp_{water} [14]	4182	J/kg.K	V_{air}	0.75	m/s
$R_{out}(t = 0)$	$8.365 \cdot 10^{-4}$	m	H_{air}	0.01	$kg_{wv}/kg_{dry\ air}$
Constant Rate Numerical Parameters			**Falling Rate Numerical Parameters**		
Parameter	**Value**	**Unit**	**Parameter**	**Value**	**Unit**
Δt	1.0	s	(δt)	$1.0 \cdot 10^{-5}$	s
$(\delta \xi)$	$1.0 \cdot 10^{-6}$	-	Φ_s	0.1 %	-
Φ_ξ	0.05 %	-	Φ_T	$1.0 \cdot 10^{-10}$ %	-

* independent parameters

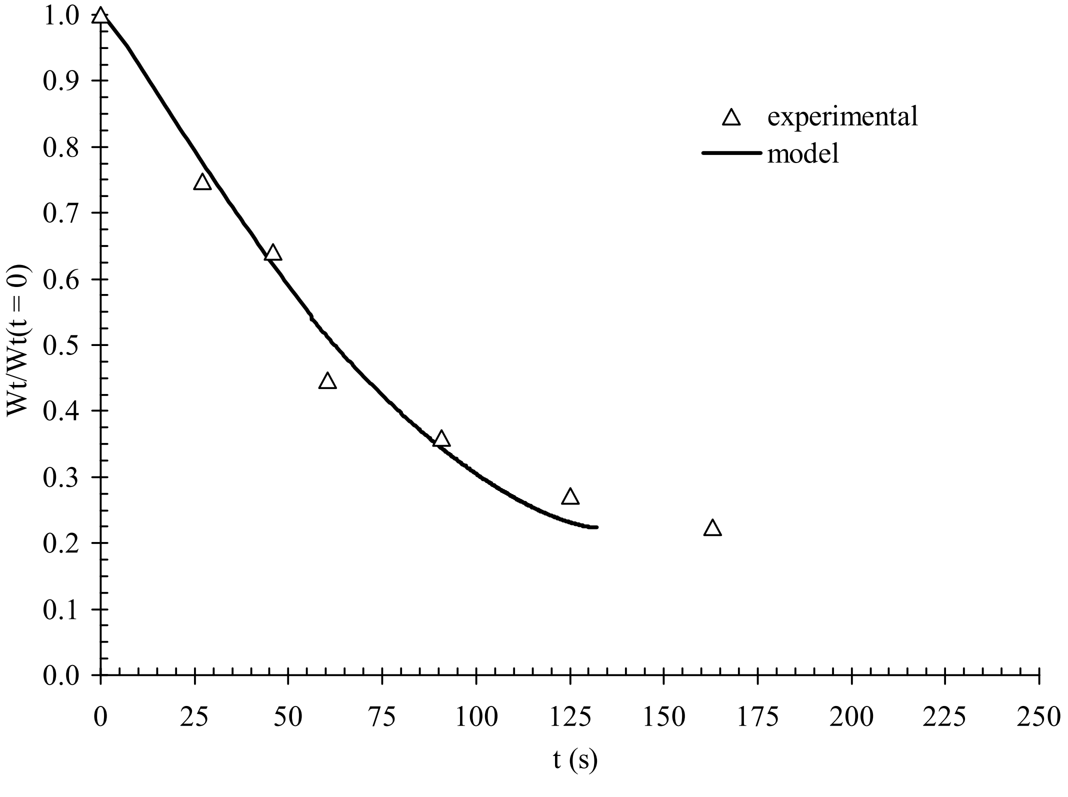

Figure 5.13 Weight history of a skimmed milk droplet dried at 90°C

Figure 5.14 shows model predictions and experimental measurements of drying of a skimmed milk droplet at 90°C. Similar to what has been observed in Figure 5.10, volume average droplet temperature reaches the air wet-bulb temperature in constant rate period (Figure 5.14). Similar trend in experimental temperature measurements is also observed. In the falling rate period, average droplet temperature gradually increases to dry-bulb temperature of air. The difference between the volume average droplet temperature and the surface temperature of the droplet is large probably because of the respectively high value of crust heat transfer resistance.

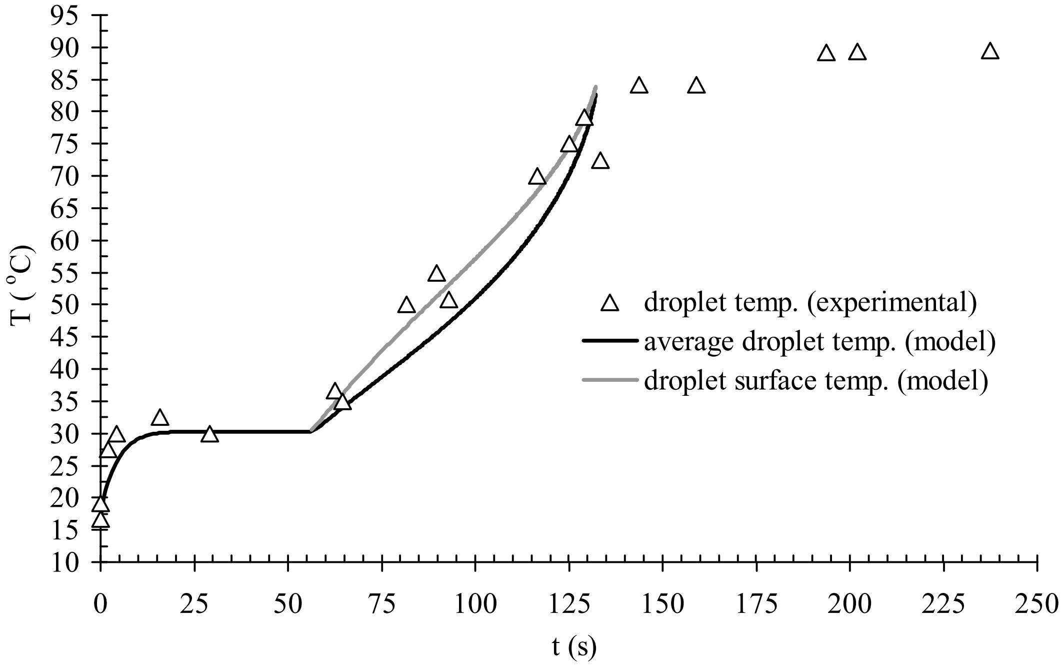

Figure 5.14 Temperature history of a skimmed milk droplet dried at 90°C

It is observed in Figure 5.14 that the model predictions and the experimental [22] measurements are in good agreement except for a slight deviation observed in the constant rate period, which is probably the result of the fact that solid-liquid interactions are neglected in the model calculations. Predicted temperature and concentration profiles are also given in Figures 5.15&16, respectively.

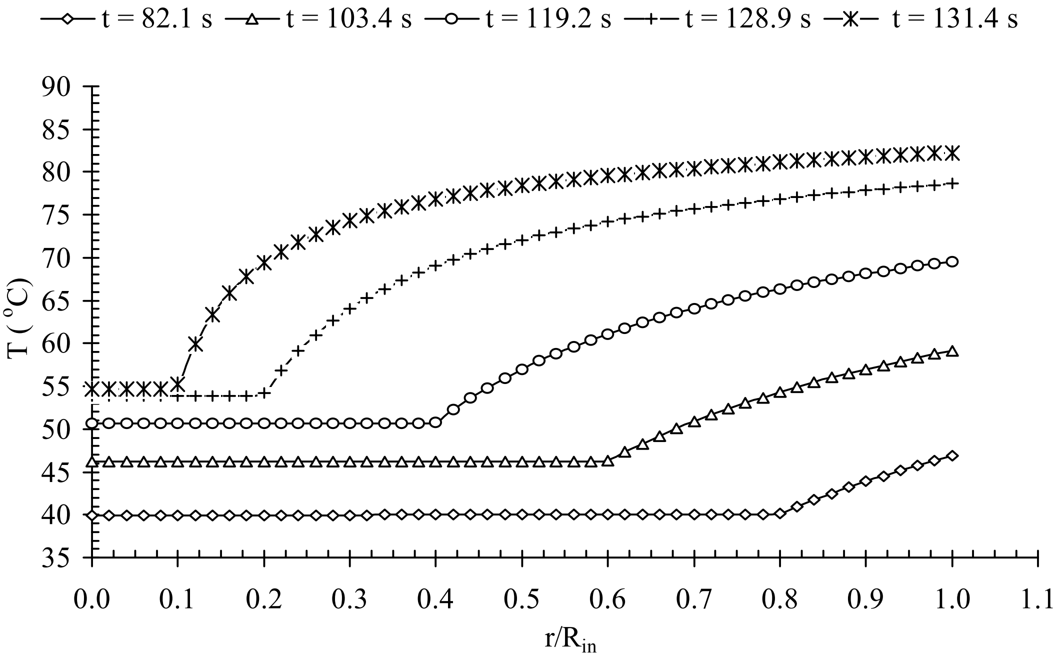

Figure 5.15 Temperature profiles of a skimmed milk droplet dried at 90°C

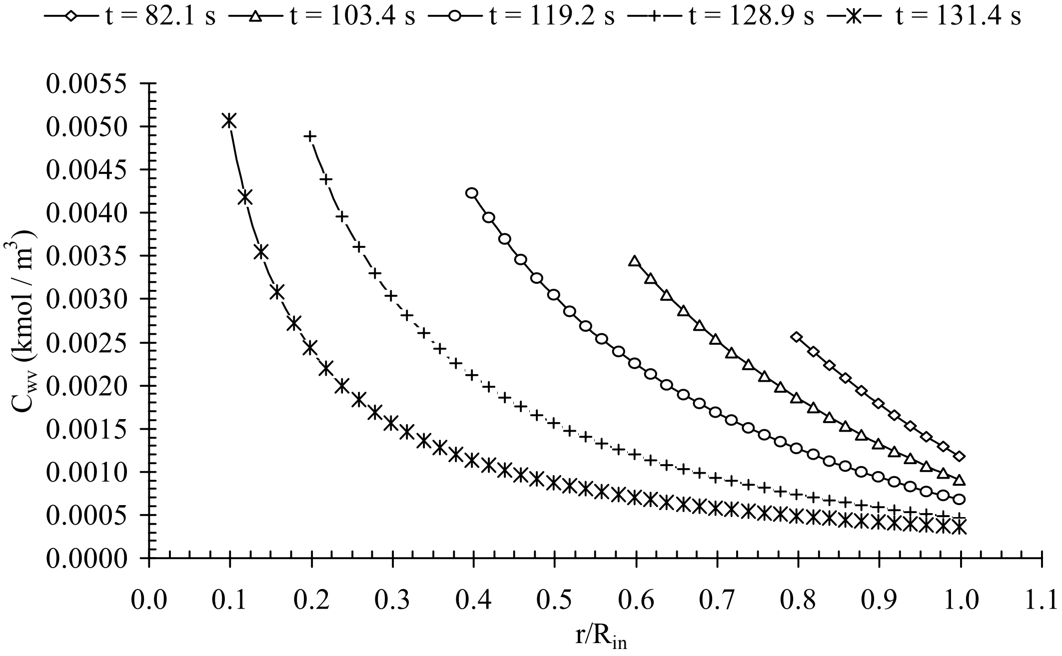

Figure 5.16 Concentration profiles of a skimmed milk droplet dried at 90°C

5.3 Drying of Sodium Sulfate Decahydrate Droplets

Sodium sulfate decahydrate droplets, which have 0.14 initial mass fraction of sodium sulfate (Na_2SO_4) in water, are dried at air temperatures of 90°C and 110°C [22]. Properties of decahydrate crystal are estimated using reference [8]. It is assumed that crystal water is not evaporated during drying. Model parameters used for drying at 90°C are given in Table 5.5.

Table 5.5 Parameters used for drying of a $Na_2SO_4 \cdot 10H_2O$ droplet at 90°C

Drying Parameters					
Parameter	**Value**	**Unit**	**Parameter**	**Value**	**Unit**
ρ_{solid} [8]	1464	kg/m^3	R_{in}	$7.438 \cdot 10^{-4}$	m
k_{solid} [8]	0.548	W/m.K	ε	0.842	-
Cp_{solid} [8]	1826	J/kg.K	$*Wt_{init}$	3.134	mg
ρ_{water} [14]	1000	kg/m^3	$*Wt_{crit}$	1.850	mg
k_{water} [14]	0.646	W/m.K	$*Wt_{final}$	0.400	mg
Cp_{water} [14]	4185	J/kg.K	V_{air}	1.00	m/s
$R_{out}(t = 0)$	$8.954 \cdot 10^{-4}$	m	H_{air}	0.01	$kg_{wv}/kg_{dry\ air}$
Constant Rate Numerical Parameters			**Falling Rate Numerical Parameters**		
Parameter	**Value**	**Unit**	**Parameter**	**Value**	**Unit**
Δt	1.0	s	(δt)	$1.0 \cdot 10^{-6}$	s
$(\delta\xi)$	$1.0 \cdot 10^{-6}$	-	Φ_s	0.1 %	-
Φ_ξ	0.05 %	-	Φ_T	$1.0 \cdot 10^{-10}$ %	-

* independent parameters

Weight history of a sodium sulfate decahydrate droplet dried at 90°C is given in Figure 5.17. Vertical axis gives dimensionless droplet weight and horizontal axis gives time. It is observed that the experimental drying rate drastically decreases as drying proceeds. Experimentation [22] on drying of sodium sulfate decahydrate droplets shows that solid crust formed in the falling rate period has a dense and relatively less porous structure, which creates an additional resistance to flow of water vapor. The resistance to vapor flow probably causes the drying rate decrease sharply in the falling rate period (Figure 5.17). Contrarily, model predictions do not represent such a significant decrease in drying rates. This occurs probably because of the high porosity value (0.842) used by the model.

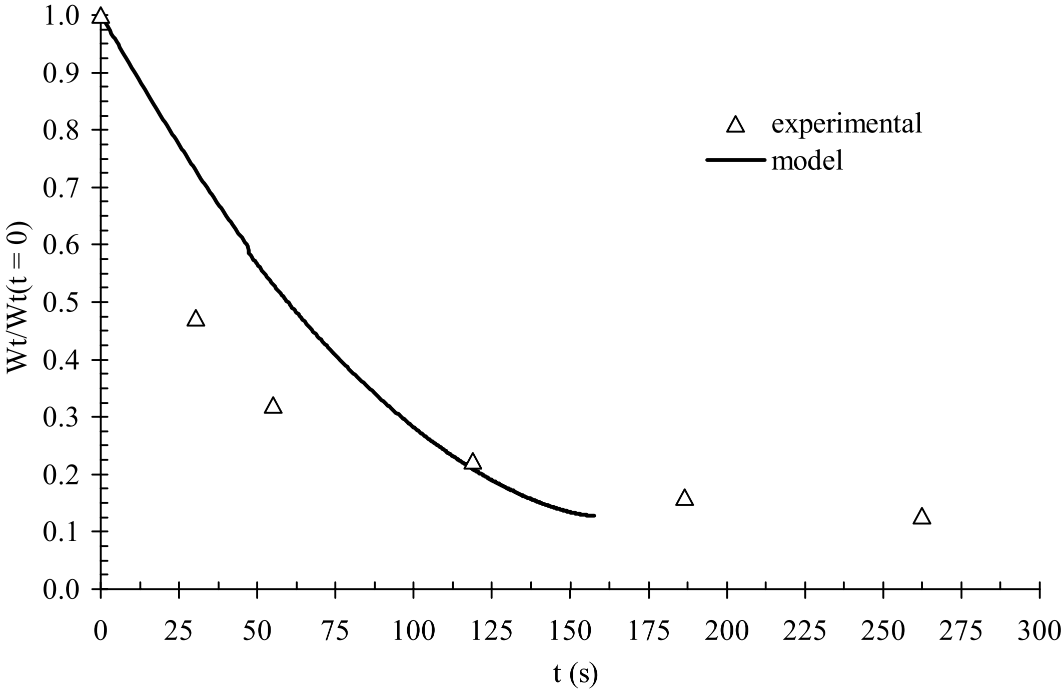

Figure 5.17 Weight history of a $Na_2SO_4 \cdot 10H_2O$ droplet dried at 90°C

It is observed in Figure 5.17 that the model fails to predict the weight history of the droplet dried at 90°C. In constant rate period, predictions of the evaporation rate of water are smaller that the actual case. This occurs probably because the temperature of the droplet increases gradually in the constant rate period (Figure 5.18), while calculated average droplet temperature is kept constant at the wet-bulb temperature. Further, decahydrate crystals melt at 34°C and form anhydrous sulfate solution [8]. Upon evaporation of water, droplet temperature decreases and decahydrate crystals are reformed. Due to this melting and re-crystallization process different hydrates are formed, which probably changes the density of the solid content of the droplet. This unique property of decahydrate crystals can also be the cause for the deviation of the predicted droplet weight values from the experimental measurements in the falling rate period (Figure 5.17).

Figure 5.18 gives model predictions and the experimental temperature measurements of drying of a sodium sulfate decahydrate droplet at 90°C. It is observed in Figure 5.18 that experimental temperature measurements gradually increase in constant rate period, contrary to what has been observed in drying of colloidal silica and skimmed milk droplets. As the droplet loses moisture in constant rate period, concentration of decahydrate crystals increases [22], which directly increases the vapor pressure depression effect, which could be a reason for the gradual increase of experimental temperature measurements in the constant rate period. Contrarily, calculated average temperature values do not change significantly in constant rate period probably because the model does not take into account the effect of vapor pressure depression.

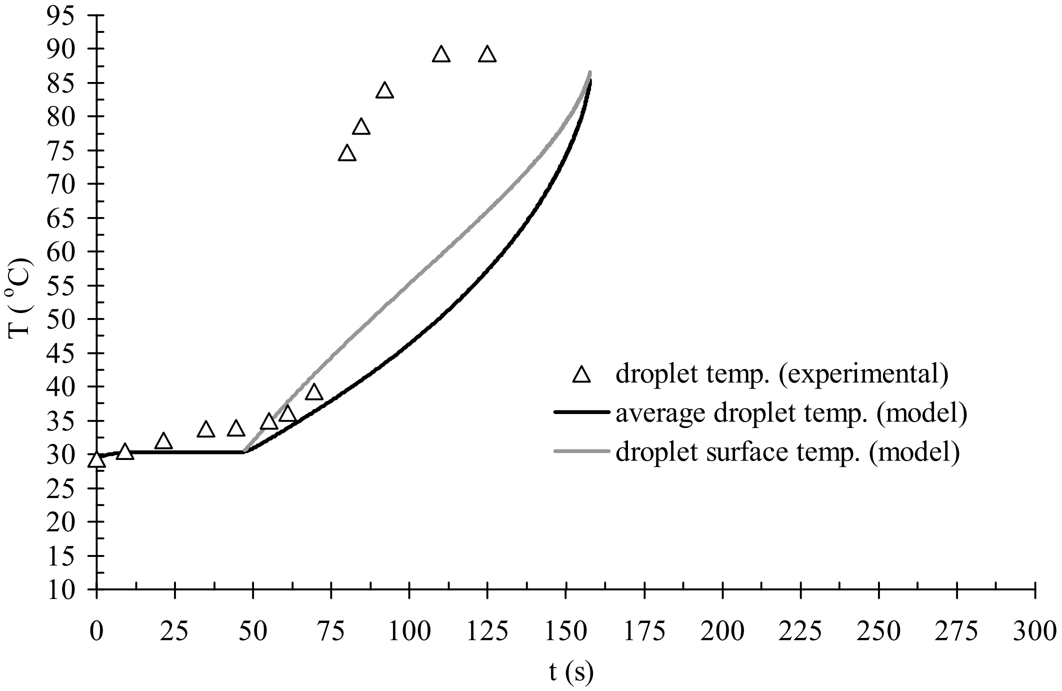

Figure 5.18 Temperature history of a $Na_2SO_4 \cdot 10H_2O$ droplet dried at 90°C

In the falling rate period, experimental temperature measurements increase sharply (Figure 5.18) probably because of the formation of a rigid dry crust [22]. However, model predictions do not show such an increase of average droplet temperature probably since the model uses a high porosity value of 0.842. Similarly, average droplet temperature and the predicted surface temperature significantly differ, since a low thermal conductivity value of the dry crust (0.089 W/m.K) creates a large crust heat transfer resistance.

It is observed in Figure 5.18 that the model predictions deviate significantly from the experimental measurements. During the course of drying, evaporation rates are calculated using the vapor pressure expression of pure water, which could be the main reason for model calculations being significantly different from experimental measurements. Predicted temperature and concentration profiles are also shown in Figures 5.19&20, respectively.

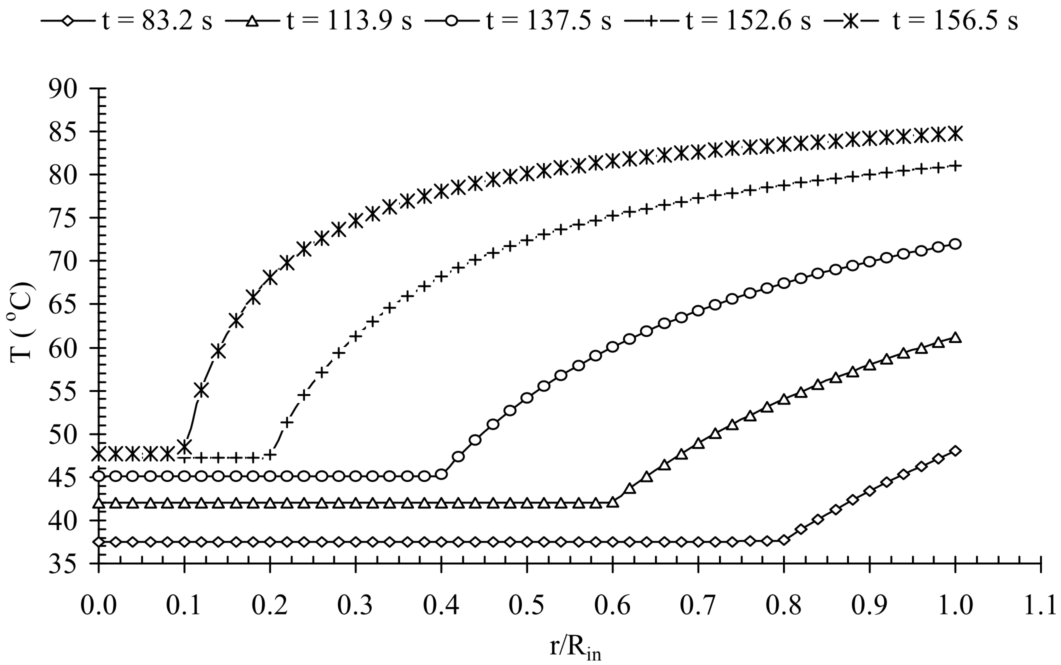

Figure 5.19 Temperature profiles of a $Na_2SO_4 \cdot 10H_2O$ droplet dried at 90°C

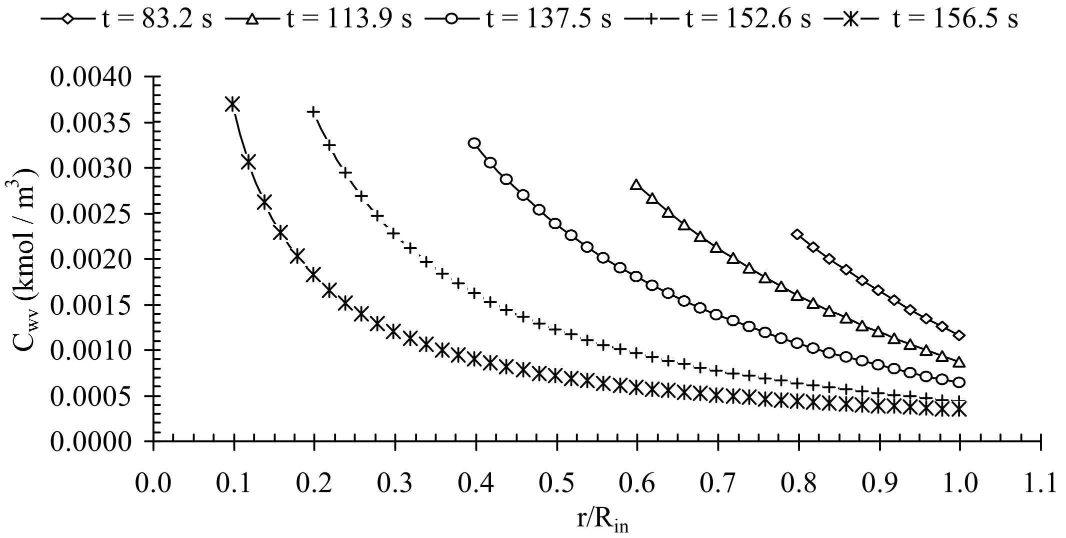

Figure 5.20 Concentration profiles of a $Na_2SO_4 \cdot 10H_2O$ droplet dried at 90°C

Model parameters used for drying of a $Na_2SO_4 \cdot 10H_2O$ droplet at 110°C are shown in Table 5.6. The model uses a higher porosity value of 0.935 compared to the value of the porosity (0.842) used for drying at air temperature of 90°C.

Table 5.6 Parameters used for drying of a $Na_2SO_4 \cdot 10H_2O$ droplet at 110°C

Drying Parameters					
Parameter	**Value**	**Unit**	**Parameter**	**Value**	**Unit**
ρ_{solid} [8]	1464	kg/m^3	R_{in}	$8.052 \cdot 10^{-4}$	m
k_{solid} [8]	0.549	W/m.K	ε	0.935	-
Cp_{solid} [8]	1828	J/kg.K	$*Wt_{init}$	3.300	mg
ρ_{water} [14]	1000	kg/m^3	$*Wt_{crit}$	2.252	mg
k_{water} [14]	0.668	W/m.K	$*Wt_{final}$	0.207	mg
Cp_{water} [14]	4190	J/kg.K	V_{air}	1.00	m/s
$R_{out}(t = 0)$	$9.175 \cdot 10^{-4}$	m	H_{air}	0.01	$kg_{wv}/kg_{dry\ air}$
Constant Rate Numerical Parameters			**Falling Rate Numerical Parameters**		
Parameter	**Value**	**Unit**	**Parameter**	**Value**	**Unit**
Δt	1.0	s	(δt)	$5.0 \cdot 10^{-6}$	s
$(\delta \xi)$	$1.0 \cdot 10^{-6}$	-	Φ_s	0.1 %	-
Φ_ξ	0.05 %	-	Φ_T	$1.0 \cdot 10^{-10}$ %	-

* independent parameters

Weight history of a $Na_2SO_4 \cdot 10H_2O$ droplet dried at air temperature of 110°C is shown in Figure 5.21. Similar to what has been observed in drying at 90°C, experimental evaporation rate significantly decreases as drying proceeds due to formation of a rigid crust layer [22]. However, model predictions do not represent such a decrease in drying rate (Figure 5.21). Model results also deviate significantly from experimental measurements because of the similar reasons mentioned for drying at air temperature of 90°C.

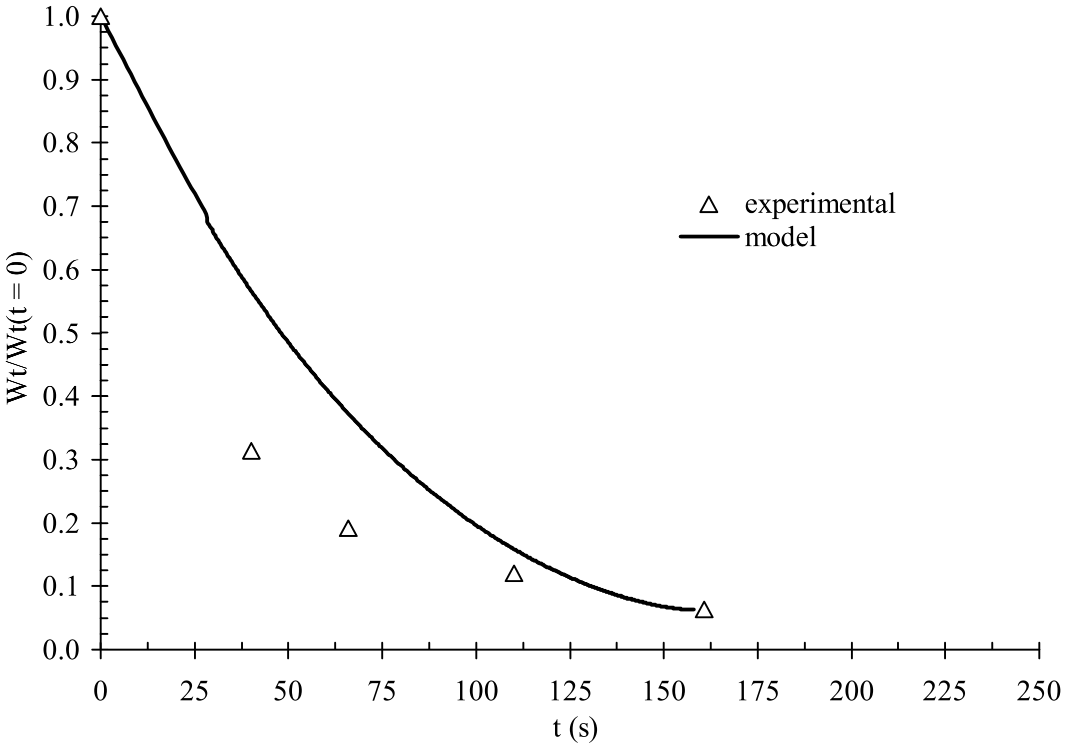

Figure 5.21 Weight history of a $Na_2SO_4 \cdot 10H_2O$ droplet dried at 110°C

Figure 5.22 gives model predictions and the experimental temperature measurements for drying of a sodium sulfate decahydrate droplet at 110°C. Similar to what has been observed in drying at 90°C, experimental measurements gradually increase in constant rate period due to increasing effect of solid-liquid interactions [8,22]. In the falling rate period, temperature measurements of the droplet sharply increase, since the dry crust layer is has a dense non-porous structure [22]. Average temperature of the droplet shows slight variations in constant rate period. Since the model uses a high porosity value (0.935), both average droplet temperature and the surface temperature of the droplet do not sharply increase in falling rate period. Similarly, a respectively higher difference between average and surface temperature of the droplet could be the result of using a very high porosity value in calculations (0.842 for drying at 90°C and 0.935 for drying at 110°C).

It is also observed in Figure 5.22 that the model predictions and the experimental measurements are not in good agreement both in constant and falling rate periods. Similar discussion, which is held for drying at 90°C, is also valid for drying at air temperature of 110°C. Predicted temperature and concentration profiles for drying of a $Na_2SO_4 \cdot 10H_2O$ droplet at 110°C are also given in Figures 5.23&24.

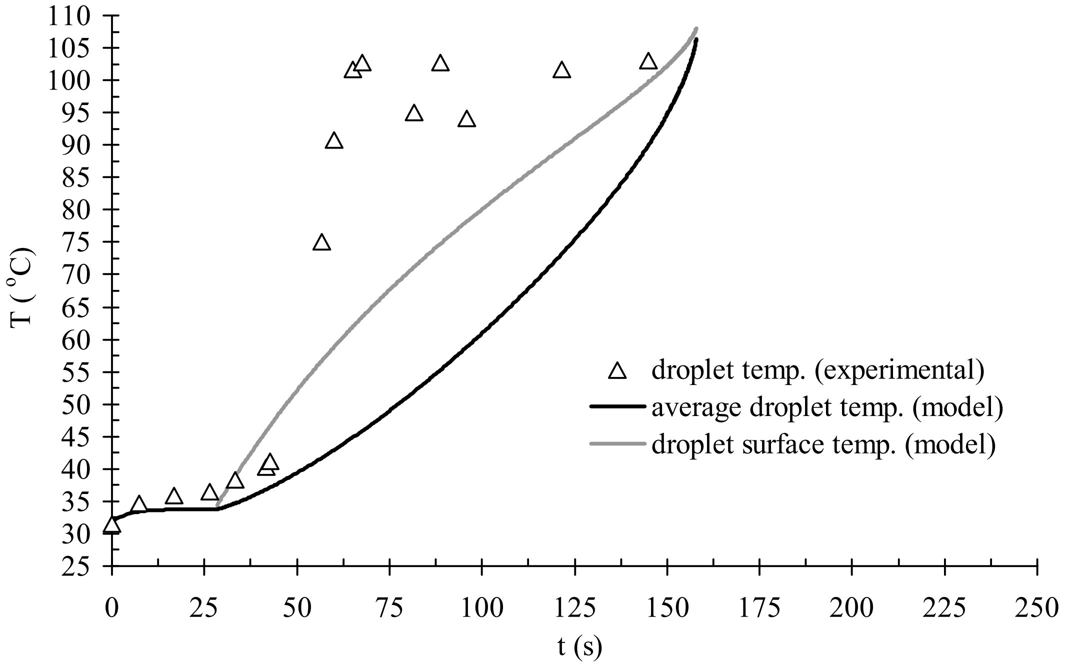

Figure 5.22 Temperature history of a $Na_2SO_4 \cdot 10H_2O$ droplet dried at 110°C

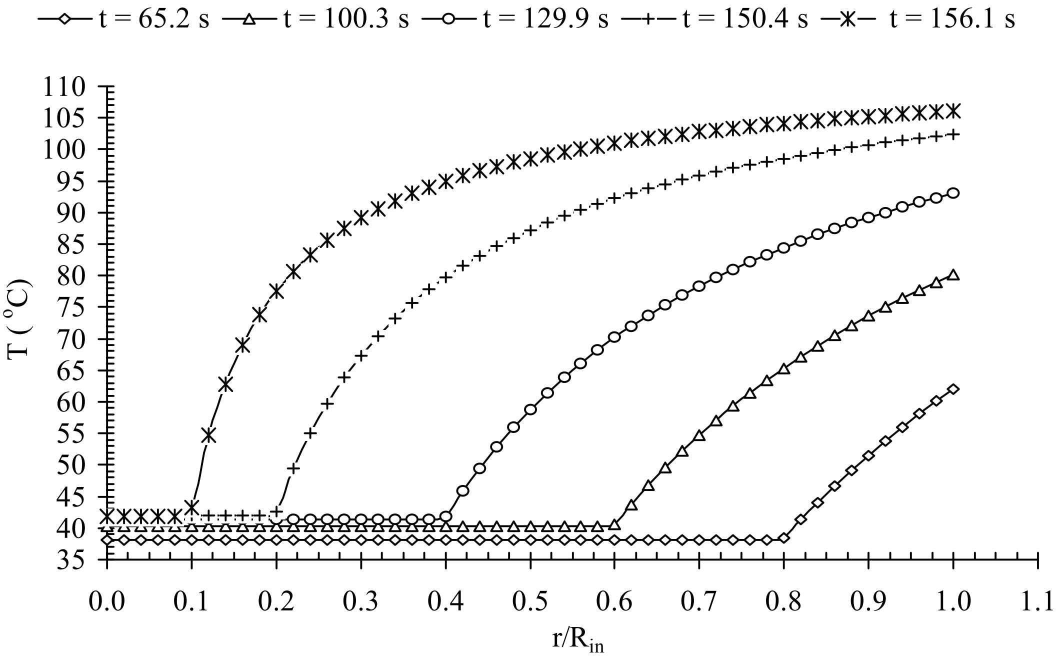

Figure 5.23 Temperature profiles of a $Na_2SO_4 \cdot 10H_2O$ droplet dried at 110°C

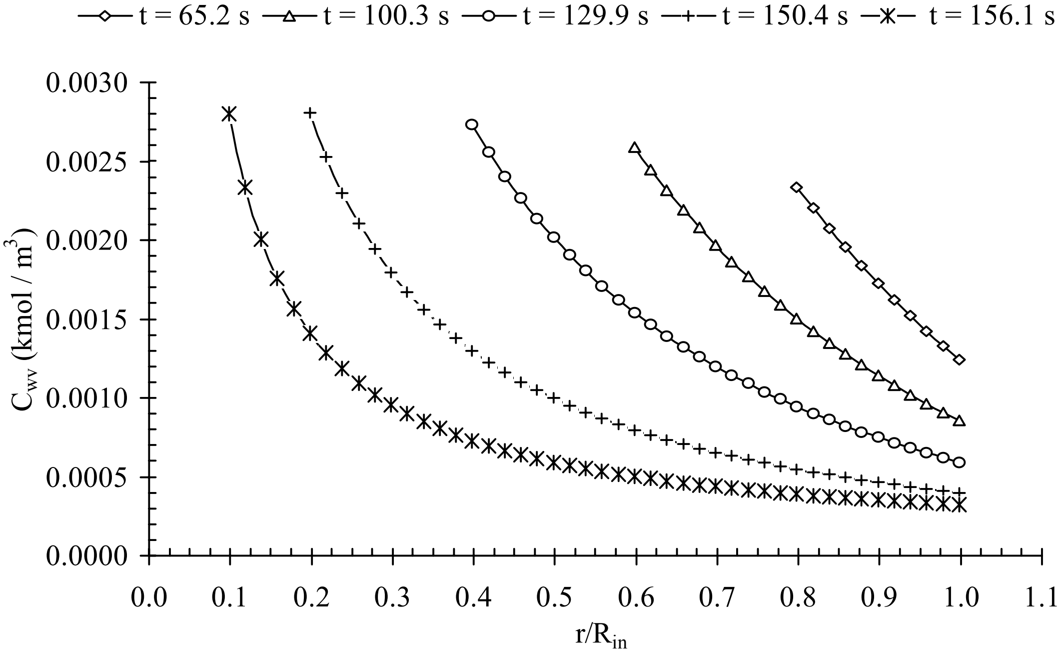

Figure 5.24 Concentration profiles of a $Na_2SO_4 \cdot 10H_2O$ droplet dried at 110°C

5.4 Drying & Numerical Model Parameters

There are a number of drying and numerical parameters that the model utilizes in predicting both temperature and concentration profiles of the droplets. Three adjustable drying parameters that the model uses are the outer radius of the droplet $R_{out}(t = 0)$, inner radius of the droplet R_{in} and the porosity ε, which are all calculated based on the experimental droplet weight measurements with a proper critical weight estimation. An improper estimation of the critical weight significantly changes the duration of the constant rate period (Figure 5.26) and although the effect of an improper choice is not clearly observed in droplet weight predictions (Figure 5.25), droplet temperature predictions (Figure 5.26) deviate drastically from experimental measurements, especially in the falling rate period. Thus, the critical weights of droplets in all of the runs are chosen that will yield best fits of the model predictions to experimental measurements [22]. Since similar effects are observed in all of the runs, the effect of different choices of critical weight is shown only for drying of a skimmed milk droplet at 50°C (Figures 5.25&26).

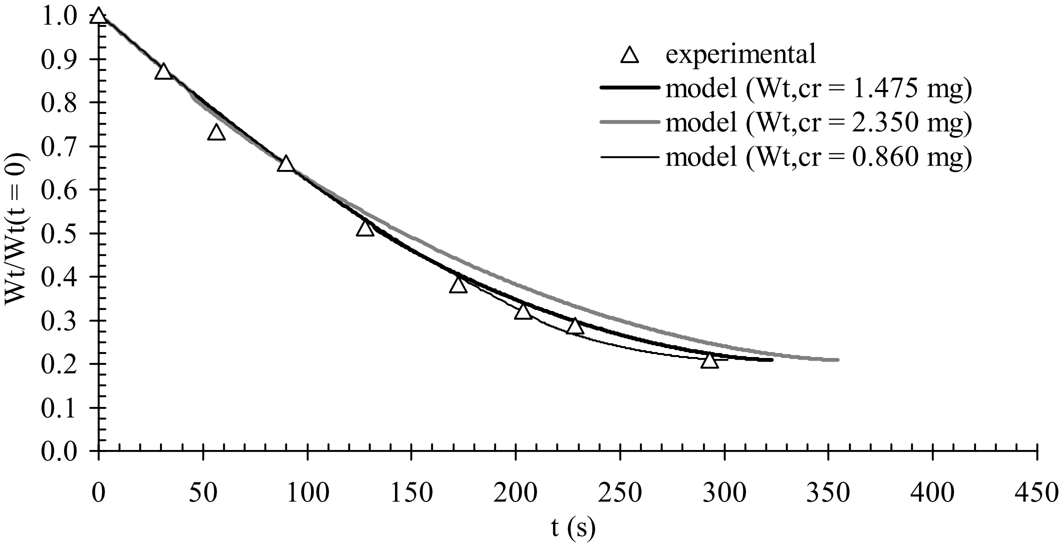

Figure 5.25 Effect of different critical weight choices on weight history

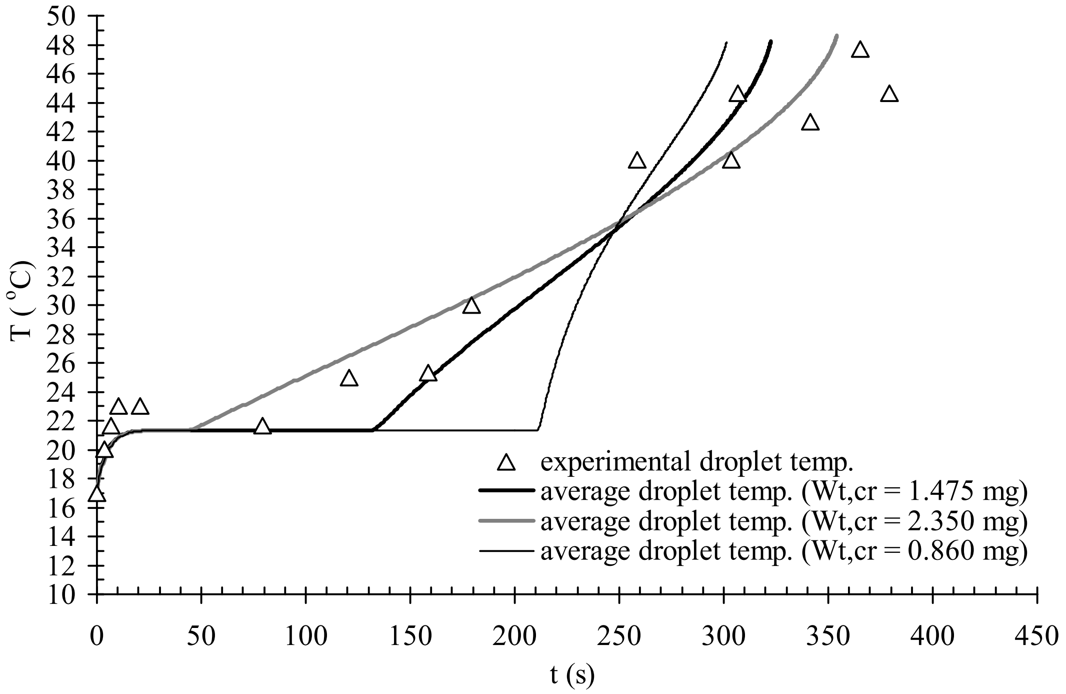

Figure 5.26 Effect of different critical weight choices on temperature history

Table 5.7 Comparison of experimental and predicted droplet diameters

Dried Material	**Temperature (°C)**	**$D_{experimental}$ (mm)**	**$D_{predicted}$ (mm)**	**$\Delta D/D_{experimental}$**
Colloidal Silica	101	2.06	1.89	0.083
Colloidal Silica	178	2.00	1.86	0.070
Skimmed Milk	50	1.76	1.79	-0.017
Skimmed Milk	90	1.71	1.84	-0.076
$Na_2SO_4 \cdot 10H_2O$	90	1.46	1.75	-0.199
$Na_2SO_4 \cdot 10H_2O$	110	1.85	1.67	0.097

Table 5.7 above gives the experimental [22] and the predicted droplet diameters, where $D_{predicted}$ is calculated using the value of $R_{out}(t = 0)$. It is observed that, except for the sodium sulfate decahydrate droplets, predicted droplet diameters are close to experimental measurements, which indicates that the critical weights of the droplets

are chosen properly. Similarly, the other two adjustable drying parameters of the model R_{in} and ε are calculated using the estimated value of the critical weight.

There are three numerical parameters that the model uses for the constant rate period, which are the time step Δt, incremental change, $(\delta\xi)$, in dimensionless outer radius of the droplet $\xi_{out}(t)$ and the termination criterion, Φ_ξ, of the loop to predict the position of the dimensionless outer radius. Since the model utilizes an implicit numerical solution technique, the choice of Δt is arbitrary. However, an improper choice of $(\delta\xi)$ directly changes the error in predicting the position of $\xi_{out}(t)$ and the calculations are not carried out within the error bound prescribed by Φ_ξ. The choice of $(\delta\xi)$ in the order of 10^{-6} has generated results having the errors in the order of 1 %.

The model utilizes three numerical parameters for the falling rate period calculations, which are the incremental time (δt), termination criterion, Φ_s, of the loop to predict the dimensionless interface position $s'(t)$, and the termination criterion, Φ_T, of the loop to predict the interface temperature T_M. When choosing the values for (δt), Φ_s and Φ_T in calculations, the relationship of these parameters shown in Figure 5.27 is taken into account. The arrows in Figure 5.27 show how the proper choices of the parameters affect each other. In order to predict the interface position within an error bound in the order of 0.1 %, (δt) should be in the order of 10^{-6} s. Similarly, the error bound of the predictions of interface temperature should be in the order of 10^{-10} %. If, either (δt) or Φ_T is improperly chosen, the interface position calculations will not be within the error bound specified by Φ_s. Similarly, same rule applies between (δt) and Φ_T, and (δt) and Φ_s (Figure 5.27).

Φ_T is chosen to be in the order of 10^{-10} %. Such a high accuracy is required since the concentration of water vapor at interface position, which is in the order of 10^{-2} to10^{-3} kmol/m^3, is directly calculated using the interface temperature T_M.

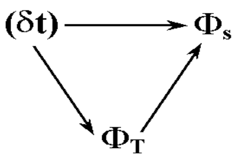

Figure 5.27 Relationship of the falling rate numerical parameters

5.5 Comparison of Different Model Results

The results of the new model developed are compared with other available model results [11,22]. Figures 5.28-39 give the comparison of the new model predictions with the model results of Nesic&Vodnik [22], where the experimental measurements are obtained from reference [22]. Similarly, in Figures 5.40-43, the comparison of the new model predictions with the model results of Farid [11] is given, where the experimental measurements are obtained from reference [21].

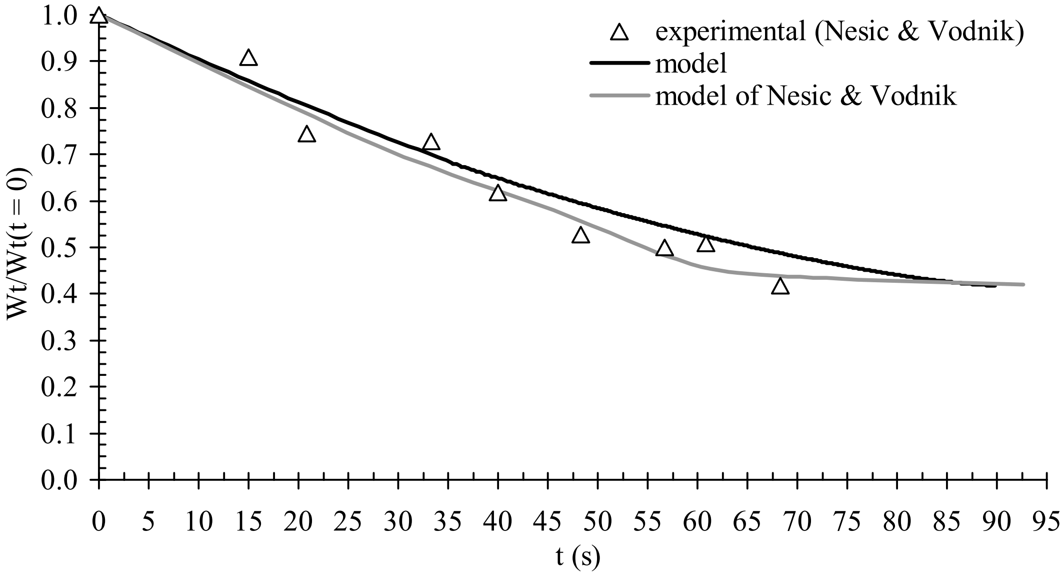

Figure 5.28 Predictions for weight history of a colloidal silica droplet at 101°C

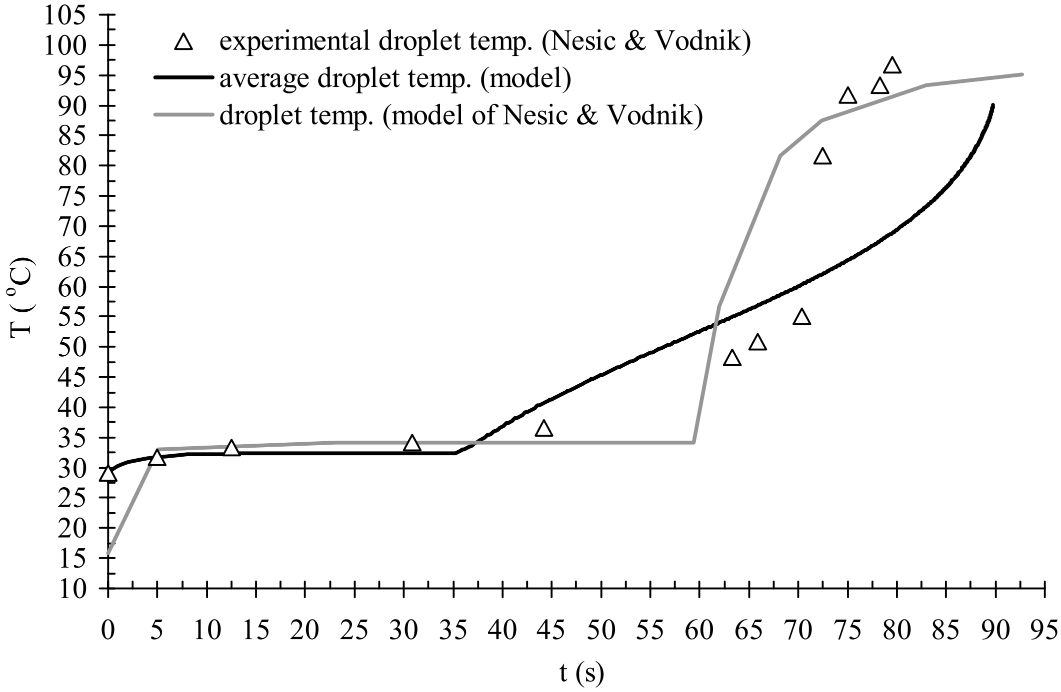

Figure 5.29 Predictions for temperature history of a colloidal silica droplet at 101°C

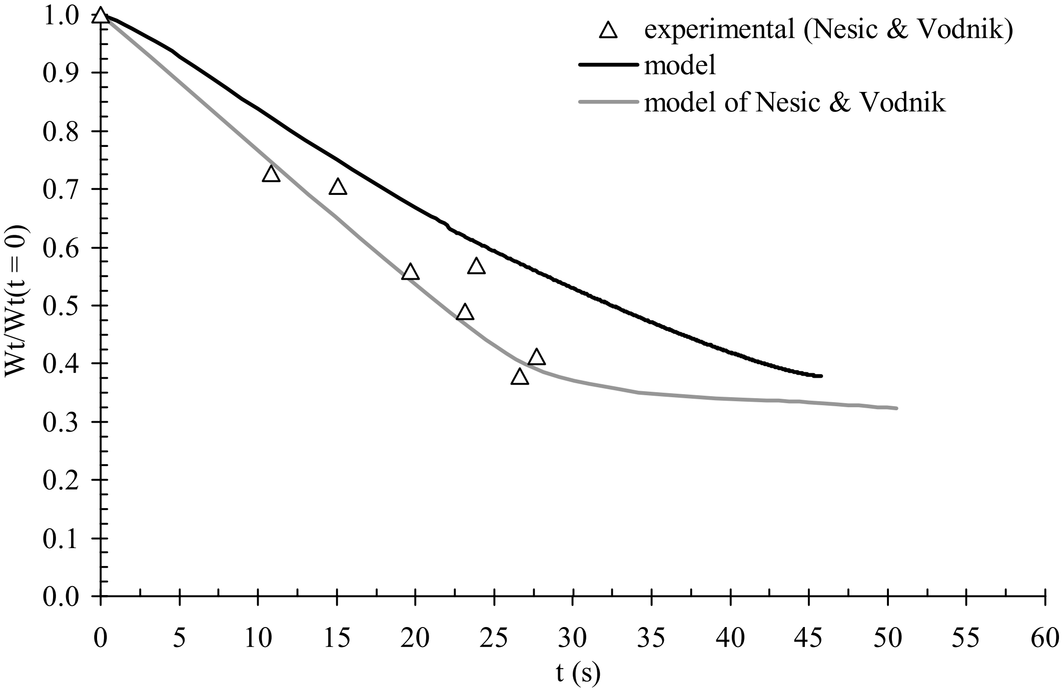

Figure 5.30 Predictions for weight history of a colloidal silica droplet at 178°C

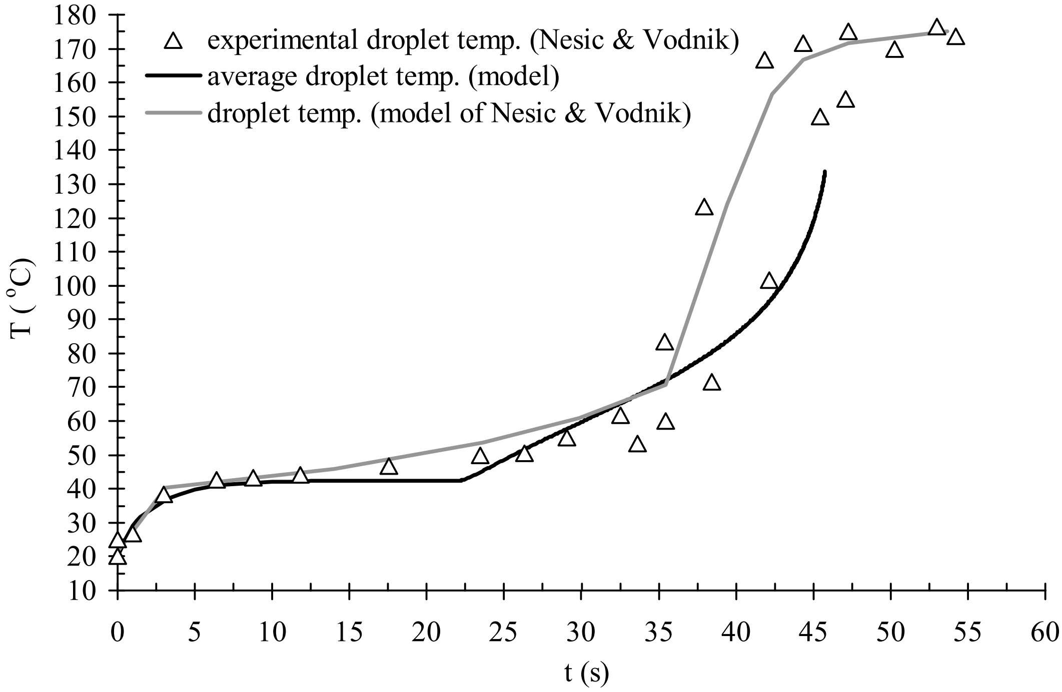

Figure 5.31 Predictions for temperature history of a colloidal silica droplet at 178°C

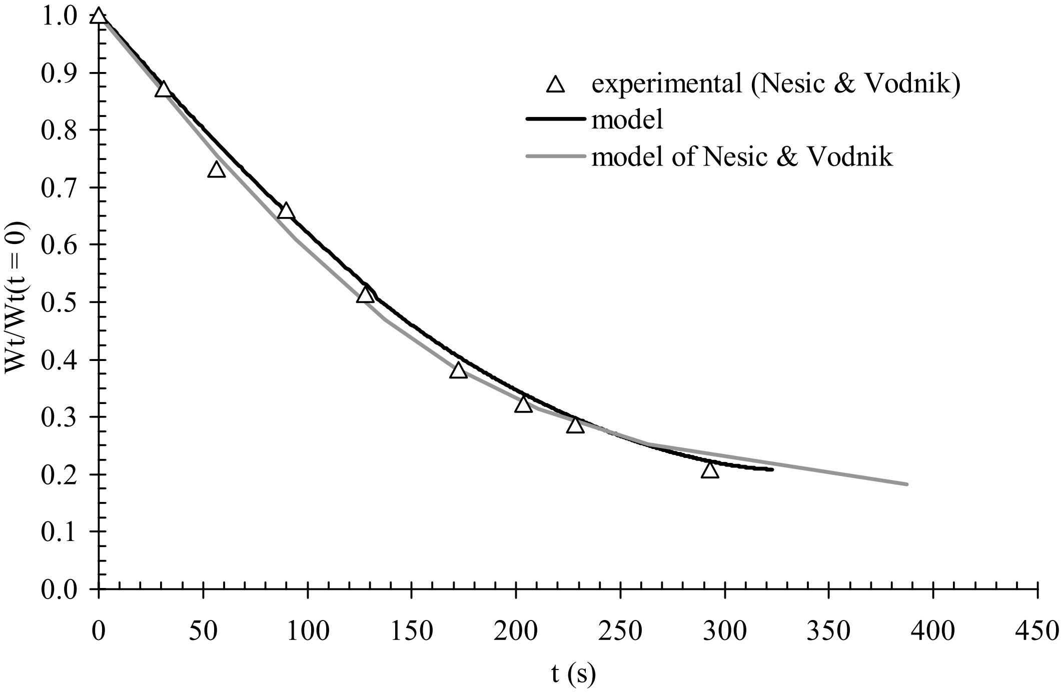

Figure 5.32 Predictions for weight history of a skimmed milk droplet at 50°C

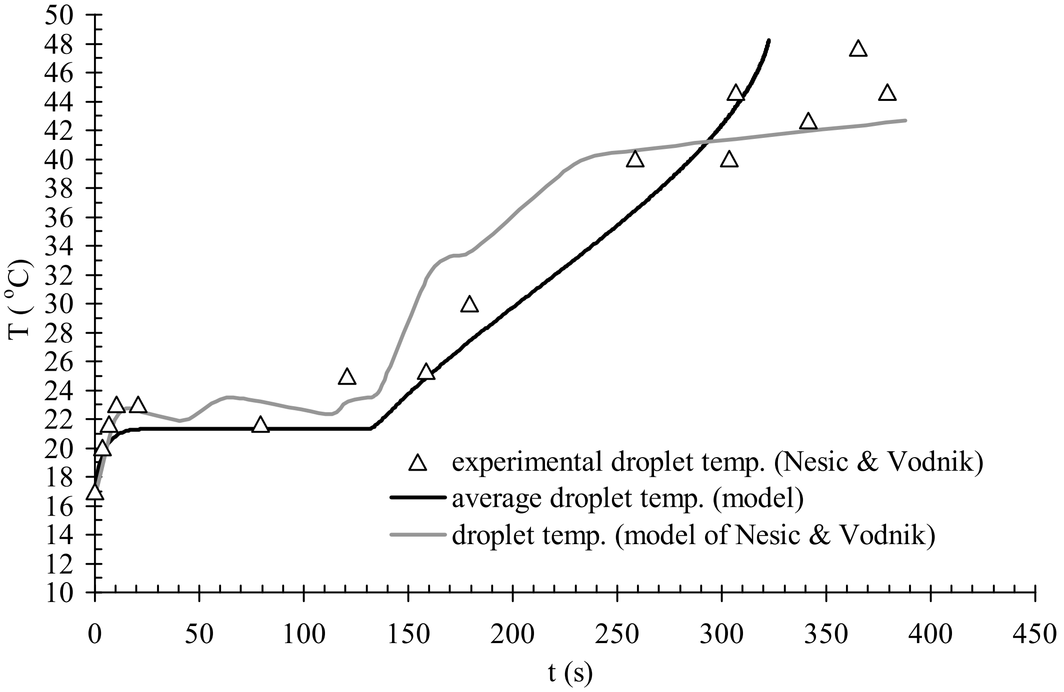

Figure 5.33 Predictions for temperature history of a skimmed milk droplet at 50°C

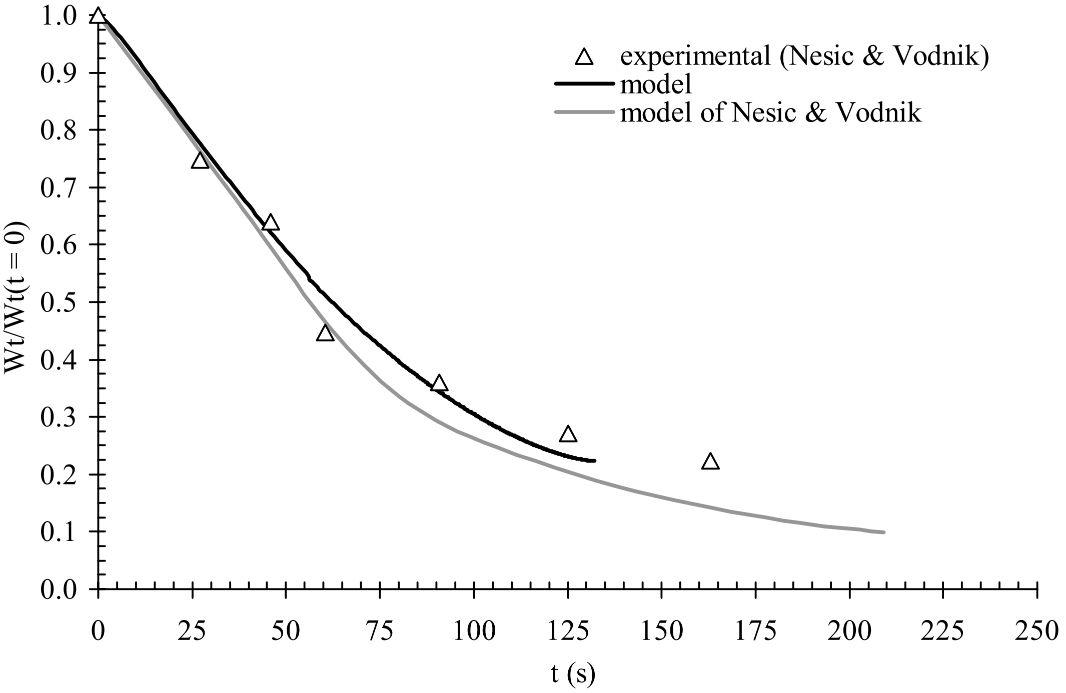

Figure 5.34 Predictions for weight history of a skimmed milk droplet at 90°C

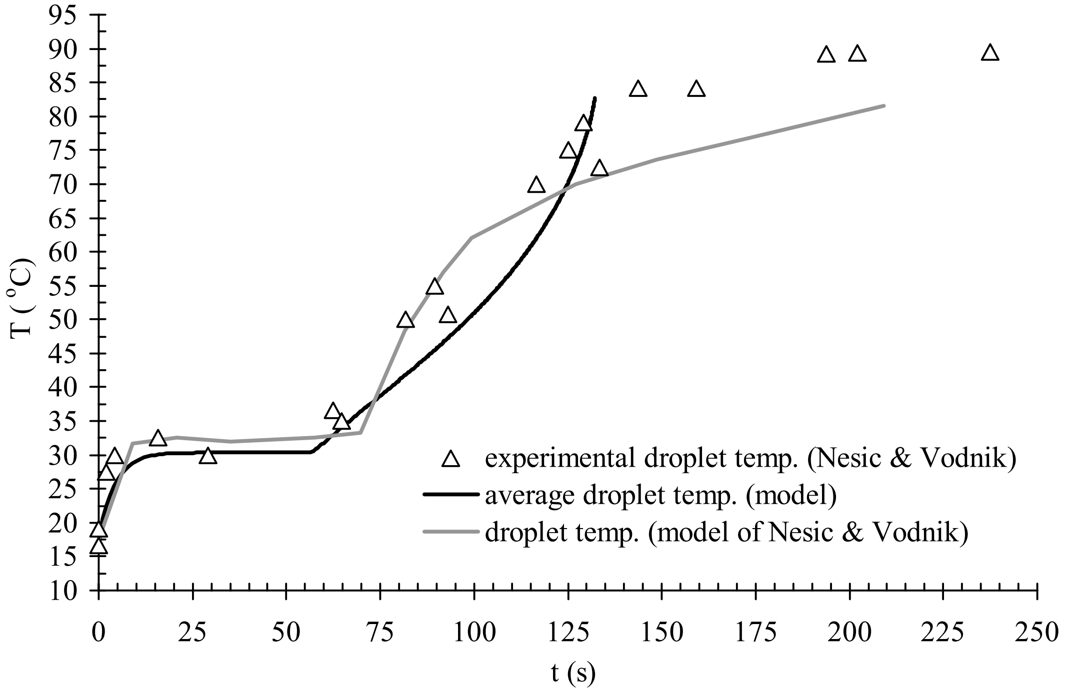

Figure 5.35 Predictions for temperature history of a skimmed milk droplet at 90°C

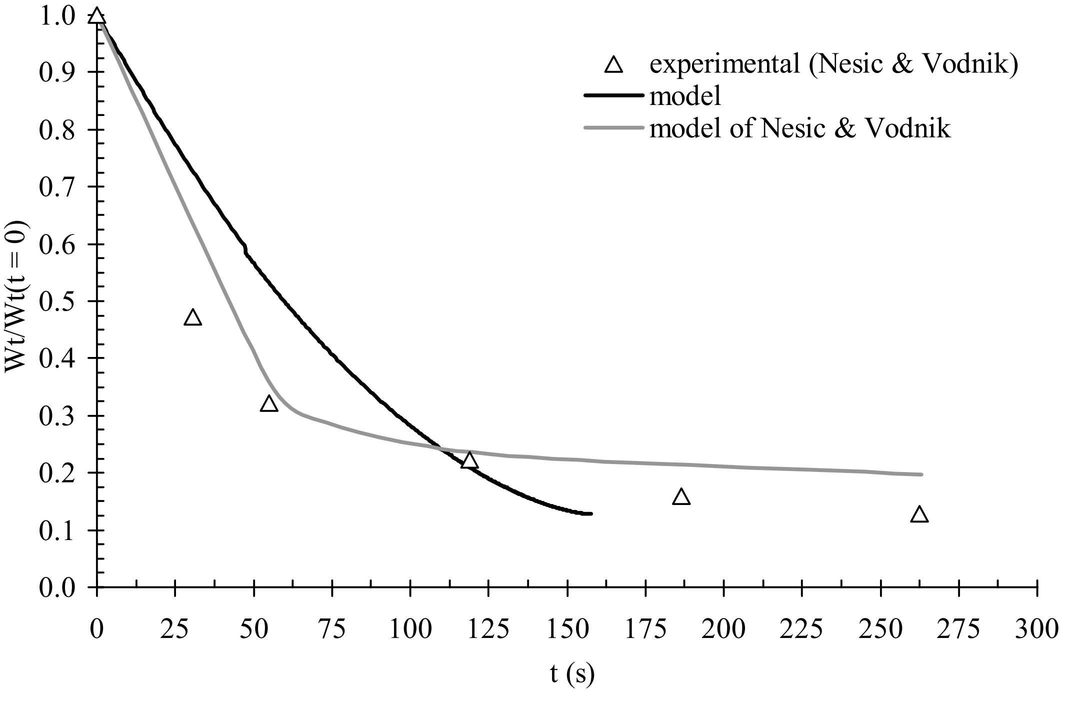

Figure 5.36 Predictions for weight history of a $Na_2SO_4 \cdot 10H_2O$ droplet at 90°C

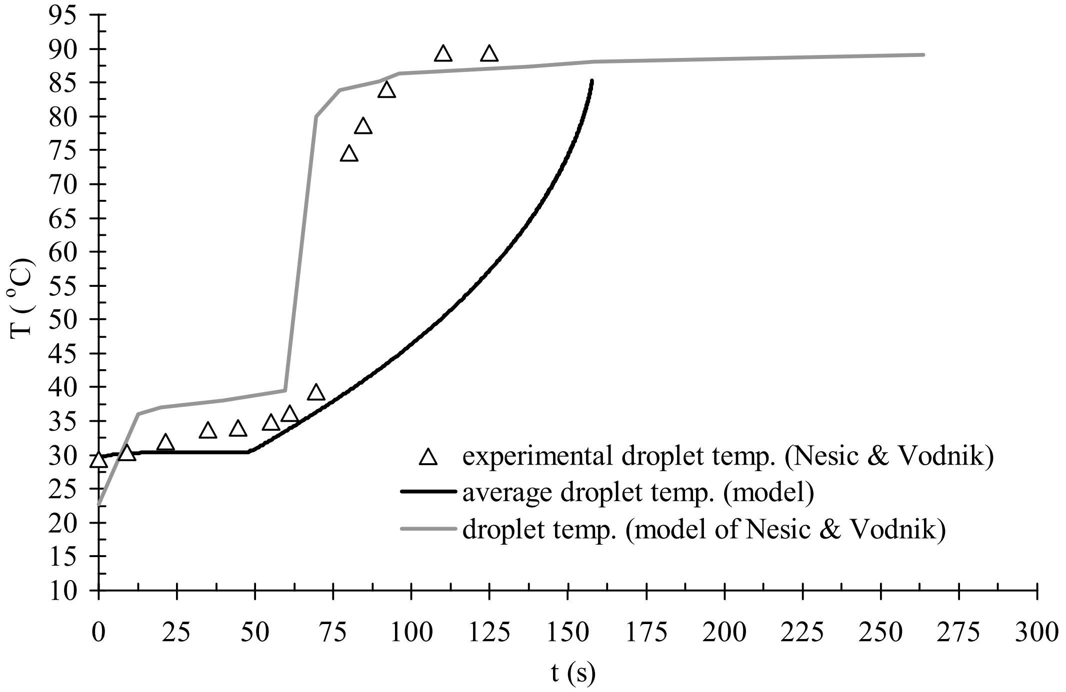

Figure 5.37 Predictions for temperature history of a $Na_2SO_4 \cdot 10H_2O$ droplet at 90°C

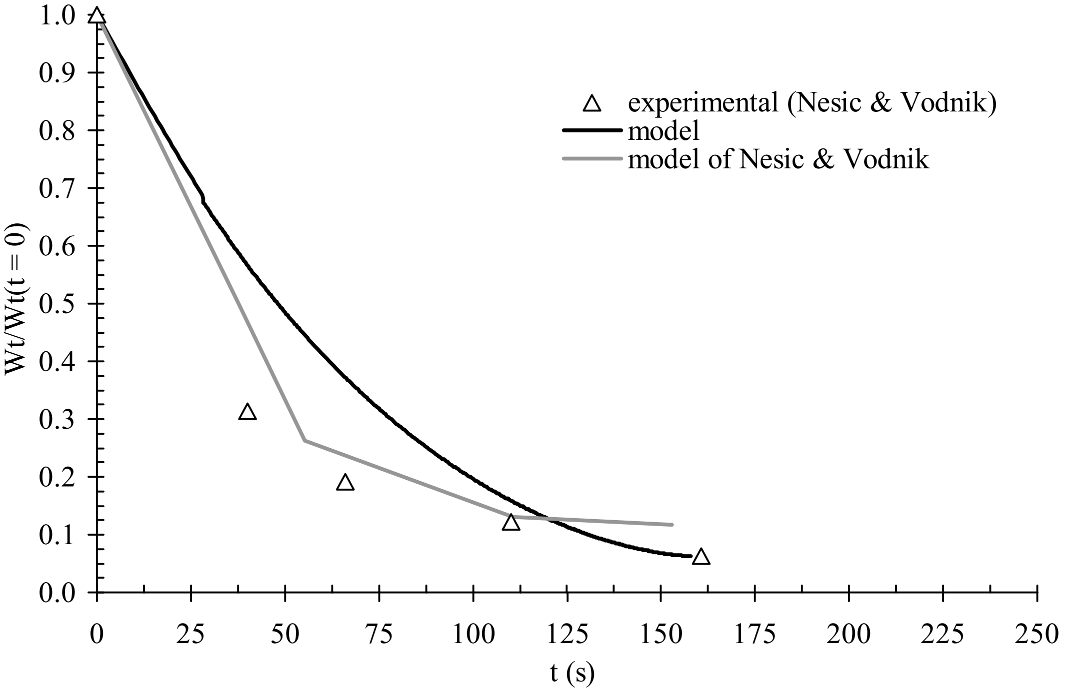

Figure 5.38 Predictions for weight history of a $Na_2SO_4 \cdot 10H_2O$ droplet at 110°C

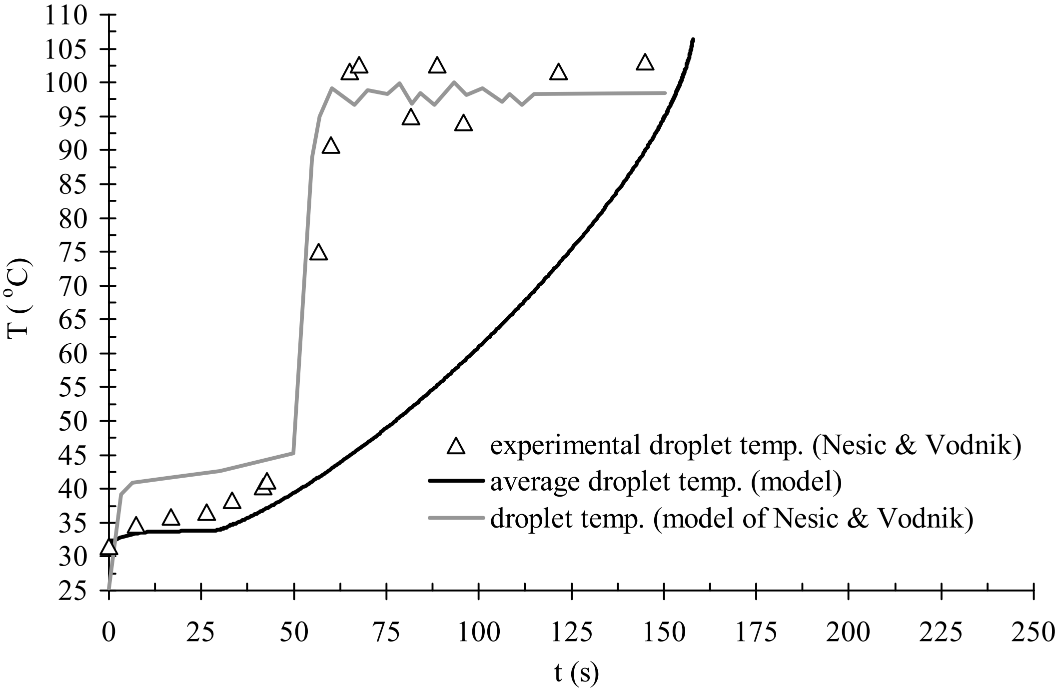

Figure 5.39 Predictions for temperature history of a $Na_2SO_4 \cdot 10H_2O$ droplet at 110°C

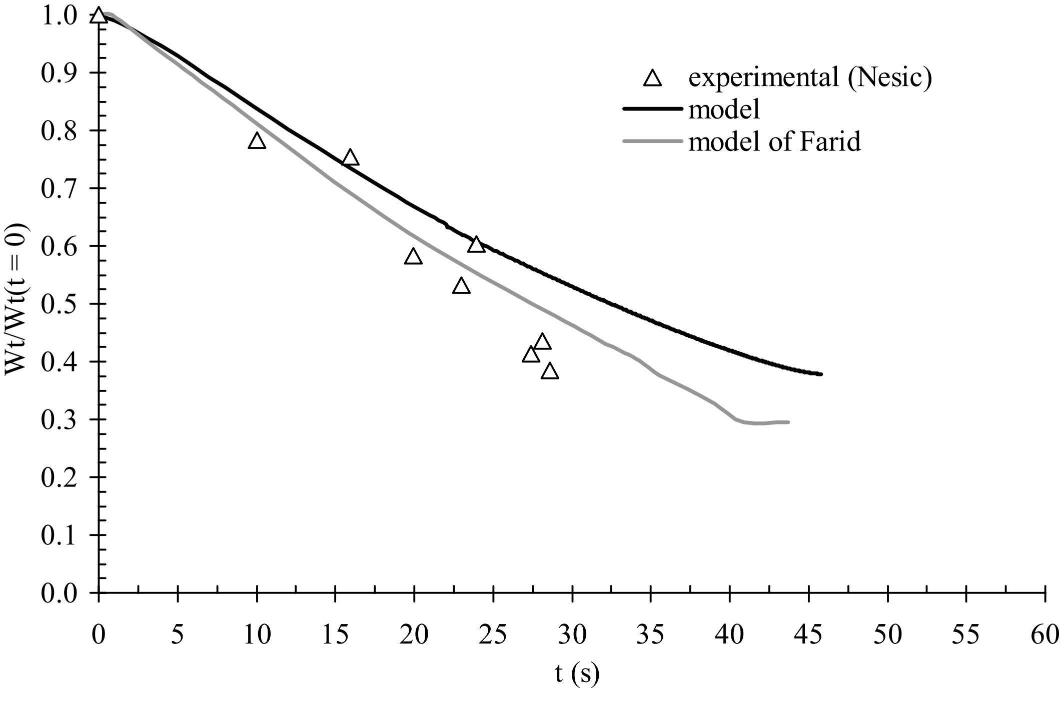

Figure 5.40 Results for weight history of a colloidal silica droplet at 178°C

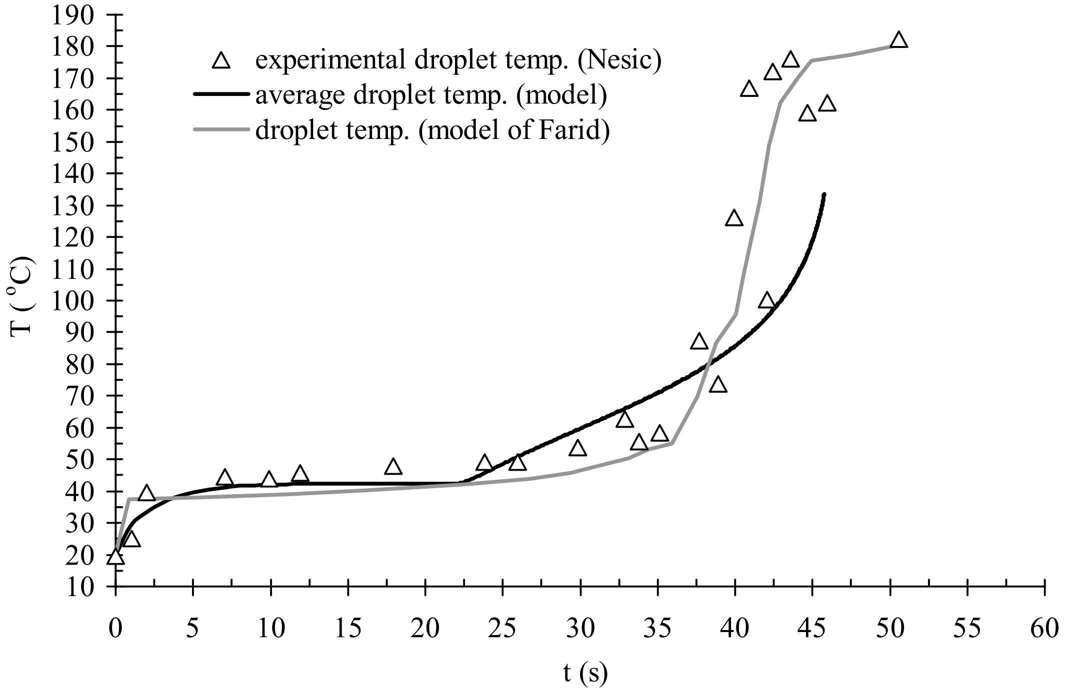

Figure 5.41 Results for temperature history of a colloidal silica droplet at 178°C

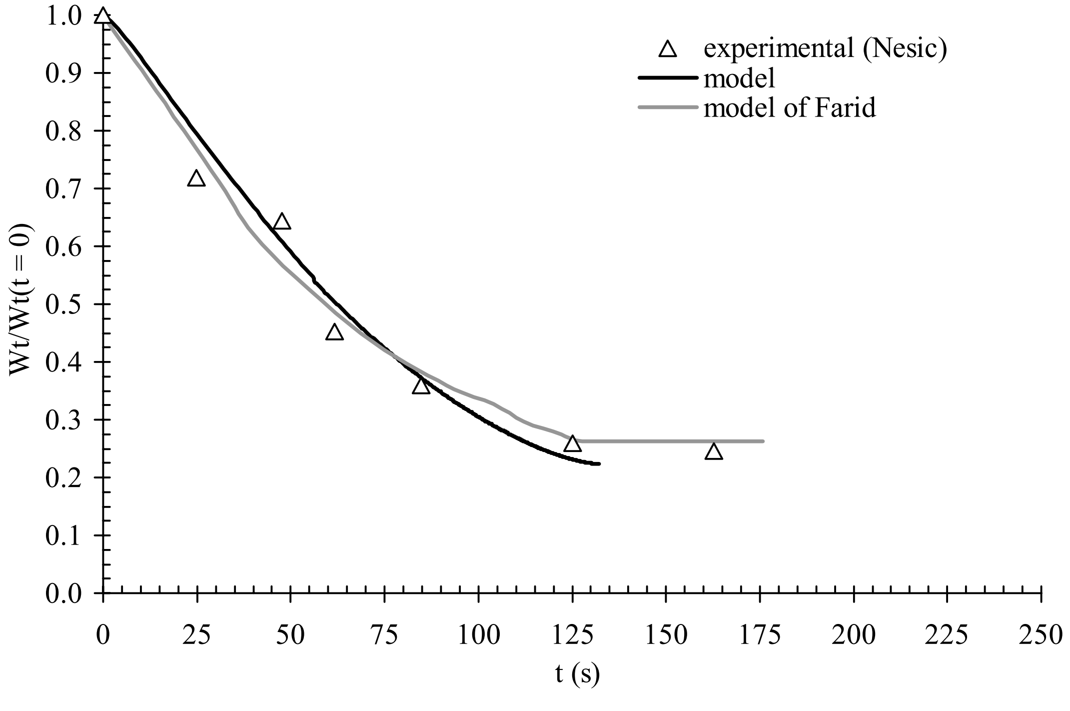

Figure 5.42 Results for weight history of a skimmed milk droplet at 90°C

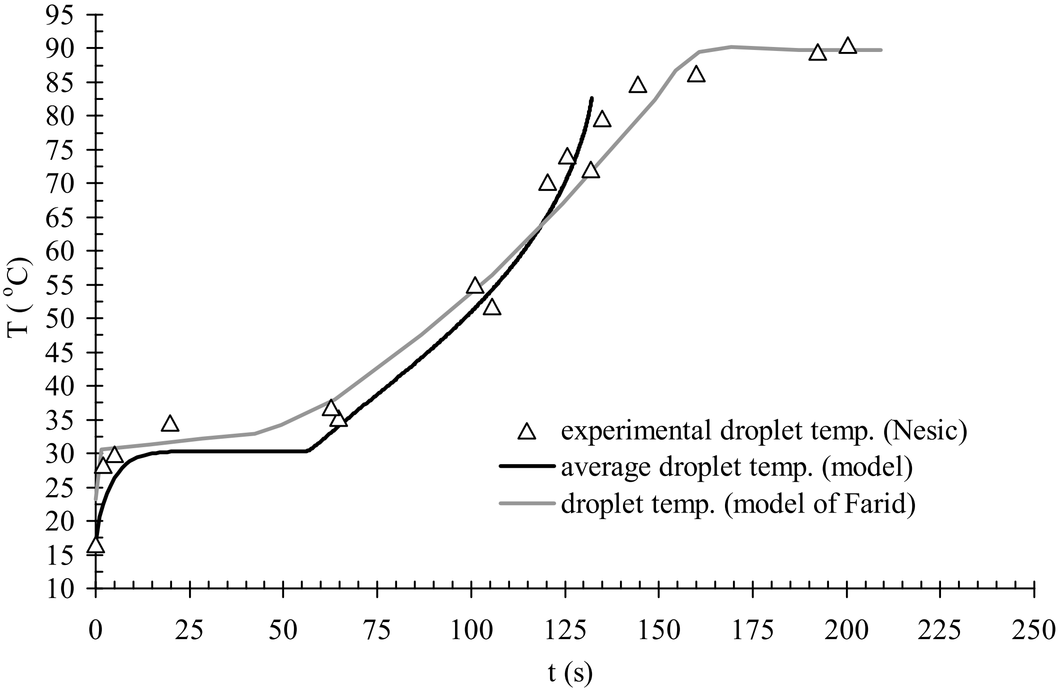

Figure 5.43 Results for temperature history of a skimmed milk droplet at 90°C

CHAPTER 6

CONCLUSION

It is aimed to describe the drying behavior of a single droplet both in constant and falling rate periods using receding evaporation front approach coupled with the utilization of heat and mass transfer equations. Fick's law of diffusion and Fourrier's law of conduction with effective coefficients are used to describe mass and heat transfer, respectively. A special attention is addressed to develop two different numerical solution methods, namely the Variable Grid Network (VGN) algorithm for constant rate period and the Variable Time Step (VTS) algorithm for falling rate period, with the requirement of moving boundary analysis. For the assessment of the validity of the model, experimental [22] weight and temperature histories of colloidal silica (SiO_2), skimmed milk and sodium sulfate decahydrate ($Na_2SO_4 \cdot 10H_2O$) droplets are compared with the model predictions. Further, proper choices of the numerical parameters are sought in order to have successful iteration loops.

Experimental weight histories of colloidal silica droplets show a unique behavior, in that drying rates observed in constant and falling rate periods do not change significantly. High value of dry crust thermal conductivity (0.596 W/m.K for both drying at 101^oC and 178^oC) is addressed for this unique behavior. Temperature histories [22], on the other hand, represent the traditional [3,8,22] behavior: an initial adjustment period followed by the slight variation of temperature in constant rate period and gradual increase of droplet temperature in the falling rate period.

The model successfully estimated both weight and temperature histories of colloidal silica droplets dried at air temperatures of 101^{o}C and 178^{o}C, except for a slight deviation of average droplet temperature from experimental measurements at the beginning of falling rate period and a significant deviation through the end of the falling rate period. Model's simplifying assumption of neglecting the transition period and the heating effect of the filament support [22] are addressed for these deviations, respectively.

Experimental weight and temperature histories of skimmed milk droplets show similar behavior to the one observed in drying of colloidal silica droplets with the exception that observed drying rates in constant and falling rate periods are quite different from each other. Respectively lower dry crust thermal conductivity (0.130 W/m.K for both drying at 50^{o}C and 90^{o}C) is addressed for the significant difference of drying rates.

The model successfully estimated both weight and temperature histories of skimmed milk droplets dried at air temperatures of 50^{o}C and 90^{o}C, except for a slight deviation of average droplet temperature from experimental measurements in constant rate period, where the assumption of negligible solid-liquid interactions is thought to be the reason for such a slight deviation.

Experimental weight and temperature histories of sodium sulfate decahydrate ($Na_2SO_4 \cdot 10H_2O$) droplets show quite unique behavior, in that observed drying rates in constant and falling rate periods drastically change. Similarly, contrary to what has been observed in drying of both colloidal silica and skimmed milk droplets, droplet temperature in constant rate period gradually increases, which is thought to be the result of increasing effect of solid-liquid interactions due to solvent loss. Formation of a rigid and non-porous dry crust [22] is addressed for the sharp increase of experimental [22] temperature readings and the drastic decrease of drying rate in falling rate period.

The model failed to estimate both weight and temperature histories of sodium sulfate decahydrate droplets dried at air temperatures of 90^{o}C and 110^{o}C. Using the vapor pressure expression of pure water, which neglects the non-idealities introduced by solid-liquid interactions, in model calculations and the model's underestimation of drastic changes occurring in droplet morphology [8] due to formation of different hydrates are thought to be the reasons of the model resulting poor estimations. However, the developed model gives the flexibility to use a proper vapor pressure expression without much effort for estimation of the drying history of droplets having highly soluble solids with strong solid-liquid interactions.

Initial droplet diameters, which were calculated based on the estimations of the critical droplet weights using experimental data, were predicted in the range of 1.5-2.0 mm, which are in good agreement with the experimental measurements.

It is concluded that the study has resulted a new reliable drying model that can be used to estimate the drying histories of different materials.

CHAPTER 7

RECOMMENDATIONS

One of the main objectives of this study is to develop a single droplet drying model that can be used as a part of the computational modeling of a typical spray drier. In conjunction with this objective, it is recommended that in order to use model independently, without any experimental data, to predict both weight and temperature histories of drying of a single droplet, an empirical correlation, which gives critical moisture content for different drying conditions, should be developed. Furthermore, the model should be improved to take into account the morphological changes occurring during drying, such as shrinkage of the droplet in the transition period. In addition, it is recommended to use a proper vapor pressure expression, which takes into account the solid-liquid interactions, in predicting both weight and temperature histories of droplets having highly soluble solids.

REFERENCES

[1]: Buckingham, E., U.S. Dept. Agr. Bur. Solids Bull., 38, (1907)

[2]: Ceaglske, N. H., Hougen, O. A., Trans. Am. Inst. Chem. Eng., 33, 283 (1937)

[3]: Charlesworth, D. H., Marshall, W. R., A.I.Ch.E. Journal, 6, 9 (1960)

[4]: Chen, P., Pei, D. C. T., Int. J. Heat Mass Transfer, 32, 297 (1989)

[5]: Chen, X. D., Xie,G. Z., Trans. Ins. Ch.E., Part C, 75, 213 (1997)

[6]: Chen, X. D., Farid, M. M., Reid, D., Fletcher, A., Pearce, D., Chen, N. X., CHEMECA 99, Newcastle, Australia, (1999)

[7]: Cheong, H. W., Jeffreys, G. V., Mumford, C .J., A.I.Ch.E. Journal, 32, 1334 (1986)

[8]: Cheong, H. W., Ph.D. Thesis, University of Aston in Birmingham, England, (1983)

[9]: Crank, J., Free and Moving Boundary Problems, Clarendon, Oxford, (1984)

[10]: Duffie, J. A., Marshall, W. R., Chem. Eng. Prog., 49, 417 (1953)

[11]: Farid, M. M., Chem. Eng. Sci., 58, 2985 (2003)

[12]: Gurr, C. G., Marshall, T. K., Hutton, J. T., Soil Sci., 74, 335 (1952)

[13]: Hamming, R. W., Numerical Methods for Scientists and Engineers, McGraw-Hill, New York, (1973)

[14]: Incropera, P. F., Dewitt, P. D., Fundamentals of Heat and Mass Transfer, Wiley, New York, (1996)

[15]: Keey, R. B., Drying of Loose and Particulate Materials, Hemisphere, New York, (1992)

[16]: Kuzmak, J. M., Sereda, P. J., Soil Sci., 84, 419 (1957)

[17]: Langrish, T. A. G., Kockel, T. K., Chem. Eng. Journal, 84, 69 (2001)

[18]: Luikov, A. V., Int. J. Heat Mass Transfer, 18, 1 (1975)

[19]: Mikhailov, M. D., Int. J. Heat Mass Transfer, 18,797 (1975)

[20]: Mujumdar, A. S., Handbook of Industrial Drying, Marcel Dekker, New York, (1995)

[21]: Nesic, S., Drying'89, 386 (1989)

[22]: Nesic, S., Vodnik, J., Chem. Eng. Sci., 46, 527 (1991)

[23]: Ochoa-Tapia, J. A., Stroeve, P., Whitaker, S., Chem. Eng. Sci., 49, 709 (1994)

[24]: Przesmycki, Z., Strumillo, C., Drying'85, 126 (1985)

[25]: Rahman, S., Food Properties Handbook, CRC Press, New York, (1995)

[26]: Ranz, W. E., Marshall, W. R., Chem. Eng. Prog., 48, 141 (1952)

[27]: Sandler, S. I., Chemical and Engineering Thermodynamics, Wiley, New York, (1999)

[28]: Sano, Y., Keey, R. B., Chem. Eng. Sci., 37, 881 (1982)

[29]: Sano, Y., Yamamoto, S., Proc. Third Int. Drying Symp., 1, 535 (1982)

[30]: Sherwood, T. K., Ind. Eng. Chem., 21, 12, 976 (1929)

[31]: Trommelen, A. M., Crosby, E. J., A.I.Ch.E. Journal, 16, 857 (1970)

[32]: Wang, C. Y., Beckermann, C., Int. J. Heat Mass Transfer, 36, 2747 (1993)

[33]: Wijlhuizen, A. E., Kerkhof, R. J. A. M., Bruin, S., Chem. Eng. Sci., 34, 651 (1979)

APPENDIX-A

PHYSICAL PROPERTIES USED BY THE MODEL

Properties of air are given below as

$$\rho_{air} = 1.293\left(\frac{273.15}{273.15+T}\right) \tag{A.1}$$

$$k_{air} = 1.731\left(0.014+4.296\cdot10^{-5}\,T\right) \tag{A.2}$$

$$\mu_{air} = 1.720\cdot10^{-5} + 4.568\cdot10^{-8}\,T \tag{A.3}$$

$$Cp_{air} = 969.542+6.801\cdot10^{-2}\,T'+16.569\cdot10^{-5}\,T'^{2}-67.828\cdot10^{-9}\,T'^{3} \tag{A.4}$$

where T is in ^{o}C and T' in K. The units of ρ_{air}, k_{air}, μ_{air}, and Cp_{air} are kg/m^3, W/m.K, kg/m.s and J/kg.K, respectively. Density, thermal conductivity and viscosity of air are obtained from reference [8] and heat capacity is obtained from reference [27].

Properties of water vapor are given as

$$D_{wv} = 0.220\cdot10^{-4}\left(\frac{T'}{273.15}\right)^{1.75} \tag{A.5}$$

$$Cp_{wv} = 1.883-1.674\cdot10^{-4}\,T+8.439\cdot10^{-7}\,T^{2}-2.697\cdot10^{-10}\,T^{3} \tag{A.6}$$

where the unit of diffusivity of water vapor in air is m^2/s and the unit of heat capacity of water vapor is J/kg.K. D_{wv} and Cp_{wv} are obtained from references [8] and [20], respectively.

Thermal conductivity of air-water vapor mixture obtained from reference [20] is

$$k_m = 2.425\cdot10^{-2} - 7.889\cdot10^{-5}T - 1.790\cdot10^{-8}T^2 - 8.570\cdot10^{-12}T^3 \qquad (A.7)$$

where the unit of k_m is W/m.K.

APPENDIX-B

PROGRAM FILE LISTING OF VGN ALGORITHM

```
PROGRAM DRY CONSTANT
C    ================================================
C    MODELING CONSTANT RATE PERIOD OF DROPLET DRYING
C    ================================================
IMPLICIT NONE
INTEGER I,J,NGRID,NMID,NCRIT
PARAMETER (NGRID = 501)
DOUBLE PRECISION A,B,C,D,P,Q,PHIT,TOLD,DT,ALPH11,ALPH22,ALPH33,
1                ALPH44,ALPH55,KCO,KH,KM,R,TGAS,TOUT,RR,RGAS,TINT,
2                CGAS,TOLS,WT,DS,ERRS,PI,POR,MW,RRIN,KS,CPW,KW,
3                RHOS,RHOW,ROUT,RIN,RO,CPS,DR11,DR22,TINTER,DIA,
4                VAIR,TDUM,CW,DRR,DSS,RNEW,TOT11,DAT,TAVE11,
5                TAVE22,TAVE,TOT22
DIMENSION A(NGRID),B(NGRID),C(NGRID),D(NGRID),P(NGRID),Q(NGRID),
1         TOLD(NGRID),R(NGRID),PHIT(NGRID),RNEW(NGRID),TDUM(NGRID),
2         TOT11(NGRID),TOT22(NGRID),DAT(15)
COMMON/PARAM/RGAS,TGAS,KS,KW,POR,RHOW,CPW,RHOS,CPS,DT,DSS,RR
C
C    INPUT AND OUTPUT FILES
C
OPEN(6,FILE='A-TPROFILE.RES')
OPEN(7,FILE='A-GRID.RES')
OPEN(8,FILE='A-WEIGHT.RES')
OPEN(9,FILE='A-AVERTEMP.RES')
OPEN(10,FILE='DATA-C.TXT')
C
C    ARGUMENT LIST
C    -------------
C    A,B,C,D   : COEFFICIENT VECTORS OF MATRIX SYSTEM FOR
                 TEMPERATURE
C    PHIT      : SOLUTION VECTOR OF TEMPERATURE PROFILE (K)
C    TOLD      : TEMPERATURE PROFILE AT TIME LEVEL T (K)
C    DT        : TIME STEP (S)
C    ALPH11-55 : MODEL CONSTANTS
C    KCO       : THERMAL CONDUCTIVITY OF WET CORE (W/M.K)
C    KH        : CONVECTIVE HEAT TRANSFER COEFFICIENT (W/M^2.K)
```

```
C     KM        : CONVECTIVE MASS TRANSFER COEFFICIENT (M/S)
C     R         : GRID VECTOR (DIMENSIONLESS) AT TIME LEVEL T
C     TGAS      : DRYING AIR TEMPERATURE (K)
C     TOUT      : TIME (S)
C     RR        : OUTER RADIUS OF DROPLET (M)
C     RGAS      : UNIVERSAL GAS CONSTANT (ATM.M^3/KMOL.K)
C     TINT      : INITIAL DROPLET TEMPERATURE (K)
C     CGAS      : AIR HUMIDITY (KMOL/M^3)
C     TOLS      : ERROR CRITERION OF INTERFACE POSITION
C     WT        : DROPLET WEIGHT (MG)
C     DS        : CALCULATED DECREASE IN ROUT (DIMENSIONLESS)
C     ERRS      : ERROR IN CALCULATION OF INTERFACE POSITION
C     POR       : POROSITY
C     MW        : MOLECULAR WEIGHT OF WATER
C     RRIN      : INNER RADIUS OF DROPLET (M)
C     CPS       : HEAT CAPACITY OF SOLID (J/KG.K)
C     KS        : THERMAL CONDUCTIVITY OF SOLID (W/M.K)
C     CPW       : HEAT CAPACITY OF WATER (J/KG.K)
C     KW        : THERMAL CONDUCTIVITY OF WATER (W/M.K)
C     RHOS      : DENSITY OF SOLID (KG/M^3)
C     RHOW      : DENSITY OF WATER (KG/M^3)
C     ROUT      : DIMENSIONLESS OUTER RADIUS
C     RIN       : DIMENSIONLESS INNER RADIUS
C     RO        : CENTER OF DROPLET
C     DR11,DR22 : DELTA DISTANCES BETWEEN TWO NODES IN WET CORE AND
C                 FREE WATER REGIONS, RESPECTIVELY
C     DSS       : ESTIMATED DECREASE IN ROUT
C     RNEW      : GRID VECTOR (DIMENSIONLESS) AT TIME LEVEL T+DT
C     TINTER    : INTERPOLATED TEMPERATURE VALUES (K)
C     DIA       : DROPLET DIAMETER (M)
C     VAIR      : DRYING AIR VELOCITY (M/S)
C     CW        : WATER VAPOR CONCENTRATION AT SURFACE (KMOL/M^3)
C     DRR       : INCREMENTAL DECREASE OF ROUT(DIMLESS)
C     TAVE      : AVERAGE DROPLET TEMPERATURE (K)
C     KAIR      : THERMAL CONDUCTIVITY OF AIR (W/M.K)
C     MUAIR     : VISCOSITY OF AIR (KG/M.S)
C     DAB       : DIFFUSIVITY OF WATER VAPOR IN AIR (M^2/S)
C     NU        : NUSSELT NUMBER
C     SH        : SHERWOOD NUMBER
C     RE        : REYNOLDS NUMBER
C     PR        : PRANDTL NUMBER
C     SC        : SCHMIDT NUMBER
C     CPAIR     : HEAT CAPACITY OF AIR (J/KG.K)
C     RHOAIR    : DENSITY OF AIR (KG/M^3)
C     TS        : DROPLET SURFACE TEMPERATURE (K)
C     NGRID     : NUMBER OF GRIDS
C     NMID      : GRID NUMBER CORRESPONDING TO RIN
C     ===============================================
C     DRYING AND NUMERICAL PARAMETERS OF THE MODEL SHOULD
C     BE SUPPLIED FROM 'DATA-C.TXT' FILE. THE PARAMETERS
C     SHOULD BE IN ARRAY FORM AS:
C
C     OUTER RADIUS OF DROPLET (M)
C     INNER RADIUS OF DROPLET (M)
C     POROSITY OF DROPLET
C     INITIAL DROPLET TEMPERATURE (C)
C     DRYING AIR TEMPERATURE (C)
C     DRYING AIR VELOCITY (M/S)
```

```
C    DENSITY OF WATER (KG/M^3)
C    THERMAL CONDUCTIVITY OF WATER (W/M.K)
C    HEAT CAPACITY OF WATER (J/KG.K)
C    DENSITY OF SOLID (KG/M^3)
C    THERMAL CONDUCTIVITY OF SOLID (W/M.K)
C    HEAT CAPACITY OF SOLID (J/KG.K)
C    TIME STEP (S)
C    INCREMENTAL DECREASE OF ROUT(DIMLESS)
C    ERROR CRITERION OF INTERFACE POSITION
C
DO 10 I=1,15
READ(10,*) DAT(I)
10    CONTINUE
RR    =DAT(1)
RRIN  =DAT(2)
POR   =DAT(3)
TINT  =DAT(4)+273.15D0
TGAS  =DAT(5)+273.15D0
VAIR  =DAT(6)
RHOW  =DAT(7)
KW    =DAT(8)
CPW   =DAT(9)
RHOS  =DAT(10)
KS    =DAT(11)
CPS   =DAT(12)
DT    =DAT(13)
DRR   =DAT(14)
TOLS  =DAT(15)
C
WRITE(*,*)'DRYING PARAMETERS OF THE MODEL'
WRITE(*,*)'================================='
WRITE(*,*)'OUTER RADIUS OF DROPLET        :',RR
WRITE(*,*)'INNER RADIUS OF DROPLET        :',RRIN
WRITE(*,*)'POROSITY OF DROPLET            :',POR
WRITE(*,*)'INITIAL DROPLET TEMPERATURE    :',TINT
WRITE(*,*)'DRYING AIR TEMPERATURE         :',TGAS
WRITE(*,*)'DRYING AIR VELOCITY            :',VAIR
WRITE(*,*)'DENSITY OF WATER               :',RHOW
WRITE(*,*)'THERMAL CONDUCTIVITY OF WATER  :',KW
WRITE(*,*)'HEAT CAPACITY OF WATER         :',CPW
WRITE(*,*)'DENSITY OF SOLID               :',RHOS
WRITE(*,*)'THERMAL CONDUCTIVITY OF SOLID  :',KS
WRITE(*,*)'HEAT CAPACITY OF SOLID         :',CPS
WRITE(*,*)'================================='
WRITE(*,*)'NUMERICAL PARAMETERS OF THE MODEL'
WRITE(*,*)'================================='
WRITE(*,*)'TIME STEP                            :',DT
WRITE(*,*)'INCREMENTAL DECREASE OF ROUT         :',DRR
WRITE(*,*)'ERROR CRITERION OF INTERFACE POSITION:',TOLS
WRITE(*,*)'================================='
C
WRITE(*,*)'ARE YOU SURE TO CONTINUE (1=YES,2=NO)'
READ(*,*)NCRIT
IF (NCRIT.EQ.1) GO TO 200
IF (NCRIT.EQ.2) GO TO 500
C
200   WRITE(*,*)'NUMERICAL CALCULATIONS STARTED'
```

```
C
C    DIMENSIONLESS FORMS
C
ROUT   = RR/RR
RIN    = RRIN/RR
RO     = 0.0D0
C
PI     = 3.1415D0
MW     = 18.02D0
RGAS   = 82.06D-3
CGAS   = 8.10D-3/(RGAS*TGAS)
C
C    ASSIGN INITIAL CONDITIONS AND GENERATE GRIDS
C
CALL GRIDS(NGRID,RO,ROUT,RIN,NMID,DR11,DR22,R)
DO 20 I = 1, NGRID
TOLD(I)=TINT
20   CONTINUE
C
C    CALCULATION OF INITIAL WEIGHT OF DROPLET
C
WT=(((4*PI*(RRIN**3)*POR*RHOW)/3)+((4*PI*(RRIN**3)*(1.0D0-
1   POR)*RHOS)/3)+((4*PI*RHOW*((ROUT*RR)**3-RRIN**3))/3))*1.0D6
C
WRITE(8,*) WT
WRITE(9,*) TINT-273.15D0
C
C    SOLUTION ALGORITHM
C
TOUT = 0.0D0
300  TOUT = TOUT+DT
DO 30 I=1,NGRID
TOT11(I)=0.0D0
TOT22(I)=0.0D0
30   CONTINUE
WRITE(6,*)'TIME =',TOUT
DSS  = 0.0D0
400  ROUT = ROUT-DRR
DSS  = DSS+DRR
DIA  = 2*(ROUT*RR)
CALL GRIDS(NGRID,RO,ROUT,RIN,NMID,DR11,DR22,RNEW)
DO 40 I=1,NGRID
CALL LINT(TOLD,R,NGRID,RNEW(I),TINTER)
TDUM(I)=TINTER
40   CONTINUE
DO 50 I=1,NGRID
TOLD(I)=TDUM(I)
50   CONTINUE
CALL CONV(TGAS,TOLD(NGRID),DIA,VAIR,KH,KM)
CALL COFT(NGRID,NMID,TOLD,RNEW,DR11,DR22,KH,A,B,C,D)
CALL TDMA(PHIT,A,B,C,D,NGRID,P,Q)
CW=(EXP(20.21D0-(5104.05D0/PHIT(NGRID)))/760)/(RGAS*PHIT(NGRID))
DS=((DT*KM*MW)/(RHOW*RR))*(CW-CGAS)
ERRS=(ABS(DS-DSS)/DSS)*100
IF (ERRS.GT.TOLS) GO TO 400
C
WRITE(6,*)'ROUT =',ROUT*RR
WRITE(6,*)'RIN  =',RIN*RR
```

```
WRITE(6,*)'NMID =',NMID
WRITE(6,*)'DR11 =',DR11
WRITE(6,*)'DR22 =',DR22
WRITE(7,*)'ROUT =',ROUT*RR
WRITE(7,*)'ROUTD=',ROUT
C
WT=(((4*PI*(RRIN**3)*POR*RHOW)/3)+((4*PI*(RRIN**3)*(1.0D0-
1   POR)*RHOS)/3)+((4*PI*RHOW*((ROUT*RR)**3-RRIN**3))/3))*1.0D6
C
DO 60 I=2,NMID-1
TOT11(I-1)=PHIT(I)*(RNEW(I)**2)
60   CONTINUE
DO 70 I=NMID+1,NGRID-1
TOT22(I-NMID)=PHIT(I)*(RNEW(I)**2)
70   CONTINUE
TAVE11=(DR11/2)*(PHIT(1)*(RNEW(1)**2)+2*SUM(TOT11)
1       +PHIT(NMID)*(RNEW(NMID)**2))
TAVE22=(DR22/2)*(PHIT(NMID)*(RNEW(NMID)**2)+2*SUM(TOT22)
1       +PHIT(NGRID)*(RNEW(NGRID)**2))
TAVE=(TAVE11+TAVE22)/((RNEW(NGRID)**3)/3)
C
WRITE(*,*)'================================================='
WRITE(*,*)'TIME                       :',TOUT
WRITE(*,*)'CENTER TEMPERATURE         :',PHIT(1)-273.15D0
WRITE(*,*)'SURFACE TEMPERATURE        :',PHIT(NGRID)-273.15D0
WRITE(*,*)'AVERAGE TEMPERATURE        :',TAVE-273.15D0
WRITE(*,*)'DROPLET WEIGHT             :',WT
WRITE(*,*)'ESTIMATED DECREASE IN ROUT :',DSS
WRITE(*,*)'CALCULATED DECREASE IN ROUT:',DS
WRITE(*,*)'ERROR IN CALCULATION       :',ERRS
WRITE(*,*)'ROUT (DIMLESS)             :',ROUT
WRITE(*,*)'ROUT (M)                   :',ROUT*RR
WRITE(*,*)'NODE OF RIN                :',NMID
C
WRITE(8,*) WT
WRITE(9,*) TAVE-273.15D0
C
DO 80 I=1,NGRID,2
WRITE(6,100) PHIT(I)
WRITE(7,100) RNEW(I)
80   CONTINUE
DO 90 I=1,NGRID
TOLD(I)=PHIT(I)
R(I)  =RNEW(I)
90   CONTINUE
IF (NMID.EQ.500) GO TO 500
GO TO 300
C
100  FORMAT(10(2X,F14.6))
500   WRITE(*,*)'PROGRAM TERMINATED'
STOP
END
C
C
C    =========================================================
      SUBROUTINE COFT (NGRID,NMID,TOLD,R,DR11,DR22,KH,A,B,C,D)
C    =========================================================
C
```

```
C    SUBROUTINE TO GENERATE MATRIX SYSTEM FOR TEMPERATURE PROFILE
C
IMPLICIT NONE
INTEGER NGRID,NMID,I
DOUBLE PRECISION A,B,C,D,TOLD,DR11,DR22,DT,KCO,KW,KH,TGAS,RR,R,
1                ALPH11,ALPH33,ALPH44,RGAS,CGAS,ALPH22,KS,POR,
2                RHOW,CPW,RHOS,CPS,RIN,DRR,DSS
DIMENSION A(NGRID),B(NGRID),C(NGRID),D(NGRID),TOLD(NGRID),R(NGRID)
COMMON/PARAM/RGAS,TGAS,KS,KW,POR,RHOW,CPW,RHOS,CPS,DT,DSS,RR
C
C    DEFINITION OF PARAMETERS
C
KCO    = POR*KW+(1.0D0-POR)*KS
ALPH11 = ((POR*RHOW*CPW+(1.0D0-POR)*RHOS*CPS)/KCO)*RR**2
ALPH22 = ((RHOW*CPW)/KW)*RR**2
ALPH33 = KH/(RHOW*RR)
ALPH44 = KW/(RHOW*RR**2)
C
C    INITIALIZE VECTORS TO ZERO AND GENERATE GRIDS
C
DO 10 I = 1, NGRID
C(I)   = 0.0D0
A(I)   = 1.0D0
B(I)   = 0.0D0
D(I)   = 0.0D0
10   CONTINUE
C
C    COEFFICIENT VECTORS AT NODE 1
C
C(1) = 0.0D0
A(1) = 1.0D0
B(1) = 1.0D0
D(1) = 0.0D0
C
C    COEFFICIENT VECTORS FROM NODE 2 TO NODE NMID-1
C
DO 20 I = 2, NMID-1
C(I) = DT/(ALPH11*DR11**2) - DT/(ALPH11*R(I)*DR11)
A(I) = 1.0D0 + 2*DT/(ALPH11*DR11**2)
B(I) = DT/(ALPH11*DR11**2) + DT/(ALPH11*R(I)*DR11)
D(I) = TOLD(I)
20   CONTINUE
C
C    COEFFICIENT VECTORS AT NODE NMID
C
C(NMID)  = KCO/DR11
A(NMID)  = KCO/DR11+KW/DR22
B(NMID)  = KW/DR22
D(NMID)  = 0.0D0
C
C    COEFFICIENT VECTORS FROM NODE NMID+1 TO NODE NGRID-1
C
DO 30 I=NMID+1,NGRID-1
C(I) = DT/(ALPH22*DR22**2) - DT/(ALPH22*R(I)*DR22)
A(I) = 1.0D0 + 2*DT/(ALPH22*DR22**2)
B(I) = DT/(ALPH22*DR22**2) + DT/(ALPH22*R(I)*DR22)
D(I) = TOLD(I)
30   CONTINUE
```

```
C
C    COEFFICIENT VECTORS AT NODE N
C
I=NGRID
C(I)  = -ALPH44/DR22
A(I)  = ((2.384D3*(DSS))/DT)-ALPH33-ALPH44/DR22
B(I)  = 0.0D0
D(I)  = ((3.154D6*(DSS))/DT)-ALPH33*TGAS
RETURN
END
C
C
C    ==================================
      SUBROUTINE LINT (F,X,N,XINT,FINT)
C    ==================================
C
C    THIS SUBROUTINE CALCULATES THE VALUE OF A GIVEN VECTOR
C    F AT A GIVEN POSITION XINT BY LINEAR INTERPOLATION.
C
C    ARGUMENT LIST
C    -------------
C    F    : FUNCTION VECTOR
C    X    : POSITION VECTOR WHERE F VALUES ARE AVAILABLE
C    N    : NUMBER OF GRIDS
C    XINT : NEW POSITION WHERE F TO BE CALCULATED
C    FINT : VALUE OF FUNCTION F LINEARLY INTERPOLATED
C
IMPLICIT NONE
INTEGER I,N
DOUBLE PRECISION F(N),X(N),M,XINT,FINT
C
IF (XINT.LT.X(1)) THEN
FINT=F(1)
RETURN
END IF
C
IF (XINT.GT.X(N)) THEN
FINT=F(N)
RETURN
END IF
C
DO 10 I=1,N
IF (XINT.EQ.X(I)) THEN
FINT=F(I)
RETURN
END IF
10   CONTINUE
C
DO 20 I=1,N-1
IF ((XINT.GT.X(I)).AND.(XINT.LT.X(I+1))) THEN
M =(F(I+1)-F(I))/(X(I+1)-X(I))
FINT =M*XINT-M*X(I)+F(I)
END IF
20   CONTINUE
RETURN
END
C
C
```

```
C    ========================================
      SUBROUTINE CONV (TGAS,TS,DIA,VEL,KH,KM)
C    ========================================
C
C    THIS SUBROUTINE CALCULATES THE CONVECTIVE HEAT AND MASS
C    TRANSFER COEFFICIENTS
C
IMPLICIT NONE
DOUBLE PRECISION TGAS,TS,DIA,VEL,TAV,KAIR,MUAIR,DAB,NU,SH,
1                RE,CPAIR,KH,KM,RHOAIR,TGASC,TSC,TAVC,PR,SC
C
TGASC= TGAS-273.15D0
TSC  = TS-273.15D0
TAV  = (TGAS+TS)/2
TAVC = (TGASC+TSC)/2
C
RHOAIR= 1.2929D0*(273.15D0/TAV)
KAIR  = 1.731D0*(0.014D0+4.296D-5*TAVC)
MUAIR = 1.720D-5+4.568D-8*TAVC
DAB   = 0.22D-4*((TAV/273.15D0)**1.75D0)
CPAIR = 34.518D0*(28.088D0+0.197D-2*TAV+0.480D-5*TAV**2
1        -1.965D-9*TAV**3)
C
RE    =(DIA*VEL*RHOAIR)/MUAIR
PR    =(CPAIR*MUAIR)/KAIR
SC    =MUAIR/(RHOAIR*DAB)
NU    =2.0D0+0.65D0*(RE**0.5D0)*(PR**0.33D0)
SH    =2.0D0+0.65D0*(RE**0.5D0)*(SC**0.33D0)
C
KH    =(NU*KAIR)/DIA
KM    =(SH*DAB)/DIA
RETURN
END
C
C
C    =================================================
      SUBROUTINE GRIDS (NTOT,A,B,R1,NPL,DLTPL,DLTEL,R)
C    =================================================
C
C    THIS SUBROUTINE GENERATES GRIDS GIVEN THE POSITION
C    OF AN INTERFACE
C
C    ARGUMENT LIST
C    -------------
C    NTOT : NUMBER OF GRIDS
C    A    : LEFT BOUNDARY
C    B    : RIGHT BOUNDARY
C    R1   : INTERFACE POSITION
C    NPL  : INTERFACE GRID NUMBER
C    DLTPL: DELTA DISTANCE IN REGION A TO R1
C    DLTEL: DELTA DISTANCE IN REGION R1 TO B
C    R    : GRID VECTOR
C
IMPLICIT NONE
INTEGER NTOT,NPL,NEL,I,IFAC
DOUBLE PRECISION A,B,R1,DLTPL,DLTEL,R,R0,T
DIMENSION R(NTOT)
C
```

```
IF (R1.EQ.A) THEN
NEL =NTOT
NPL =0
DLTPL =(R1-A)/(NPL-1)
DLTEL =(B-R1)/(NEL-1)
R(1)  =A
DO 10 I=2,NTOT
R(I) =R(I-1) + DLTEL
10   CONTINUE
RETURN
END IF
C
IF (R1.EQ.B) THEN
NEL =0
NPL =NTOT
DLTPL =(R1-A)/(NPL-1)
DLTEL =(B-R1)/(NEL-1)
R(1)  =A
DO 20 I=2,NTOT
R(I) =R(I-1)+DLTPL
20   CONTINUE
RETURN
END IF
C
R0     =(R1-A)/(B-R1)
T      =DFLOAT(NTOT)
NEL    =(T-1.0D0)/(R0+1.0D0)
NPL    =NTOT-1-NEL
DLTPL =(R1-A)/NPL
DLTEL =(B-R1)/NEL
C
R(1) =A
DO 30 I=1,NPL
R(I+1) =A+DLTPL*I
30   CONTINUE
C
IFAC=0
DO 40 I=NPL+1,NTOT-1
IFAC   =IFAC+1
R(I+1) =R1+DLTEL*IFAC
40   CONTINUE
NPL =NPL+1
RETURN
END
C
C
C    ====================================
      SUBROUTINE TDMA (PHI,A,B,C,D,N,P,Q)
C    ====================================
C
C    SUBROUTINE TO SOLVE TRIDIAGONAL SYSTEM
C
C    ARGUMENT LIST
C    -------------
C    N              : NUMBER OF SIMULTANEOUS EQUATIONS.
C    PHI            : SOLUTION VECTOR
C    A,B,C,D        : COEFFICIENT VECTORS OF LENGTH N
C    P,Q            : DUMMY VECTORS USED IN RECURRENCE RELATIONS
```

```
C
C    THE SYSTEM SHOULD BE ARRANGED AS:
C    A(I)*T(I)=B(I)*T(I+1) + C(I)*T(I-1) + D(I)
C
INTEGER I,K,M,N,NL
DOUBLE PRECISION A,B,C,D,DENOM,P,PHI,Q
DIMENSION A(N),B(N),C(N),D(N),P(N),PHI(1),Q(N)
C
C    EVALUATE P(1)&Q(1)
C
P(1) =B(1)/A(1)
Q(1) =D(1)/A(1)
C
C    USE RECURRENCE RELATIONS TO FIND P(I),Q(I),I = 2,3,...,N
C
DO 10 I=2,N
DENOM =1.0/(A(I)-C(I)*P(I-1))
P(I)  =B(I)*DENOM
10   Q(I)  =(D(I)+C(I)*Q(I-1))*DENOM
PHI(N)=Q(N)
C
C    BACK SUBSTITUTE P(I),Q(I),I = N-1,N-2,....,1 TO FIND PHI(N-1),
C    PHI(N-2),....,PHI(1)
C
NL =N-1
DO 20 K=1,NL
M =N-K
20   PHI(M) =P(M)*PHI(M+1)+Q(M)
RETURN
END
```

APPENDIX-C

PROGRAM FILE LISTING OF VTS ALGORITHM

```
PROGRAM DRY FALLING
C    ================================================
C    MODELING FALLING RATE PERIOD OF DROPLET DRYING
C    ================================================
IMPLICIT NONE
INTEGER I,J,NGRID,NMID,NCRIT
PARAMETER (NGRID = 501)
DOUBLE PRECISION A,B,C,D,P,Q,PHIT,TOLD,DT,DR,ALPH11,TAVE,TDUM,RR,
1                ALPH33,ALPH44,KCO,KCR,KH,LENGTH,R,TGAS,TOUT,TIME,
2                COLD,RGAS,TINT,AC,BC,CC,DC,PHIC,CGAS,KM,DCR,ERR,
3                ALPH77,TOL,ALPH22,WT,ALPH55,ALPH66,DTT,DS,TOLS,
4                ERRS,PI,POR,RHOS,RHOW,CPS,MW,KS,CPGAS,KGAS,CPW,KW,
5                DVAP,DRR,DIA,VAIR,TOT,DTGUESS,DAT
DIMENSION A(NGRID),B(NGRID),C(NGRID),D(NGRID),COLD(NGRID),
1         AC(NGRID),BC(NGRID),CC(NGRID),DC(NGRID),PHIC(NGRID),
2         P(NGRID),Q(NGRID),TOLD(NGRID),R(NGRID),PHIT(NGRID),
3         TOT(NGRID),TOUT(NGRID),DAT(16)
COMMON/PARAM/DR,DT,TGAS,RR,RGAS,CGAS,DRR,POR,KW,KS,RHOW,CPW,RHOS,
1             CPS,MW
C
C    INPUT AND OUTPUT FILES
C
OPEN(6,FILE='A-PROFILE-T.RES')
OPEN(7,FILE='A-TIME.RES')
OPEN(8,FILE='A-WEIGHT.RES')
OPEN(9,FILE='A-PROFILE-C.RES')
OPEN(10,FILE='A-AVERTEMP.RES')
OPEN(11,FILE='A-DS.RES')
OPEN(12,FILE='A-SURFTEMP.RES')
OPEN(13,FILE='DATA-F.TXT')
C
C    ARGUMENT LIST
C    -------------
C    A,B,C,D     : COEFFICIENT VECTORS OF MATRIX SYSTEM FOR
                   TEMPERATURE
```

```
C    AC,BC,CC,DC : COEFFICIENT VECTORS OF MATRIX SYSTEM FOR
C                  CONCENTRATION
C    PHIT        : SOLUTION VECTOR OF TEMPERATURE PROFILE (K)
C    TOLD        : TEMPERATURE PROFILE AT TIME LEVEL T (K)
C    DT          : TIME STEP (S)
C    DTT         : INCREMENTAL TIME STEP (S)
C    DTGUESS     : INITIAL GUESS OF TIME STEP (S)
C    ALPH11-77   : MODEL CONSTANTS
C    KCO         : THERMAL CONDUCTIVITY OF WET CORE (W/M.K)
C    KCR         : THERMAL CONDUCTIVITY OF DRY CRUST (W/M.K)
C    KH          : CONVECTIVE HEAT TRANSFER COEFFICIENT (W/M^2.K)
C    KM          : CONVECTIVE MASS TRANSFER COEFFICIENT (M/S)
C    R           : GRID VECTOR (DIMENSIONLESS)
C    TGAS        : DRYING AIR TEMPERATURE (K)
C    TIME        : TIME (S)
C    TOUT        : TIME VECTOR
C    RR          : RADIUS OF DROPLET (M)
C    RGAS        : UNIVERSAL GAS CONSTANT (ATM.M^3/KMOL.K)
C    TINT        : INITIAL DROPLET TEMPERATURE (K)
C    CGAS        : AIR HUMIDITY (KMOL/M^3)
C    TOL         : ERROR CRITERION OF INTERFACE TEMPERATURE
C    TOLS        : ERROR CRITERION OF INTERFACE POSITION
C    WT          : DROPLET WEIGHT (MG)
C    DS          : CALCULATED DECREASE IN INTERFACE POSITION
C                  (DIMENSIONLESS)
C    ERRS        : ERROR IN CALCULATION OF INTERFACE POSITION
C    ERR         : ERROR IN CALCULATION OF INTERFACE TEMPERATURE
C    POR         : POROSITY
C    MW          : MOLECULAR WEIGHT OF WATER
C    CPS         : HEAT CAPACITY OF SOLID (J/KG.K)
C    KS          : THERMAL CONDUCTIVITY OF SOLID (W/M.K)
C    CPW         : HEAT CAPACITY OF WATER (J/KG.K)
C    KW          : THERMAL CONDUCTIVITY OF WATER (W/M.K)
C    RHOS        : DENSITY OF SOLID (KG/M^3)
C    RHOW        : DENSITY OF WATER (KG/M^3)
C    CPGAS       : HEAT CAPACITY OF WATER VAPOR (J/KG.K)
C    KGAS        : THERMAL CONDUCTIVITY OF AIR-WATER VAPOR MIXTURE
C                  (W/M.K)
C    LENGTH      : DIMENSIONLESS DROPLET RADIUS
C    DR          : DELTA DISTANCES BETWEEN TWO NODES (DIMENSIONLESS)
C    DIA         : DROPLET DIAMETER (M)
C    VAIR        : DRYING AIR VELOCITY (M/S)
C    COLD        : WATER VAPOR CONCENTRATION AT TIME LEVEL T
C                  (KMOL/M^3)
C    PHIC        : SOLUTION VECTOR OF CONCENTRATION PROFILE
C                  (KMOL/M^3)
C    DRR         : DELTA DISTANCES BETWEEN TWO NODES (M)
C    TAVE        : AVERAGE DROPLET TEMPERATURE (K)
C    KAIR        : THERMAL CONDUCTIVITY OF AIR (W/M.K)
C    MUAIR       : VISCOSITY OF AIR (KG/M.S)
C    DVAP        : DIFFUSIVITY OF WATER VAPOR IN AIR (M^2/S)
C    DCR         : EFFECTIVE DIFFUSIVITY OF CRUST (M^2/S)
C    NU          : NUSSELT NUMBER
C    SH          : SHERWOOD NUMBER
C    RE          : REYNOLDS NUMBER
C    PR          : PRANDTL NUMBER
C    SC          : SCHMIDT NUMBER
C    CPAIR       : HEAT CAPACITY OF AIR (J/KG.K)
```

```
C    RHOAIR      : DENSITY OF AIR (KG/M^3)
C    NGRID       : NUMBER OF GRIDS
C    NMID        : GRID NUMBER CORRESPONDING TO INTERFACE POSITION
C    ===============================================
C    DRYING AND NUMERICAL PARAMETERS OF THE MODEL SHOULD
C    BE SUPPLIED FROM 'DATA-F.TXT' FILE. THE PARAMETERS
C    SHOULD BE IN ARRAY FORM AS:
C
C    RADIUS OF DROPLET (M)
C    POROSITY OF DROPLET
C    INITIAL DROPLET TEMPERATURE (C)
C    DRYING AIR TEMPERATURE (C)
C    DRYING AIR VELOCITY (M/S)
C    DENSITY OF WATER (KG/M^3)
C    THERMAL CONDUCTIVITY OF WATER (W/M.K)
C    HEAT CAPACITY OF WATER (J/KG.K)
C    DENSITY OF SOLID (KG/M^3)
C    THERMAL CONDUCTIVITY OF SOLID (W/M.K)
C    HEAT CAPACITY OF SOLID (J/KG.K)
C    ERROR CRITERION OF INTERFACE TEMPERATURE
C    ERROR CRITERION OF INTERFACE POSITION
C    INCREMENTAL TIME (S)
C    INITIAL GUESS FOR TIME STEP (S)
C    TIME ELAPSED FOR CONSTANT RATE PERIOD (S)
C
DO 10 I=1,16
READ(13,*) DAT(I)
10    CONTINUE
RR     =DAT(1)
POR    =DAT(2)
TINT   =DAT(3)+273.15D0
TGAS   =DAT(4)+273.15D0
VAIR   =DAT(5)
RHOW   =DAT(6)
KW     =DAT(7)
CPW    =DAT(8)
RHOS   =DAT(9)
KS     =DAT(10)
CPS    =DAT(11)
TOL    =DAT(12)
TOLS   =DAT(13)
DTT    =DAT(14)
DTGUESS=DAT(15)
TIME   =DAT(16)
C
WRITE(*,*)'DRYING PARAMETERS OF THE MODEL'
WRITE(*,*)'================================='
WRITE(*,*)'INNER RADIUS OF DROPLET        :',RR
WRITE(*,*)'POROSITY OF DROPLET            :',POR
WRITE(*,*)'INITIAL DROPLET TEMPERATURE    :',TINT
WRITE(*,*)'DRYING AIR TEMPERATURE         :',TGAS
WRITE(*,*)'DRYING AIR VELOCITY            :',VAIR
WRITE(*,*)'DENSITY OF WATER               :',RHOW
WRITE(*,*)'THERMAL CONDUCTIVITY OF WATER  :',KW
WRITE(*,*)'HEAT CAPACITY OF WATER         :',CPW
WRITE(*,*)'DENSITY OF SOLID               :',RHOS
WRITE(*,*)'THERMAL CONDUCTIVITY OF SOLID  :',KS
WRITE(*,*)'HEAT CAPACITY OF SOLID         :',CPS
```

```
WRITE(*,*)'=================================='
WRITE(*,*)'NUMERICAL PARAMETERS OF THE MODEL'
WRITE(*,*)'=================================='
WRITE(*,*)'ERROR CRITERION OF INTERFACE TEMP.    :',TOL
WRITE(*,*)'ERROR CRITERION OF INTERFACE POSITION:',TOLS
WRITE(*,*)'INCREMENTAL TIME                      :',DTT
WRITE(*,*)'INITIAL GUESS OF TIME STEP            :',DTGUESS
WRITE(*,*)'TIME ELAPSED FOR CONSTANT RATE PERIOD:',TIME
WRITE(*,*)'=================================='
C
WRITE(*,*)'ARE YOU SURE TO CONTINUE (1=YES,2=NO)'
READ(*,*)NCRIT
IF (NCRIT.EQ.1) GO TO 200
IF (NCRIT.EQ.2) GO TO 700
C
200   WRITE(*,*)'NUMERICAL CALCULATIONS STARTED'
C
C    INITIAL POSITION OF INTERFACE
C
NMID   = NGRID-1
C
DIA    = 2*RR
PI     = 3.1415D0
MW     = 18.02D0
RGAS   = 82.06D-3
CGAS   = 8.10D-3/(RGAS*TGAS)
LENGTH = 1.0D0
DR     = LENGTH/(NGRID-1)
DRR    = DR*RR
C
C    INITIALIZE VECTORS TO ZERO AND GENERATE GRIDS
C
DO 20 I = 1, NGRID
PHIT(I) = 0.0D0
PHIC(I) = 0.0D0
R(I)    = (I-1)*DR
20   CONTINUE
C
C    INITIAL CONDITION FOR TEMPERATURE PROFILE
C
DO 30 I = 1, NGRID
TOLD(I) = TINT
30    CONTINUE
C
C    INITIAL CONDITION FOR CONCENTRATION PROFILE
C
DO 40 I=1,NMID-1
COLD(I) = 0.0D0
40   CONTINUE
DO 50 I = NMID, NGRID
COLD(I) = (EXP(20.21D0-(5104.05D0/TINT))/760)/(RGAS*TINT)
50   CONTINUE
C
C    SOLUTION ALGORITHM
C
300  DO 60 I=1,NGRID
TOT(I) = 0.0D0
60   CONTINUE
```

```
DT   = DTGUESS
NMID = NMID-1
CALL CONV(TGAS,TOLD(NGRID),DIA,VAIR,KH,KM)
400   DT = DT-DTT
TDUM = TOLD(NMID)
500  CALL COFC (NGRID,NMID,COLD,TOLD,TDUM,KM,AC,BC,CC,DC)
CALL TDMA (PHIC,AC,BC,CC,DC,NGRID,P,Q)
CALL COFT (NGRID,NMID,TOLD,PHIC,KH,A,B,C,D,ALPH22)
CALL TDMA (PHIT,A,B,C,D,NGRID,P,Q)
ERR=((ABS(PHIT(NMID)-TDUM))/PHIT(NMID))*100
IF (ERR.LT.TOL) GO TO 600
TDUM=PHIT(NMID)
GO TO 500
600  DS=((DT*ALPH22)/(2*DR))*(3*PHIC(NMID)-
4*PHIC(NMID+1)+PHIC(NMID+2))
ERRS=(ABS(DS-DR)/DR)*100
IF (ERRS.GT.TOLS) GO TO 400
DO 70 I=1,NGRID
TOLD(I)=PHIT(I)
COLD(I)=PHIC(I)
70   CONTINUE
C
TIME=TIME+DT
C
WT=((4*PI*(1-POR)*RHOS*RR**3)/3
1        +(4*PI*POR*RHOW*(R(NMID)*RR)**3)/3)*1.0D6
C
DO 80 I=2,NGRID-1
TOT(I)=((R(I)*RR)**2)*PHIT(I)
80   CONTINUE
TAVE=(DRR/2)*(PHIT(1)*((R(1)*RR)**2)+2*SUM(TOT)+
1      PHIT(NGRID)*((R(NGRID)*RR)**2))/((RR**3)/3)
C
WRITE(6,*) '  TIME = ',TIME
WRITE(9,*) '  TIME = ',TIME
WRITE(6,*) '  NMID = ',NMID
WRITE(9,*) '  NMID = ',NMID
WRITE(6,*) '    DS = ',DS
WRITE(9,*) '    DS = ',DS
WRITE(7,*)  TIME
WRITE(8,*)  WT
WRITE(11,*) DS
WRITE(10,*) TAVE-273.15D0
WRITE(12,*) PHIT(NGRID)-273.15D0
WRITE(6,*) TIME
C
WRITE(*,*)'================================================'
WRITE(*,*)'TIME                        :',TIME
WRITE(*,*)'TIME STEP                   :',DT
WRITE(*,*)'CENTER TEMPERATURE          :',PHIT(1)-273.15D0
WRITE(*,*)'INTERFACE TEMPERATURE       :',PHIT(NMID)-273.15D0
WRITE(*,*)'SURFACE TEMPERATURE         :',PHIT(NGRID)-273.15D0
WRITE(*,*)'AVERAGE TEMPERATURE         :',TAVE-273.15D0
WRITE(*,*)'DROPLET WEIGHT              :',WT
WRITE(*,*)'ESTIMATED DECREASE IN S     :',DR
WRITE(*,*)'CALCULATED DECREASE IN S    :',DS
WRITE(*,*)'ERROR IN CALCULATION        :',ERRS
WRITE(*,*)'INTERFACE NODE              :',NMID
```

```
C
DO 90 I=1,NGRID,10
WRITE(6,100) PHIT(I)-273.15D0
90   CONTINUE
C
DO 110 I=NMID,NGRID,10
WRITE(9,100) PHIC(I)
110  CONTINUE
C
IF (NMID.EQ.15) GO TO 700
IF (NMID.LT.470) DTGUESS=DT
GO TO 300
C
100  FORMAT(10(2X,F14.6))
700   STOP
END
C
C
C    ==============================================================
      SUBROUTINE COFT (NGRID,NMID,TOLD,CNEW,KH,A,B,C,D,ALPH22)
C    ==============================================================
C
C    SUBROUTINE TO GENERATE MATRIX SYSTEM FOR TEMPERATURE PROFILE
C
IMPLICIT NONE
INTEGER NGRID,NMID,I
DOUBLE PRECISION A,B,C,D,CNEW,TOLD,DR,DT,KCO,KCR,KH,TGAS,RR,R,
1                ALPH11,ALPH33,ALPH44,RGAS,ALPH77,DCR,KM,CGAS,
2                ALPH22,ALPH55,ALPH66,DRR, CPGAS,KGAS,POR,KW,KS,
3                DVAP,RHOW,CPW,RHOS,CPS,MW
DIMENSION A(NGRID),B(NGRID),C(NGRID),D(NGRID),TOLD(NGRID),
1         CNEW(NGRID),R(NGRID)
COMMON/PARAM/DR,DT,TGAS,RR,RGAS,CGAS,DRR,POR,KW,KS,RHOW,CPW,RHOS,
1             CPS,MW
C
C    DEFINITION OF PARAMETERS
C
CPGAS  = 1.883D0-1.6737D-4*(((TOLD(NMID)+TOLD(NGRID))/2)-273.15D0)
1         +8.4386D-7*((((TOLD(NMID)+TOLD(NGRID))/2)-273.15D0)**2)
2         -2.6966D-10*((((TOLD(NMID)+TOLD(NGRID))/2)-273.15D0)**3)
KGAS   = 2.425D-2-7.889D-5*(((TOLD(NMID)+TOLD(NGRID))/2)-273.15D0)
1         -1.790D-8*((((TOLD(NMID)+TOLD(NGRID))/2)-273.15D0)**2)
2         -8.570D-12*((((TOLD(NMID)+TOLD(NGRID))/2)-273.15D0)**3)
KCO    = POR*KW+(1.0D0-POR)*KS
KCR    = POR*KGAS+(1.0D0-POR)*KS
DVAP   = 0.22D-4*((((TOLD(NMID)+TOLD(NGRID))/2)/273.15D0)**1.75D0)
DCR    = (2*POR*DVAP)/(3.0D0-POR)
ALPH11 = ((POR*RHOW*CPW+(1.0D0-POR)*RHOS*CPS)/KCO)*RR**2
ALPH22 = (DCR*MW/(POR*RHOW))/RR**2
ALPH33 = (DCR*MW*CPGAS)/KCR
ALPH44 = ((RHOS*CPS*(1.0D0-POR))/KCR)*RR**2
ALPH55 = (KCR/(POR*RHOW))/RR**2
ALPH66 = (KCO/(POR*RHOW))/RR**2
ALPH77 = (POR/DCR)*RR**2
C
C    INITIALIZE VECTORS TO ZERO AND GENERATE GRIDS
C
```

```
DO 10 I = 1, NGRID
C(I)   = 0.0D0
A(I)   = 1.0D0
B(I)   = 0.0D0
D(I)   = 0.0D0
R(I)   = (I-1)*DR
10   CONTINUE
C
C    COEFFICIENT VECTORS AT NODE 1
C
C(1) = 0.0D0
A(1) = 1.0D0
B(1) = 1.0D0
D(1) = 0.0D0
C
C    COEFFICIENT VECTORS FROM NODE 2 TO NODE NMID-1
C
DO 20 I = 2, NMID-1
C(I) = DT/(ALPH11*DR**2) - DT/(ALPH11*R(I)*DR)
A(I) = 1.0D0 + 2*DT/(ALPH11*DR**2)
B(I) = DT/(ALPH11*DR**2) + DT/(ALPH11*R(I)*DR)
D(I) = TOLD(I)
20   CONTINUE
C
C    COEFFICIENT VECTORS AT NODE NMID
C
C(NMID)  = -ALPH66/DR
A(NMID)  = (2.384D3*DR)/DT-ALPH55/DR-ALPH66/DR
B(NMID)  = -ALPH55/DR
D(NMID)  = (3.154D6*DR)/DT
C
C    COEFFICIENT VECTORS FROM NODE NMID+1 TO NODE NGRID-1
C
DO 30 I=NMID+1,NGRID-1
C(I)=DT/(ALPH44*DR**2)-(DT/(2*ALPH44*DR))*(2/R(I)
1             +(ALPH33/(2*DR))*(CNEW(I+1)-CNEW(I-1)))
A(I)=1+2*DT/(ALPH44*DR**2)-(DT/ALPH44*(ALPH33/(R(I)*DR)*(CNEW(I+1)
1      -CNEW(I-1))+ALPH33/DR**2*(CNEW(I+1)-2*CNEW(I)+CNEW(I-1))))
B(I) = DT/(ALPH44*DR**2)+(DT/(2*ALPH44*DR))*(2/R(I)
1             +(ALPH33/(2*DR))*(CNEW(I+1)-CNEW(I-1)))
D(I) = TOLD(I)
30   CONTINUE
C
C    COEFFICIENT VECTORS AT NODE N
C
I=NGRID
C(I)  = 1.0D0
A(I)  = 1.0D0+(KH*RR*DR)/KCR
B(I)  = 0.0D0
D(I)  = (TGAS*KH*RR*DR)/KCR
RETURN
END
C
C
C    ==========================================================
      SUBROUTINE COFC (NGRID,NMID,COLD,TOLD,TINT,KM,AC,BC,CC,DC)
C    ==========================================================
C
```

```
C     SUBROUTINE TO GENERATE MATRIX SYSTEM FOR CONCENTRATION PROFILE
C
IMPLICIT NONE
INTEGER NGRID,NMID,I
DOUBLE PRECISION AC,BC,CC,DC,COLD,TINT,DR,DT,KCO,KCR,KH,TGAS,RR,R,
1                ALPH11,ALPH33,ALPH44,RGAS,ALPH77,DCR,KM,CGAS,
2                ALPH22,ALPH55,ALPH66,DRR,CPGAS,KGAS,POR,KW,KS,
3                DVAP,RHOW,CPW,RHOS,CPS,MW,TOLD
DIMENSION AC(NGRID),BC(NGRID),CC(NGRID),DC(NGRID),COLD(NGRID),
1         R(NGRID),TOLD(NGRID)
COMMON/PARAM/DR,DT,TGAS,RR,RGAS,CGAS,DRR,POR,KW,KS,RHOW,CPW,RHOS,
1            CPS,MW
C
C     DEFINITION OF PARAMETERS
C
CPGAS  = 1.883D0-1.6737D-4*(((TOLD(NMID)+TOLD(NGRID))/2)-273.15D0)
1         +8.4386D-7*((((TOLD(NMID)+TOLD(NGRID))/2)-273.15D0)**2)
2         -2.6966D-10*((((TOLD(NMID)+TOLD(NGRID))/2)-273.15D0)**3)
KGAS   = 2.425D-2-7.889D-5*(((TOLD(NMID)+TOLD(NGRID))/2)-273.15D0)
1         -1.790D-8*((((TOLD(NMID)+TOLD(NGRID))/2)-273.15D0)**2)
2         -8.570D-12*((((TOLD(NMID)+TOLD(NGRID))/2)-273.15D0)**3)
KCO    = POR*KW+(1.0D0-POR)*KS
KCR    = POR*KGAS+(1.0D0-POR)*KS
DVAP   = 0.22D-4*((((TOLD(NMID)+TOLD(NGRID))/2)/273.15D0)**1.75D0)
DCR    = (2*POR*DVAP)/(3.0D0-POR)
ALPH11 = ((POR*RHOW*CPW+(1.0D0-POR)*RHOS*CPS)/KCO)*RR**2
ALPH22 = (DCR*MW/(POR*RHOW))/RR**2
ALPH33 = (DCR*MW*CPGAS)/KCR
ALPH44 = ((RHOS*CPS*(1.0D0-POR))/KCR)*RR**2
ALPH55 = (KCR/(POR*RHOW))/RR**2
ALPH66 = (KCO/(POR*RHOW))/RR**2
ALPH77 = (POR/DCR)*RR**2
C
C     INITIALIZE VECTORS TO ZERO AND GENERATE GRIDS
C
DO 10 I = 1, NGRID
AC(I)   = 1.0D0
BC(I)   = 0.0D0
CC(I)   = 0.0D0
DC(I)   = 0.0D0
R(I)   = (I-1)*DR
10   CONTINUE
C
C     COEFFICIENT VECTORS FROM NODE 1 TO NMID-1
C
DO 20 I=1,NMID-1
CC(1)= 0.0D0
AC(1)= 1.0D0
BC(1)= 0.0D0
DC(1)= 0.0D0
20   CONTINUE
C
C     COEFFICIENT VECTORS AT NODE NMID
C
CC(NMID) = 0.0D0
AC(NMID) = 1.0D0
BC(NMID) = 0.0D0
DC(NMID) = (EXP(20.21D0-(5104.05D0/TINT))/760)/(RGAS*TINT)
```

```
C
C    COEFFICIENT VECTORS FROM NODE NMID+1 TO NODE NGRID-1
C
DO 30 I=NMID+1,NGRID-1
CC(I)=DT/(ALPH77*DR**2)-DT/(ALPH77*R(I)*DR)
AC(I)= 1.0D0 + 2*DT/(ALPH77*DR**2)
BC(I)=DT/(ALPH77*DR**2)+DT/(ALPH77*R(I)*DR)
DC(I)=COLD(I)
30   CONTINUE
C
C    COEFFICIENT VECTORS AT NODE N
C
CC(I) = 1.0D0
AC(I) = 1.0D0+(KM*RR*DR)/DCR
BC(I) = 0.0D0
DC(I) = (CGAS*KM*RR*DR)/DCR
RETURN
END
C
C
C    ========================================
      SUBROUTINE CONV (TGAS,TS,DIA,VEL,KH,KM)
C    ========================================
C
C    THIS SUBROUTINE CALCULATES THE CONVECTIVE HEAT AND MASS
C    TRANSFER COEFFICIENTS
C
IMPLICIT NONE
DOUBLE PRECISION TGAS,TS,DIA,VEL,TAV,KAIR,MUAIR,DAB,NU,SH,
1                RE,CPAIR,KH,KM,RHOAIR,TGASC,TSC,TAVC,PR,SC
C
TGASC= TGAS-273.15D0
TSC  = TS-273.15D0
TAV  = (TGAS+TS)/2
TAVC = (TGASC+TSC)/2
C
RHOAIR= 1.2929D0*(273.15D0/TAV)
KAIR  = 1.731D0*(0.014D0+4.296D-5*TAVC)
MUAIR = 1.720D-5+4.568D-8*TAVC
DAB   = 0.22D-4*((TAV/273.15D0)**1.75D0)
CPAIR = 34.518D0*(28.088D0+0.197D-2*TAV+0.480D-5*TAV**2
1        -1.965D-9*TAV**3)
C
RE    =(DIA*VEL*RHOAIR)/MUAIR
PR    =(CPAIR*MUAIR)/KAIR
SC    =MUAIR/(RHOAIR*DAB)
NU    =2.0D0+0.65D0*(RE**0.5D0)*(PR**0.33D0)
SH    =2.0D0+0.65D0*(RE**0.5D0)*(SC**0.33D0)
C
KH    =(NU*KAIR)/DIA
KM    =(SH*DAB)/DIA
RETURN
END
C
C
C    ====================================
      SUBROUTINE TDMA (PHI,A,B,C,D,N,P,Q)
C    ====================================
```

```
C
C    SUBROUTINE TO SOLVE TRIDIAGONAL SYSTEM
C
C    ARGUMENT LIST
C    -------------
C    N             : NUMBER OF SIMULTANEOUS EQUATIONS.
C    PHI           : SOLUTION VECTOR
C    A,B,C,D       : COEFFICIENT VECTORS OF LENGTH N
C    P,Q           : DUMMY VECTORS USED IN RECURRENCE RELATIONS
C
C    THE SYSTEM SHOULD BE ARRANGED AS:
C    A(I)*T(I)=B(I)*T(I+1) + C(I)*T(I-1) + D(I)
C
INTEGER I,K,M,N,NL
DOUBLE PRECISION A,B,C,D,DENOM,P,PHI,Q
DIMENSION A(N),B(N),C(N),D(N),P(N),PHI(1),Q(N)
C
C    EVALUATE P(1)&Q(1)
C
P(1) =B(1)/A(1)
Q(1) =D(1)/A(1)
C
C    USE RECURRENCE RELATIONS TO FIND P(I),Q(I),I = 2,3,...,N
C
DO 10 I=2,N
DENOM =1.0/(A(I)-C(I)*P(I-1))
P(I)  =B(I)*DENOM
10   Q(I)  =(D(I)+C(I)*Q(I-1))*DENOM
PHI(N)=Q(N)
C
C    BACK SUBSTITUTE P(I),Q(I),I = N-1,N-2,....,1 TO FIND PHI(N-1),
C    PHI(N-2),....,PHI(1)
C
NL =N-1
DO 20 K=1,NL
M =N-K
20   PHI(M) =P(M)*PHI(M+1)+Q(M)
RETURN
END
```